Augmin complex components control branching of sensory neuron dendrites in *Drosophila* larvae

Dissertation

zur

Erlangung des Doktorgrades (Dr. rer. nat.)

der

Mathematisch-Naturwissenschaftlichen Fakultät

der

Rheinischen Friedrich-Wilhelms-Universität Bonn

Vorgelegt von

Yun Zhang

aus

Hubei, China

Bonn

December, 2015

Angefertigt mit Genehmigung der Mathematisch-Naturwissenschaftlichen
Fakultät der Rheinischen Friedrich-Wilhelms-Universität Bonn

Erstgutachter: Dr. Gaia Tavosanis

Zweitgutachter: Prof. Dr. Walter Witke

Tag der Promotion: 18.12.2015

Erscheinungsjahr: 2016

Hiermit erkläre ich ehrenwörtlich, dass ich die vorliegende Dissertation selbständig und ohne unerlaubte Hilfe angefertigt habe. Ich habe weder anderweitig versucht, eine Dissertation oder Teile einer Dissertation einzureichen beziehungsweise einer Prüfungskommission vorzulegen, noch mich einer Doktorprüfung zu unterziehen.

Bonn, den

Yun Zhang

Table of Content

Index of figures

Index of tables

Abbreviations

ADP	Adenosine diphosphate
ATP	Adenosine triphosphate
AEL	After egg laying
BDNF	Brain-derived neurotrophic factor
CAMSAP	Calmodulin-regulated spectrin-associated protein
CNS	Central nervous system
C-terminal	Carboxyl-terminal
da	Dendritic arborization
DNA	Deoxyribonucleic acid
dNTP	Deoxynucleoside triphospate
DGC	Dendritic growth cone
Drosophila	*Drosophila melanogaster*
EM	Electron microscopy
GFP	Green fluorescent protein
GTP	Guanosine triphosphate
GDP	Guanosine diphosphate
γ-TuRC	Gamma Tubulin ring complex
MAP	Microtubule associated protein
MARCM	Mosaic analysis with a repressible cell marker
MTOC	Microtubule organizing center
N-terimal	Amino-terminal
PCR	Polymerase chain reaction
PNS	Peripheral nervous system
RNA	Ribonucleic acid
SD	Standard deviation
UAS	Upstream activating sequence

1 Summary

Microtubule is the major architectural element to support proper neuronal structure. It is tightly organized with intrinsic polarity and affects not only neuronal morphology but also the transport property within the cell. In many cell types, the centrosome component γ-*tubulin* is the principal microtubule nucleator. However, the mechanism underlying neuronal microtubule nucleation and organization remains unknown. During neuronal development, the centrosome is inactivated and microtubule nucleation becomes acentrosomal. Whether the microtubule centrosomal-independent nucleation contributes to the establishment of polarity in neurons remains unclear and essential to answer.

The purpose of this work is to reveal whether Augmin mediated microtubule nucleation plays a role in building up proper dendritic morphology and organizing dendritic microtubule polarity. To this purpose, I analyzed the dendrite morphology of class IV ddaC da neurons in *Drosophila* larvae carrying mutations for γ-*tubulin* and Augmin. I found that dendritic morphology and dendrite branch dynamics were changed in γ-*tubulin, dgt5, dgt6* (Augmin) and *Dgp71WD* (γ-TuRC) mutants. Interestingly, the phenotypes of these various mutants were similar, suggesting the possibility that they might act in concert. To test this possibility, I performed genetic interaction experiments between γ*tub23C, dgt5, dgt6* and *Dgp71WD* and found these molecules play coordinate roles in dendrite morphology. In Augmin complex mutant neurons, the localization of fluorescently tagged α-*tubulin* and the microtubule minus-end marker Nod were both altered, suggesting a role of Augmin in microtubule organization in these neurons. Taken together, my work suggests a role of the Augmin complex in the proper organization of microtubules in neuronal dendrites, which is important for achieving dendritic complexity in *Drosophila* PNS class IV da neurons.

2 Introduction

2.1 Dendrite

The mature nervous system consists of polarized neurons with long axonal processes and multiple dendrites. The axon is responsible for transmitting electrical impulses away from the cell body, while dendrites act to receive and integrate these stimulating inputs from other neurons or the environment via synapses. Synapses are the contact sites between presynaptic axons and postsynaptic dendrites or cell bodies and are important for information processing and memory storage. Therefore, the appropriate development of dendrites, underlying number and distribution of synaptic contacts, is essential for neuronal structure and functional plasticity (Kulkarni and Firestein 2012, Koleske 2013). Moreover, loss of dendrites is related to several psychiatric and neurological disorders, such as Alzheimer's disease (AD), Down syndrome (DS), autism spectrum disorders (ASDs) (Kaufmann and Moser, 2000, Lin and Koleske 2010). For instance, major depressive disorder (MDD) is associated with reduction of both synapse density and dendrite arbor complexity (Licznerski and Duman 2013). Destabilization of dendrites is also found within and adjacent to the infarct area in ischemic events in cortical pyramidal neurons (Brown, Boyd et al. 2010).

To establish appropriate synapsis contact and ensure proper neuronal function, the dendritic morphology needs to satisfy several requirements during development. First, a neuron's dendritic field should be fully covered with proper dendritic density to integrate and process its sensory synaptic inputs. Second, the plasticity of the dendrites needs to be carefully organized to adjust the changes of inputs they received. Third, an elaborate interaction between genetic programming and extracellular signals is required.

2.2 Dendrites of *Drosophila* PNS da neurons

Different types of neurons are classified based on the shape of their dendritic field and dendrite branching patterns. In sensory neurons of *Drosophila melanogaster* larval peripheral nervous system (PNS) (Bodmer, Barbel et al. 1987), the dendritic arborization (da) neurons are classified into four classes based on their distinct dendrite morphology and functions (Grueber, Jan et al. 2003) (Fig. 2.1).

There are fifteen dendritic arborization (da) neurons per larval hemi-segment classified into four main groups in order of increasing dendrite complexity. All da neurons are born 9h after egg laying (AEL) and dendritogenesis initiates around 13h AEL (Grueber, Jan et al. 2003). Class I neurons have the simplest dendritic pattern that is established early during differentiation (Grueber, Jan et al. 2002, Sugimura, Yamamoto et al. 2003). They are proprioceptive and control the coordination muscle contraction (Hughes and Thomas 2007). Class III neurons have more complicate dendritic pattern with actin-rich filopodia-like terminal branchlets decorating the main dendrites. These terminal branchlets are termed as “spiked protrusions” and are enriched in actin filaments organized by the actin-bundling molecule Fascin (Nagel, Delandre et al. 2012). Behavioral response to gentle touch is mediated by these neurons with low threshold (Yan, Zhang et al. 2013). Class IV neurons have the most intricate dendritic arbors that are space filling. Thus, they cover extensively their receptive field and display filling-in responses (Grueber, Ye et al. 2003). They represent polymodal nociceptors in *Drosophila* larvae. They are important for sensation of intense mechanical nociception, thermal nociception, harmful short wavelength ultraviolet radiation, dry-surface environments and harmful hyperoxia (Hwang, Zhong et al. 2007, Xiang, Yuan et al. 2010, Johnson and Carder 2012, Kim and Johnson 2014). Further, deletion of pickpocket, a DEG/ENaI type ion channel, results in a fast moving and less turning-frequency in larvae (Ainsley, Pettus et al. 2003, Gorczyca, Younger et al. 2014, Guo, Wang et al. 2014). All classes of neurons display self-avoidance, and thus their dendrite branches in general do not cross. The

mechanism underlying requires recognition and repulsion of the dendrites of the same neuron, and is mediated by Dscam (Down syndrome cell adhesion molecules), a transmembrane protein in the immunoglobulin superfamily (Soba, Zhu et al. 2007, Zipursky and Grueber 2013). This function of Dscam is cell type dependent, while Dscam does not affect dendrite self-avoidance in Drosophila motoneurons (Hutchinson et al. 2014). Other molecules as integrins also promote dendritic self-avoidance (Kim, Shrestha et al. 2012). Both class III and class IV neurons in addition avoid the dendrite of homotypic neurons and thus tile the epidermis (Grueber, Jan et al. 2002). Several signaling molecules are involved in tiling in *Drosophila* da neurons including Tricornered (TRC), a kinase of the NDR family, and genes of rapamycin complex 2 (TORC2) (Jan and Jan 2010).

The *Drosophila* da neurons of the embryonic and larval peripheral nervous system provide a powerful model for studying dendritic development and its underlying molecular mechanisms owing to the following reasons. First, they are located between the epithelium and muscle and spread their dendritic trees in a two-dimensional manner, which can be easily accessed by *in vivo* imaging with high resolution. Second, the dendrites of these neurons start to develop in the embryonic stage, reach their maximum complexity in third instar larval stage and undergo pruning during metamorphosis. Each stage is presenting different molecular mechanisms and dendritic morphology that is useful for dendrite development studying. Third, the class-specified diversity of these neurons allows comparative analysis to find the key control elements for the establishment of different dendritic branching patterns. Fourth, they are accessible to genetic screens and this allows the molecular elucidation of important steps in dendrite morphogenesis including dendrite dynamics (Gao, Brenman et al. 1999, Gao 2007, Parrish, Emoto et al. 2007, Corty, Matthews et al. 2009, Jan and Jan 2010, Grueber, Jan et al. 2003, Sugimura, Yamamoto et al. 2003).

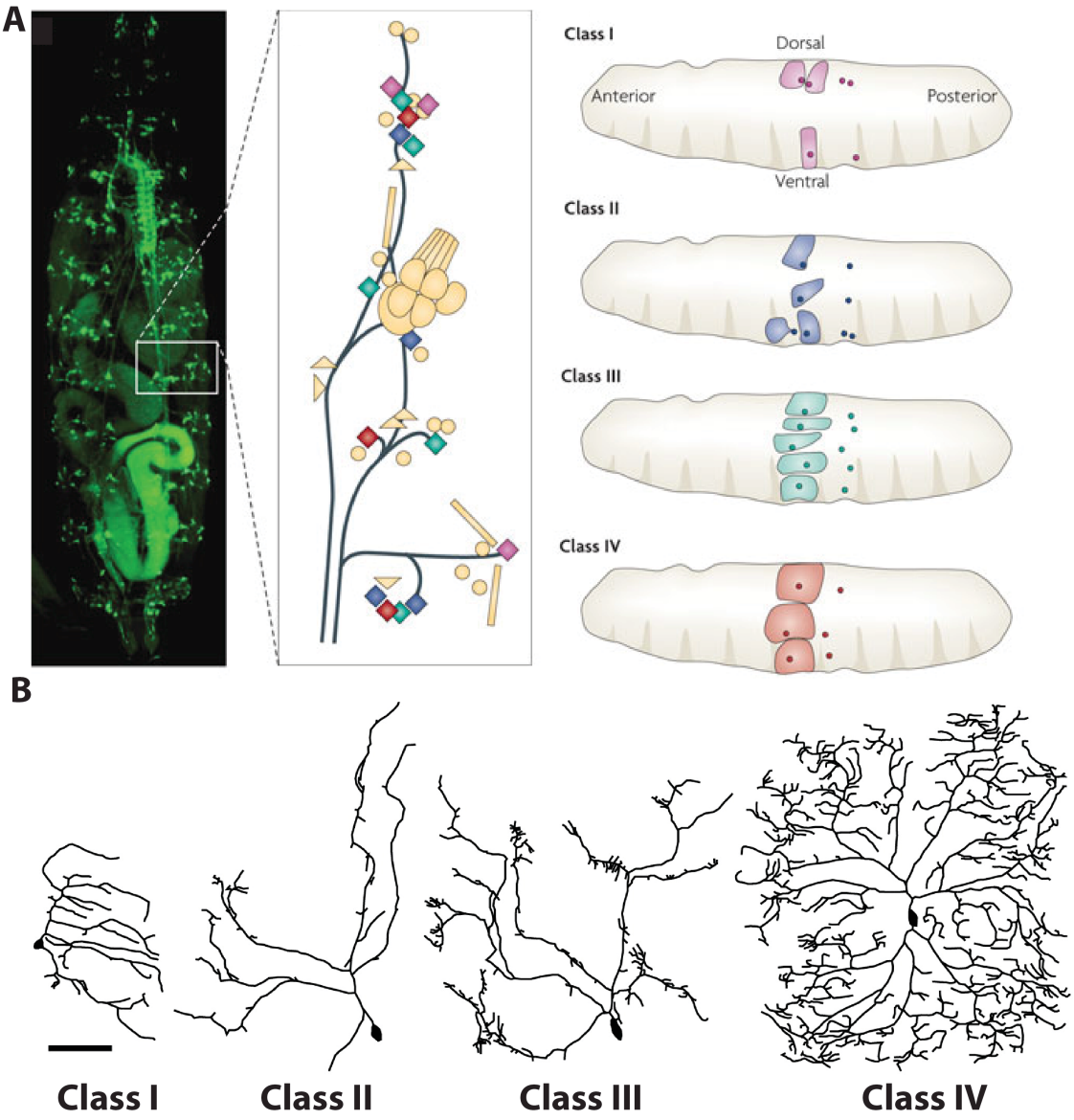

Figure 2.1 The *Drosophila* PNS dendritic arborization (da) neurons

(A) A view of *Drosophila* larva with its dendritic arborization (da) neurons labeled with GFP and schemes of their localization within a single hemi-segment. (Jan and Jan 2010). (B) Tracing of the four classes in third instar larva: class I ddaE, class II ddaB, class III ddaF, and class IV ddaC. The scale bar is 75 μm. (Jinushi-Nakao, Arvind et al. 2007)

2.3 Dendrite differentiation

The development of dendrites is an essential process for neuronal circuitry maturation. Therefore, the dendrites develop in a carefully coordinated manner with proper addition and elimination of dendrites. Dendritogenesis proceeds in 3 characteristic steps, exemplified by differentiating projection neurons within the optic tectum of *Xenopus laevis* tadpoles: (i) initiation of neurites and their differentiation into one axon and several dendrites; (ii) dynamic branching, elongation and synapse formation; (iii) deceleration of further outgrowth and stabilization of existing branches (Hossain, Hewapathirane et al. 2012). The time scale between these steps can vary among neuronal types and species, but the order of events appears conserved.

There are three types of processes involved in the differentiation of dendrites: dendritic branches (long dendritic processes), dendritic filopodia (small protrusions along dendrite stretches of up to 10 μm in length), and dendritic growth cones (DGC, a small lamellipodium-like structure at the tips of dendrites) (Crino and Eberwine 1996, Dailey and Smith 1996, Hossain, Hewapathirane et al. 2012). The growth dynamics of these dendritic structures are studied extensively in *Drosophila* larva sensory neurons, cultured rodent hippocampal neurons, tectal projection neurons of *Xenopus* tadpole and retinal ganglion cells of zebrafish using live imaging (Ziv and Smith 1996, Wu, Zou et al. 1999, Jan and Jan 2003, Niell and Smith 2004, Mumm, Williams et al. 2006, Hossain, Hewapathirane et al. 2012, Nagel, Delandre et al. 2012). In general, DGCs and filopodia are coincided with dendrite maturation. DGCs decorate the tips of dendritic branches as shown in *Xenopus* tectal neurons or hippocampal slices and are important for dendrite branching through growth cone splitting (Dailey and Smith 1996, Hossain, Hewapathirane et al. 2012). Filopodia, which later will grow into branches or spines, extend along the length of dendritic shafts (Wong and Wong 2000). Stabilized filopodia then become dendritic branches and extend further (Heiman and Shaham 2010). There are several possible triggers for

the development from filopodia to dendritic branches including activity of neurotransmitter receptors, signaling adhesion proteins, membrane tension and mRNA synthesis (Jan and Jan 2003, Heiman and Shaham 2010, Koleske 2013).

2.3.1 Dendrite stabilization

Stabilization of the dendritic arbor occurs over a long period of time and correlates with neuronal activity and synapse formation. The relation between synaptic input and dendrite development has been extensively investigated. In early development of optic tectal neurons of *Xenopus laevis*, dendritic arbors are highly dynamic, while dendrites in more mature neurons with higher complexity are significantly less dynamic (Wu, Zou et al. 1999). In zebrafish larva optic tectum neurons or *Xenopus* tectal neurons, branches are stabilized after an initial synaptic contact is maintained (Niell, Meyer et al. 2004, Li, Erisir et al. 2011). Mature neurons, which have stronger synaptic inputs, have more stable dendrites (Wu, Zou et al. 1999). Changes of presynaptic activity affect the development of dendrites in *Drosophila* aCC motor neurons, which is mediated by protein kinase A (PKA) (Tripodi, Evers et al. 2008). In *Drosophila* serotoninergic neurons, the refinement of dendrites requires presynaptic input and is driven by Wnt signaling during metamorphosis (Singh, VijayRaghavan et al. 2010). Moreover, mediated by Rho GTPases, visual stimulation increases dendrite growth rate as well as total dendritic length in *Xenopus* optical tectal neurons (Sin, Haas et al. 2002). In ventral lateral neurons of *Drosophila* larva CNS, which are important for light avoidance behavior of larvae, extended light exposure reduces dendritic length, which is mediated through rhodopsin and cAMP pathway (Yuan, Xiang et al. 2011). However, in *Drosophila* high order visual system, dendritic development is independent of light stimulation in vertical system (VS1) neurons (Scott, Reuter et al. 2003). It seems that different systems within different developmental stages requires different levels of presynaptic input. The underlying mechanisms remain unclear. As a brief statement, in young developing neurons, new synaptic input is essential for dendrite stability.

In addition, the neurotrophic factor BDNF (brain-derived neurotrophic factor),

a member of the neurotrophin family, is considered to be an important modulator, in regulating neuronal morphology through TrkB receptors. Blocking BDNF increases dendritic complexity in young retinal ganglion cells (RGCs) through TrkB (Lom and Cohen-Cory 1999, Yacoubian and Lo 2000). Moreover, BDNF enhances dendritic number and length of layer II pyramid neurons (Niblock, Brunso-Bechtold et al. 2000). In layer II or III pyramid neurons, BDNF is necessary for dendrite maintenance in later developmental stages (Gorski, Zeiler et al. 2003). In hippocampal neurons, BDNF increases mRNA and protein level of cypin, which can support dendritic branching by promoting microtubule assembly. Signaling through CREB (cAMP response element-binding protein) and cypin regulates dendrite stability and dendritic number increment (Kwon, Fernandez et al. 2011). Blocking NMDAR (N-methyl-D-aspartate receptor) results in longer dendrites of barrelette neurons and increased primary dendrites of dentate gyrus granule cells (Lee, Lo et al. 2005, Espinosa, Wheeler et al. 2009). There are also suggestions linking BDNF to microtubule associated proteins like MAP1A and MAP2 (Koleske 2013). However, further evidence is required.

2.3.2 Dendrite dynamics

The differentiation of neuronal dendrites is a highly dynamic process, as is observed by time-lapse analysis in various systems including *Drosophila* da sensory neurons, tectal neurons of *Xenopus* tadpoles and zebrafish embryos (Wu, Zou et al. 1999, Niell and Smith 2004, Hossain, Hewapathirane et al. 2012, Nagel, Delandre et al. 2012, Sugimura, Yamamoto et al. 2003) (Fig. 2.2). During development, terminal branches are more dynamic than the primary and secondary dendrites, for instance in embryonic chick retinal ganglion cells (Wong and Wong 2000). In Purkinje cells, terminal dendrites extend at a constant speed while proximal dendritic segments are quite static (Fujishima, Horie et al. 2012). *In vivo* time-lapse of single optic tectal neurons of *Xenopus* tadpoles reveals that the dendrites of young neurons undergo more dynamic changes than mature neurons (Wu, Zou et al. 1999). Nevertheless, mature neurons still preserve some degree of dendritic plasticity. After maturation, dendrite structure and stability can also be altered

in physiological conditions during adult life by hormones, injury, environmental changes, stress or learning (Tavosanis 2012). In vivo imaging of zebrafish spinal motorneurons shows a correlation between high electrical activity of cells and low growth dynamic suggesting a homeostatic regulation in dendritic dynamics (Kishore and Fetcho 2013).

The stability and dynamics of the cytoskeleton within the dendritic arbor is also crucial for dendrite stabilization and remodeling. The network of microtubules provides structural support for dendrite remodeling and stability. Microtubule associated proteins and regulators are involved in this process. For instance, MAP1A, a microtubule stabilizing protein enriched in dendrites, contributes to dendrite stability and therefore regulates dendritic growth (Szebenyi, Bollati et al. 2005). The Rho-GTPase family can disrupt microtubule organization and therefore impairs dendritic morphology (Georges, Hadzimichalis et al. 2008). More details of dendritic microtubule will be discussed in the following chapters.

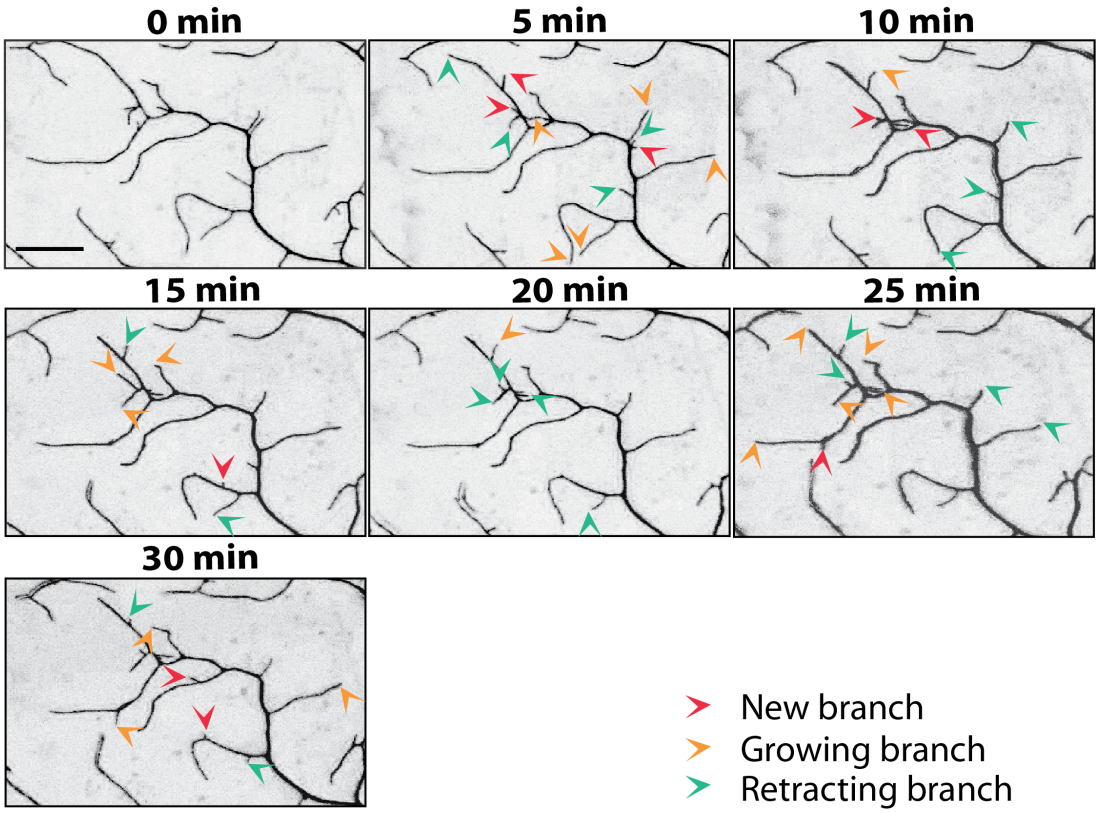

Figure 2.2 Time-lapse of dendrites of second instar *Drosophila* class IV ddaC da neurons within 30 min.

Terminal dendrites are imaged at different time points. Different colored arrows indicate different dendrite dynamics of new branches, growing branches and retracting branches. Scar bar is 10 ⌠m.

2.4 Cytoskeleton of dendrites

The architecture of the dendrites is determined by the underlying cytoskeleton. The neuronal cytoskeleton consists of actin microfilaments (7 nm diameter), intermediate filaments (10 nm diameter) and microtubules (25 nm diameter).

Microfilaments consist of actin polymers (F-actin) that can organize in bundles as well as branched networks. F-actin is a polarized polymer with fast growing barbed/plus ends and shrinking pointed/minus ends, generating a treadmilling that is at the core of force generation towards the plus end and controls cell movement or organelle transport. This dynamic is elaborately controlled by many actin-binding proteins (ABP) function in promoting actin filament nucleation, elongation, capping, severing and depolymerization (Campellone and Welch 2010).

To initiate dendritic formation, when actin filaments are destabilized, microtubules can invade into the filopodia and thus prompt the initiation of dendrites (Georges, Hadzimichalis et al. 2008). Microtubules are also polymers containing dynamic and stable regions that are carefully controlled by microtubule associated proteins (MAPs) and other regulators. They are important for neuronal structure and protein trafficking. Therefore, they may function as “information carriers” in the neurons (Dent and Baas 2014). The structure and function of the microtubules will be discussed in more details in following chapters.

Intermediate filaments assemble from anti-parallel tetramers. They lack polarity and can not serve as basis for cell motility and intracellular transport. There are a variety of intermediate filaments in the nervous system displaying characteristic sidearm projections. Neurofilaments (NFs) are intermediate filaments of neurons and localized to axons to control axonal width and thus axonal signal transmission. In *Drosophila*, they in general are absent.

2.4.1 Microtubule organization in dendrites

Parallel microtubules are the main cytoskeleton components in dendrite shafts providing support for the dendrite structure as well as for new dendrite formation. They are regularly spaced discontinuously and lie parallel to each other as shown early in cat retinal ganglion cells by serial electron micrographic reconstruction (Sasaki et al. 1983). Though actin is generally considered to play the initial role in cellular remodeling, microtubule sliding driven by the microtubule motor kinesin-1 contributes to providing the mechanical forces necessary for initial neurite extension in *Drosophila* primary cultured neurons (Lu, Fox et al. 2013).

Microtubules are polarized heterodimers of α- and β-Tubulins that line up in a head-to-tail pattern to form linear protofilaments, the basic structural element of microtubule, that assemble later into hollow tubes. They display two distinct domains along the length of the tubule: a plus-end enriched in GTP-bound Tubulin molecules and a domain closer to the minus end, enriched in GDP-bound Tubulin. Microtubules continuously undergo assembly and disassembly dynamics. As long as a GTP cap is present at their plus end, microtubules will keep growing. Once Tubulin's GTPase activity has hydrolyzed GTP to GDP and eliminated the GTP cap, the microtubule will undergo rapid catastrophic depolymerization. Different cell types display microtubules with different number of protofilaments (11-15) suggesting the number of protofilaments is important for the establishment of proper cellular morphology and function. Doublecortin, a microtubule stabilizer in developing neurons, binds preferentially to 13-protofilament microtubules *in vitro* (Bechstedt and Brouhard 2012). Recent research shows that MEC-17, a α-Tubulin acetyltransferase, is important for organizing 15-protofilament-microtubule in touch receptor neurons (TRNs) in *Caenorhabditis elegans*. Loss of MEC-17 results in microtubules with various diameters and protofilament numbers. The mutant neurons develop swelling and longer axons (Topalidou, Keller et al. 2012).

Besides the number of protofilaments, microtubules of mature neurons have more frequently undergone post-translational modifications resulting in more stable structures. Among these modifications, detyrosination and acetylation are the most common and studied ones. Both detyrosination and acetylation occur on α-Tubulin within polymerized microtubules, by removal of the C-terminal tyrosine residue or modification of lysine 40, respectively (Westermann and Weber 2003, Peris, Wagenbach et al. 2009, Janke and Bulinski 2011). Post-translational modified microtubules are enriched in axons and less detyrosinated microtubules in dendrites, suggesting that dendritic microtubules are more dynamic than axonal microtubules. In rat cortical neurons, serotonin receptor promotes microtubule dynamics by manipulating microtubule post-translational modification and thus regulates morphology and dynamics of dendritic growth cone (DGC) (Ohtani, Kozono et al. 2014). In hippocampal neurons, proline/serine-rich coiled-coil protein 1 (PSRC1), a microtubule associated protein promotes cell growth, increases acetylated and tyrosinated microtubules and suppresses neurite/axon outgrowth (Hsieh, Chiang et al. 2012). In the same system, kinesin translocation is affected by microtubule post-translational modifications (Hammond, Huang et al. 2010). This suggests that such modifications can regulate motor proteins and regulator proteins as well, for instance by representing binding sites for them. Kinesin-5, for example, accumulates on dendritic microtubules and prefers to bind to tyrosinated tubulins in superior cervical ganglia (SCG) neurons (Kahn, Sharma et al. 2014). In cerebrocortical neurons, microtubule associated protein SEPT7, a subunit of the heteropolymerizing guanosine tri-/di-phosphate-binding protein family, is required for dendritogenesis since its depletion induces shorter dendrites with less complexity. Interestingly, it limits acetylation since acetylated α-tubulin significantly accumulates in SEPT7-depleted neurons. Further evidence shows SEPT7 interacts with HDAC6, the major α-Tubulin deacetylase, to regulate acetylation of Tau (Ageta-Ishihara, Miyata et al. 2013, Noack, Leyk et al. 2014). This finding suggests a role of SEPT7 and HDAC6 in controlling dendrite development through interaction with acetylated α-Tubulin.

Another important characteristic of dendritic microtubules is their orientation. In the shaft of mature dendrites, microtubules display mixed polarity, whereas microtubules orientation remains uniform with the plus-ends-out in axon (Baas, Black et al. 1989). Utilizing fluorescent-tagged plus-end binding proteins, the dynamics of microtubule extension can be traced *in vivo* and *vitro*. For instance, in the proximal region of cultured hippocampal neuron and Purkinje neuron dendrites, microtubules have mixed orientations with approximately 50% microtubules in plus-end-out direction, which is in agreement with earlier data based on electron microscopy (Sharp, Yu et al. 1995, Stepanova, Slemmer et al. 2003). In *Drosophila* da neurons, growing dendritic microtubules display a predominant minus-end out orientation (>90%) and thus differ from the orientation of microtubules in vertebrate neurons (Stone, Roegiers et al. 2008, Hill, Parmar et al. 2012). In nematode neurons like two bipolar neurons in *Caenorhabditis elegans*, the orientation is consistent with *Drosophila* neurons with predominant minus-end-out in the dendrites and kinesin-1 is proposed to glide the plus-end-out microtubules out of the dendrites (Yan, Chao et al. 2013, Sakakibara, Ando et al. 2013).

Microtubule polarity is important for neuronal development in *Drosophila* da neurons, as exemplified by the following example. In mature *Drosophila* class IV da neurons, axon lesion induces an increase in plus-end-out microtubules in the dendrites. After the dendrite closest to the original axon has reoriented its microtubules to a uniform plus-ends-out orientation and starts growing as the new axon, the other dendrites then return to their minus-ends-out dominant orientation (Stone, Nguyen et al. 2010). These data suggest plus-end-out orientated microtubule is a sign for a dendrite turning to an axon in *Drosophila* da neurons. In young cultured hippocampal neurons, minus-ends-out microtubules start to emerge while dendrites start to form their unique morphology, suggesting the presence of minus-end-out microtubules is a significant character in dendrites. In this system, Kinesin-2, EB1 and APC are required to direct microtubule growth at dendritic branch points (Mattie, Stackpole et al. 2010). *In vitro*, EB1-kinesin complex steers growing microtubule plus ends towards the cell body, suggesting a general mechanism for microtubule polarity establishment (Chen, Rolls et al. 2014).

Remarkably, the used imaging method can only detect growing microtubules but not the already-existing ones. Thus, the orientation relation between growing and stable microtubules is an intriguing but open issue. For more extensive read on microtubule polarity orientation in neurons, I refer to a recent review (Baas and Lin 2011).

2.4.2 Microtubule nucleation in neurons

To understand the polarity of microtubules, one important aspect is how microtubules are nucleated within neurons. The centrosome is the main microtubule organizing center (MTOC) in actively dividing cells. In newly born neurons, most of the microtubules are nucleated from the centrosomes. In sympathetic neurons in culture (20hs culture, during which time axon outgrowth happens), after nocodazole treatment, microtubules have been seen to assemble in the region of the centrosome within 5 minutes, and the staining of tyrosinated tubulins suggests the attachment of most of these microtubules to the centrosome (Yu, Centonze et al. 1993). In young hippocampal neurons, microtubules are generated from centrosome as well as the cell body. The treatment with drugs that inhibit microtubule assembly does not abolish the present of microtubules, indicating that microtubules are generated from the centrosome and then transported to the dendrites in early developmental stage (Sharp, Yu et al. 1995, Stiess, Maghelli et al. 2010). There are several essential components of the centrosome-dependent microtubule nucleation, for instance NEDD1, AKAP450, pericetrin and MOZART 1 and 2 (Kollman, Merdes et al. 2011). Zebrafish NEDD1 homologue has been found to play a similar role in recruiting γ-Tubulin to the centrosome as mammalian NEDD1 and depletion of zNEDD1 yields poorly patterned neuronal structures (Manning, Lewis et al. 2010).

As the neuron develops, the centrosome loses its function as a microtubule organizing center (MTOC). Despite different morphology of MTOC, γ-Tubulin is considered to be the key microtubule nucleator in all MTOCs. Evidence shows that centrioles are not surrounded by γ-Tubulin in both developing and mature neurons. Dsas-4 centriole duplication mutants as well as centrioles

ablation don't change the microtubule orientation in axons and dendrites (Nguyen, Stone et al. 2011). In hippocampal neurons, γ-Tubulin is present through the axons and dendrites, where it potentially supports microtubule nucleation. In mature hippocampal neurons, after laser ablation of the centrosome, axons still extend and regenerate through acentrosomal microtubule nucleation (Stiess, Maghelli et al. 2010). Taken together, these recent data support the idea that microtubules are formed independently of the centrosome, opening the question of how and where microtubules are nucleated in mature neurons.

There are several possibilities for the acentrosomal microtubule nucleation. In mammalian and *Drosophila* neurons, neuronal Golgi apparatus derived compartments are enriched in dendrites, and can regulate the dynamics of dendrites (Hanus and Ehlers 2008). Such Golgi outposts, the small isolated Golgi stacks found predominately in dendrites (Ye et al. 2007), can serve as non-centrosomal microtubule nucleation sites in the dendritic arbor in *Drosophila* da neurons. This acentrosomal nucleation requires also γ-Tubulin and CP309 (the *Drosophila* homolog of AKAP450, a γ-Tubulin interacting protein) (Ori-McKenney, Jan et al. 2012). One centrosome/Golgi protein is Myomegalin (MMG), which associates with cyclic nucleotide phosphodiesterase and controls microtubules in vertebrates. In epithelial cells, it localizes in cis-Golgi and binds to γ-Tubulin or EB1 respectively. One isoform CM-MMG, which has a conserved domain (CM1), acts as a nucleation activator, recruits γ-Tubulin and promotes microtubule nucleation. The other isoform EB-MMG, which has only EB1-binding sites, localizes to microtubule plus-ends through EB1 binding (Roubin, Acquaviva et al. 2013). It will be interesting to test their function in the nervous system.

Evidence also shows that the existing microtubules can be the track of new microtubule growth in *Drosophila* dendritic da neurons at dendritic branch points (Mattie, Stackpole et al. 2010). This raises the possibility of microtubule nucleation along the existing microtubules. In neurons, there are several molecules that could be responsible for acentrosomal microtubule nucleation. Doublecortin (DCX), which stabilizes microtubule, is expressed in

differentiating neurons. It can bind to sides of microtubules lattice and copolymerize with tubulin to form 13-protofilament microtubules predominantly in vitro. Further research reveals that *in vitro* the interaction between DCX molecules are important for it to bind to microtubules and dock at growing microtubule ends (Fourniol, Sindelar et al. 2010, Bechstedt and Brouhard 2012). Further work to explore DCX as a microtubule nucleator *in vivo* would be interesting.

Additional, microtubules originated from the centrosome can be released and transported into the dendrites as templates (Bartolini and Gundersen 2006). In this scenario, microtubule-severing proteins play important role in releasing microtubules assembled at the centrosome and these severed microtubules then have the possibility to serve as seeds for further microtubule generation. One interesting molecule is Nezha (CAMSAP3) of the calmodulin-regulated spectrin-associated protein (CAMSAP) family. It anchors preferentially at the minus-ends of microtubules as a regulator of microtubule dynamics at cadherin-based adherens junction in epithelia cells which contain oriented non-centrosomal microtubules (Meng, Mushika et al. 2008). *Drosophila* CAMSAP (ssp4/Patronin) caps and stabilizes microtubule minus-ends against kinesin-13 induced depolymerization in *Drosophila* S2 cells (Goodwin and Vale 2010). In hippocampal neurons, CAMSAP2 localizes to microtubule minus ends in a γ-Tubulin independent manner and regulates dendrite development and neuronal polarity (Yau, van Beuningen et al. 2014). It is suggested that CAMSAP is responsible for microtubule minus-end nucleation. In epithelial cells, CAMSAPs preferably localize to severed microtubule minus-ends and stabilize the microtubules lattice. And these microtubule lattices can serve as “seeds” for microtubule outgrowth. Further, Katanin, a microtubule severing protein, can bind to CAMSAPs and regulate the length of CAMSAPs decorated stretches (Jiang, Hua et al. 2014). The function of microtubule severing proteins in dendrites will be discussed later.

Nevertheless, γ-Tubulin is the general nucleator required for microtubule nucleation (Kollman, Merdes et al. 2011). Still, the localization of γ-Tubulin and how microtubule nucleation happens in neurons remains an open issue.

2.5 Microtubule associated proteins in dendrites

Microtubule associated proteins (MAPs) contribute to regulation of microtubule dynamics and stabilization. They usually bind directly to the tubulin dimers through their C-terminal domains, and therefore control a wide range of functions including microtubule stabilizing, microtubule destabilizing, microtubule guiding and microtubule cross-linking with other proteins. Several MAPs classes have been described, including microtubule plus-end tracking proteins (+TIPs), structural microtubule associated proteins, microtubule severing proteins, microtubule polymerizing proteins, microtubule motor proteins and other microtubule regulators. An appropriate coordination of MAPs is required for proper establishment of dendritic arbors.

2.5.1 Microtubule plus-end tracking proteins (+TIPs)

+TIPs are preferably accumulated at the plus ends of microtubule, allowing control of microtubule dynamics and interaction with other components, including actin. Several +TIPs as DLIS-1, Dhc64, CLIP-170, and shortstop, have been shown to regulate dendritic arborization in *Drosophila* and link microtubules to actin directly or indirectly (Gao, Brenman et al. 1999, Swiech, Blazejczyk et al. 2011, Satoh, Sato et al. 2008, Kapitein and Hoogenraad 2011, Lansbergen and Akhmanova 2006). APC (adenomatous polyposis coli), which promotes microtubule assembly, was shown recently as RNA-binding protein to regulate dynamic microtubules through β2B-tubulin in cortical neurons (Preitner, Quan et al. 2014). Further, they direct microtubule growth also in dendrite development. For instance, in *Drosophila* da neurons, kinesin-2, together with EB1 and APC, are required for normal microtubule polarity in dendrites and essential for dendritic branching (Mattie, Stackpole et al. 2010). Recent researches have shown *in vivo* and *vitro* that the XsIP domain of kinesin-1 (KIF5B) and kinesin-2 (KIF7) can bind to EB1 and further conduct new microtubule growth along existing microtubules (Chen, Brinkmann et al. 2014, Doodhi, Katrukha et al. 2014). These findings will help to further explain microtubule-dependent microtubule organization in different systems.

2.5.2 Microtubule structural proteins

Classical microtubule structural proteins are divided into three families: MAP1, MAP2 and Tau. They contribute to microtubule stabilization and thus control the dendritic morphology. MAP1B is highly expressed during early neuronal development. In *Drosophila* central nervous system (CNS) and peripheral nervous system (PNS), loss of futsch, the *Drosophila* orthologue of MAP1B, leads to a disruption of dendritic growth (Hummel, Krukkert et al. 2000). MAP1A, which is enriched in mature dendrites, promotes dendritic branching and growth in Purkinje cells and pyramidal neurons (Szebenyi, Bollati et al. 2005). HMW (High molecular weight) -MAP2 associates preferentially with dendritic microtubules. In primary cultured neurons, depletion of MAP2 prevents dendritic differentiation (Farah and Leclerc 2008). Calcium/calmodulin-dependent protein kinase (II) (CAMKII) can phosphorylate MAP2 and increases its binding to microtubules (Vaillant, Zanassi et al. 2002).

2.5.3 Microtubule stabilizing/polymerizing proteins

Several MAPs are involved in microtubule stabilization and establishment of neuronal morphology. DCX-like kinases (DCLK1 and DCLK2) and Gas7b (Growth arrest specific protein 7b) are found to enhance microtubule bundling in hippocampal neurons and neuron 2A cells, respectively (Gotoh, Hidaka et al. 2013, Shin, Kashiwagi et al. 2013). Marlin-1 stabilizes microtubules through its N-terminal domain and is required for neurite extension as well as neuron migration in cortical pyramidal neurons (Vidal, Fuentes et al. 2012). Other MAPs are found to associate with MAP2 in neurons. In primary hippocampal neurons and dorsal root ganglion neurons, Protein kinase A associates with microtubules in a MAP2 dependent manner and contributes to neurite elongation (Huang, Kao et al. 2013). CRMP (Collapsin-Response-Mediator Protein) family member CRMP5 is important for neuronal polarity as it inhibits dendritic neurite outgrowth by forming a complex with Tubulin and MAP-2. It can also abrogate the function of CRMP2 in promoting neurite outgrowth (Brot, Rogemond et al. 2010). One new possible MAPs member, been found recently to play role in microtubule stabilization is SHATI/NAT8L. In cortical pyramidal neurons, SHATI colocalizes with Tubulin and its

reduction strongly simplifies dendrite complexity. These data suggest SHATI's function as a MAP in stabilizing microtubules (Toriumi, Ikami et al. 2013). MAP6, known as STOP (stable tubule-only polypeptide), which is also known to be responsible for microtubule-cold stability and interacts with the actin cytoskeleton and the Golgi apparatus, inhibits retrograde lysosomal trafficking in dendrites in primary rat neurons and results in negative regulation of dendritic complexity, particularly in distal branching (Schwenk, Lang et al. 2014).

2.5.4 Microtubule severing proteins

The function of microtubule severing proteins is critical for releasing microtubules from nucleation sites and thus allowing their transport within the neuron. Further, they are suggested to contribute for generating seeds for new microtubules generation (Sharp and Ross 2012). One severing protein Katanin consists of two subunits, P60 and P80. And it is distributed widely throughout the neurons. In cultured Rat sympathetic neurons, Katanin has been initially implicated in releasing microtubules generated at the centrosome, and regulating microtubule length throughout the cell body (Ahmad, Yu et al. 1999). The sensitivity of microtubules to severing by Katanin is regulated by microtubule acetylation in both axons and dendrites of young hippocampal neurons (Sudo and Baas 2010). In the same system, *p60-katanin* (one subunit of Katanin) is up regulated by protein kinase C activation and results in neurite retraction (Korulu, Yildiz-Unal et al. 2013). The mechanisms underlying regulation of Katanin need further investigation. In *Drosophila* da neurons, the Katanin family member Katanin p60-like 1 (Kat-60L1) is required for microtubule disruption in the proximal dendrites and plays an essential role in dendrite pruning (Lee, Jan et al. 2009). During development, Kat-60L1 contributes to dendrite morphology by increasing the number of growing microtubules and thus establishes terminal branch stability and dendrite complexity (Stewart, Tsubouchi et al. 2012). Another microtubule severing protein is Spastin, which has an ATPase domain. In contrast to Kat-60L1, although loss of Spastin also simplifies the dendrite arbor of *Drosophila* class IV da neurons, microtubule polymerization within dendrites is unaffected

(Stewart, Tsubouchi et al. 2012). Considering previous work showing that proper dosage of Spastin is required to establish not only appropriate dendritic arbor but also axon elaboration in the ventral nerve cord (VNC) (Jinushi-Nakao, Arvind et al. 2007, Ye, Kim et al. 2011), Spastin is considered to have a broader function that is not exclusively in dendrites. Interestingly, in the same system Spastin overexpression can destroy stable microtubules, while Kat-60L1 has no effect (Stewart, Tsubouchi et al. 2012). Further, reduction of Spastin does not affect the microtubule polarity and the dendrite outgrowth after pruning. And normal Spastin gene dosage is specifically required for regeneration of an axon from a dendrite (Stone, Rao et al. 2012). All these results suggest that in the *Drosophila* class IV da neuron dendrite arbors, Kat-60L1 may have a microtubule regulatory role in promoting dendrite stability with a different mechanism than Spastin. Spastin seems to be tightly controlled at the transcriptional level. The transcription factor Knot can increase dendritic arbor outgrowth through promoting the expression of Spastin (Jinushi-Nakao, Arvind et al. 2007). Dar1, which encodes a novel transcription regulator in the Krüppel-like factor family, is suggested to promote dendrite growth in part by suppressing the expression of Spastin. In *Drosophila* da neurons, depletion of Dar1 results in severe growth defects of microtubule- but not of F-actin-based dendritic branches (Ye, Kim et al. 2011).

2.5.5 Actin-microtubule cross-linkers

Some MAPs, as the MAP2/Tau family, act as actin-microtubule cross-linkers. The actin binding domain is located within the microtubule binding domain (Dehmelt and Halpain 2004). As one member of the conserved actin-microtubule linkers, Shot regulates microtubule polymerization and axon extension in *Drosophila* primary neurons (Alves-Silva, Sanchez-Soriano et al. 2012). Other MAPs regulate actin-microtubule binding through actin binding proteins. For instance EB3, a microtubule +TIPs protein, can interact with actin binding protein Drebrin and redirect microtubules into spines in hippocampal neurons. Actin-dissembling drugs or Drebrin knockdown can diminish the microtubule invasion to spines revealing this invasion event is controlled in a drebrin-dependent manner (Merriam, Millette et al. 2013). To

coordinate interaction between actin and microtubule, GTP-binding protein Septin, formed a ring-shaped complex and colocalized with actin in yeast and mammalian cells (Kinoshita, Field et al. 2002), is important for dendritic development in hippocampal neurons (Tada, Simonetta et al. 2007). Septin7, abundant in the brain, binds to microtubules and recruits them to enter the axonal filopodia and thus induces collateral branching (Hu, Bai et al. 2012, Ageta-Ishihara, Miyata et al. 2013).

2.5.6 Microtubule-based transport

In addition to functioning as structural component, another essential role of microtubules is to deliver various cargos over long distances within the dendrites. The key molecules for the anterograde and retrograde transport are motor proteins, including myosin along actin filaments, Dynein and Kinesin along microtubules (Schlager and Hoogenraad 2009). Microtubule post-translational modification sites can serve as “road signs” to direct motor transport to specific subcellular destinations (Verhey and Gaertig 2014).

The Dynein family comprises: cytoplasmic Dynein, intraflagellar transport (IFT) Dynein and axonemal Dyneins. Cytoplasmic Dynein moves along the microtubules in a minus end-directed manner in most eukaryotic cells (Roberts, Kon et al. 2013). This movement manner may affect microtubule orientation. For instance, in *Drosophila* da neuron axons, loss of Dynein results in mixed orientation of the axonal microtubules, whereas the mixed dendritic microtubule polarity remains intact (Zheng, Wildonger et al. 2008). These data suggest that Dynein is required for the uniform plus-end-out microtubule organization. In hippocampal neurons, Dynein is found to conduct bidirectional transport in dendrites (Kapitein, Schlager et al. 2010). The underlying mechanism remains an open and interesting issue.

In contrast to Dynein, Kinesins are mostly plus-end directed motors (Namba, Nakamuta et al. 2011). Depletion of Kinesin-6 (barely detected in axons) or Kinesin-12 in rat sympathetic neurons causes a reduction of minus-end-out microtubules in developing dendrites, which results in an axon-like morphology. Interestingly, depletion of either motor results in faster growing

axons with greater numbers of mobile microtubules. Therefore, these two motors may regulate the microtubule pattern in both axons and dendrites by driving minus-ends-out microtubules into developing dendrites and preventing the entry of minus-ends-in microtubules transport from the cell body into the axons (Lin, Liu et al. 2012). In *Caenorhabditis elegans* DA9 neurons, Kinesin-1 is also critical for minus-end-out microtubule organization in dendrite. In UNC-116 (kinesin-1/kinesin heavy chain) mutants, dendritic microtubule polarity is completely reversed and adopts an axonal-like plus-end-out organization. Likely, Kinesin-1 regulates dendrite microtubule polarity through directly gliding the plus-end-out microtubules out of the dendrite (Yan, Chao et al. 2013). For RNA transport in cortical primary neurons, KIF1Bβ forms RNA-protein complexes suggesting its function on mediating bi-directed transport of dendritically localized mRNAs (Charalambous, Pasciuto et al. 2013). Based on these findings, Kinesins may conduct bi-directed transportations in both axons and dendrites.

Other researches further investigate proteins interacting with motors. In hippocampal neurons, TRAK1 and TRAK2 (TRAK family adaptor proteins) are required for mitochondrial motility in axon and dendrites respectively. TRAK1 binds to both Kinesin-1 and Dynein/Dynactin, is prominently targeted to axons and needed for axonal growth and branching, whereas TRAK2 predominantly interacts with Dynein/Dynactin but not Kinesin-1, is exclusively present in primary dendrites and required for primary dendrites outgrowth (van Spronsen, Mikhaylova et al. 2013). The ubiquitin E3 ligase TRIM3 (also known as BERP) binds to KIF21B motor in hippocampal neurons. Though the degradation of KIF21B is not due to the TRIM3 E3 ligase function, depletion of TRIM3 reduces the directionality of the motor (Labonte, Thies et al. 2013). Considering the function of TRIM3 binding to Myosin V, this molecule provides an interesting prospective of actin-microtubule interface in dendrites.

2.5.7 Small GTPases-mediated control of dendrite microtubules

The dynamic interaction between actins and microtubules is required for neuronal morphogenesis. One important family that is essential for the regulation of cytoskeletal dynamics is that of the small Rho GTPases

(Gonzalez-Billault, Munoz-Llancao et al. 2012). Rho GTPases are members of Ras superfamily and are clustered in distinct subgoups: Rho (RhoA-C, RhoD, RhoL and Rnd1-3), Rac (Rac1-3) and Cdc42. In neurons, some of these Rho GTPases are essential during dendritic development and determine the complexity of dendrites (Newey, Velamoor et al. 2005).

Although small Rho GTPases were firstly shown to be involved in actin regulation, several recent studies have revealed the need for Rho GTPases in microtubule stabilization in association (Pertz 2010). The members of Rho family seem to be major players in regulating actin-microtubule cross-linking in developing neurons. Several potential regulators of Rho GTPases are quite interesting for further investigation (Conde and Cáceres 2009).

MAP1B, distributed in the dendrites of mature neurons and enriched at the postsynaptic densities, has been extensively studied for its function in promoting microtubule assembly and stabilization (Georges, Hadzimichalis et al. 2008). Recently, it has been shown that it may regulate the structure of the cytoskeleton by interacting with Rho. For instance, in cultured hippocampal neurons, Rho regulates dendrite number and microtubule dynamics through Cypin, which is a guanine deaminase that promotes microtubule assembly (Chen and Firestein 2007). Also in hippocampal neuron primary cultures, Rac1 activator Tiam1 interacts with both the actin-binding and microtubule-binding domains of MAP1B and regulates the actin cytoskeleton via Rac1 (Tortosa, Montenegro-Venegas et al. 2011, Henriquez, Bodaleo et al. 2012). Reelin, a conserved extracellular glycoprotein, regulates actin and microtubules via Rho GTPases in neurons (Leemhuis and Bock 2011). Another regulator is GSK3 signaling that cross-talks with several pathways to control neuronal polarity, including Rho GTPases. It is also suggested to be a key molecule to control microtubule dynamics via microtubule-binding proteins regulation (Kim, Hur et al. 2011). Future work will be required to reveal the link between Rho GTPases and microtubule cytoskeleton.

2.6 γ-Tubulin, γ-TuRC and the Augmin complex

2.6.1 γ-Tubulin and γ-TuRC (γ–Tubulin ring complex)

The globular protein γ-Tubulin is the major microtubule nucleator and it is found primarily at the microtubule organizing centers (MTOC) in eukaryotes. It was first discovered in *Aspergillus* (Oakley and Oakley 1990). It is a ubiquitous and highly conserved protein. Disruption of γ-Tubulin leads to animal lethality and microtubule depletion (Oakley and Oakley. 1990; Sunkel et al. 1995). Disruption or depletion of γ-Tubulin results in microtubule dis-organization in mammalian cells and *Xenopus* egg extracts (Joshi et al. 1992; Stearns and Kirschner 1994), indicating γ-Tubulin plays a key role in organization of microtubule arrays. *In vitro* synthesized radiolabeled γ-Tubulin was shown to tightly bind to microtubule ends and the binding is specific (Li and Joshi 1995). The X-ray crystal structure of γ-Tubulin is similar to α- and β-Tubulins. Researchers suggested that γ-Tubulin might regulate its affinity for αβ-Tubulin through GTP binding and hydrolysis (Aldaz et al. 2005). In *Drosophila* there are two forms of γ-Tubulin: γTub37C and γTub23C.

In *Drosophila*, *Xenopus* and human, γ-Tubulin assembles with several associated proteins to form the γ-Tubulin ring complex (γ-TuRC), consisting of GCP2, GCP3, GCP4, GCP5, GCP6 and NEDD1, according to its ring shape in electron micrographs, which acts as a scaffold or template for α/β tubulin dimers during microtubule nucleation (Moritz et al. 2000; Oegema et al. 1999; Zheng et al. 1995). In human Hela metaphase spindles, γ-TuRC are bound to minus ends of non-centrosomal spindle microtubules (Lecland and Luders 2014), which may contribute to non-centrosomal microtubule nucleation. In *Saccharomyces cerevisiae* and other related yeasts, components of γ-TuRC are absent. They retain only the γ-Tubulin small complex (γ-TuSC), which consists of 2 γ-Tubulins associated with GCP2 and GCP3, suggesting a core role of the nucleating machinery for γ-TuSC (Vinh et al. 2002). Several

reviews have presented nucleation models and structural aspects of γ-TuRC (Kollman, Merdes et al. 2011, Lin, Neuner et al. 2014).

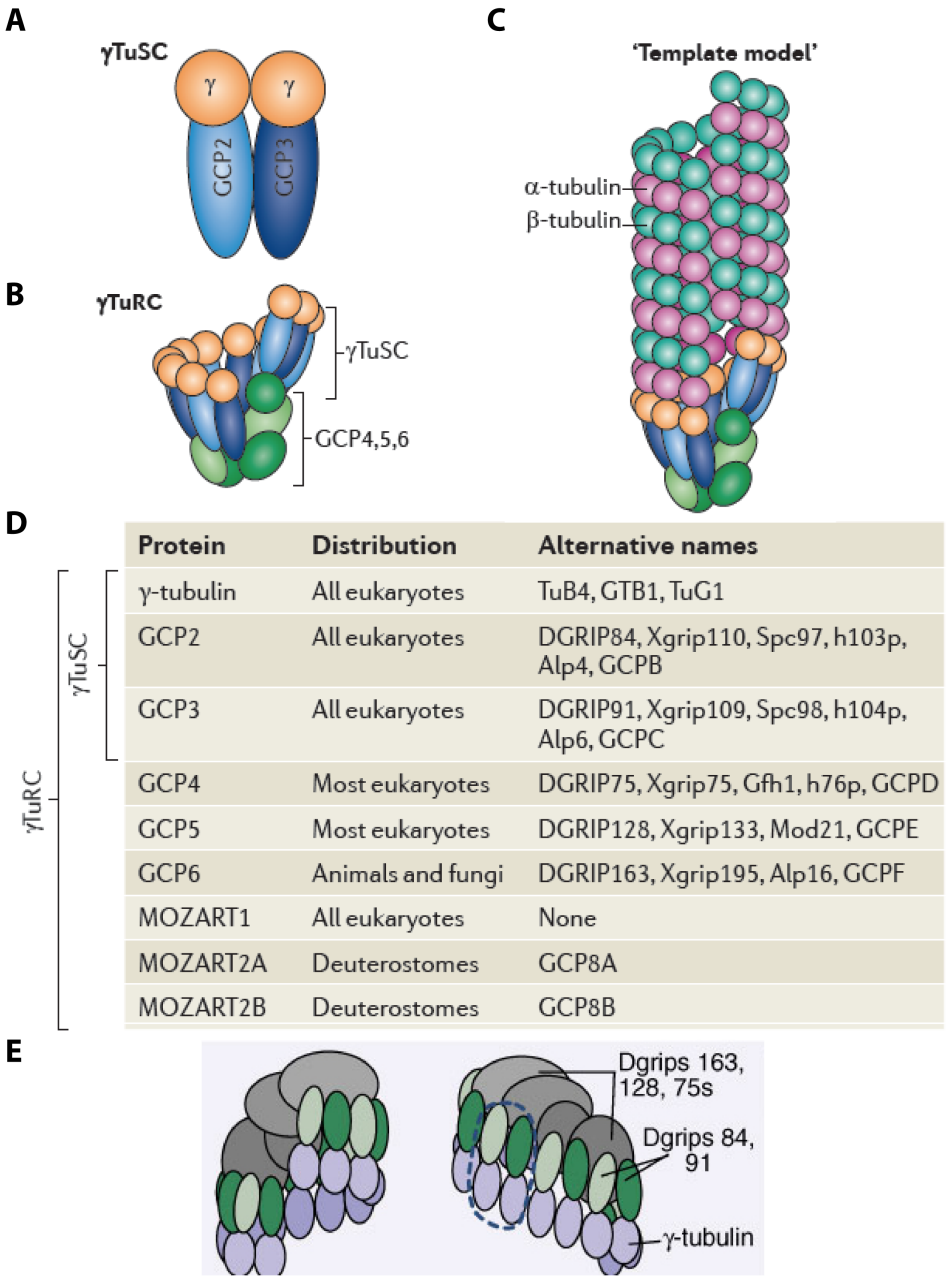

Protein	Distribution	Alternative names
γ-tubulin	All eukaryotes	TuB4, GTB1, TuG1
GCP2	All eukaryotes	DGRIP84, Xgrip110, Spc97, h103p, Alp4, GCPB
GCP3	All eukaryotes	DGRIP91, Xgrip109, Spc98, h104p, Alp6, GCPC
GCP4	Most eukaryotes	DGRIP75, Xgrip75, Gfh1, h76p, GCPD
GCP5	Most eukaryotes	DGRIP128, Xgrip133, Mod21, GCPE
GCP6	Animals and fungi	DGRIP163, Xgrip195, Alp16, GCPF
MOZART1	All eukaryotes	None
MOZART2A	Deuterostomes	GCP8A
MOZART2B	Deuterostomes	GCP8B

Figure 2.3 Structure of γ-TuRC and γ-TuSC

(A)(B) Cartoon models of γ-TuRC and γ-TuSC structure. (C) Cartoon model of microtubule nucleation. (D) Protein list of γ-TuRC and γ-TuSC components. (Kollman, Merdes et al. 2011) (E) Cartoon model of the opening and the opposite side of γ-TuRC structure in *Drosophila* (Moritz, Braunfeld et al. 2000).

2.6.2 The Augmin complex

Recent studies using *Xenopus* egg extracts and human U2OS cells have revealed that a newly forming microtubule can be nucleated at the side of an already existing microtubule. This process requires binding of γ-TuRC to the sides of existing microtubules through the Augmin complex. The resulting daughter microtubules have the same polarity as the mother microtubules (Petry et al. 2012; Kamasaki et al. 2013).

The Augmin complex was recently identified as a set of proteins that facilitated efficient spindle assembly. It is a conserved complex in *Drosophila*, vertebrate cells and plant cells, consisting of eight subunits. (Goshima et al. 2008; Lawo et al. 2009; Ho et al. 2011; Hotta et al. 2012). The *Drosophila* Augmin complex is a hetero-octamer composed of *dgt2* (*dim γ-tubulin 2*) to *dgt9* (*dim γ-tubulin 9*). Recently, analysis of biochemical reconstitution of the Augmin complex with recombinant proteins and electron microscopy reveal the subunit organization and overall architecture of the augmin complex in an elongated Y-shaped structure (Hsia et al. 2014). The human Augmin is named as HAUS and its subunits are as shown in Fig2.4.

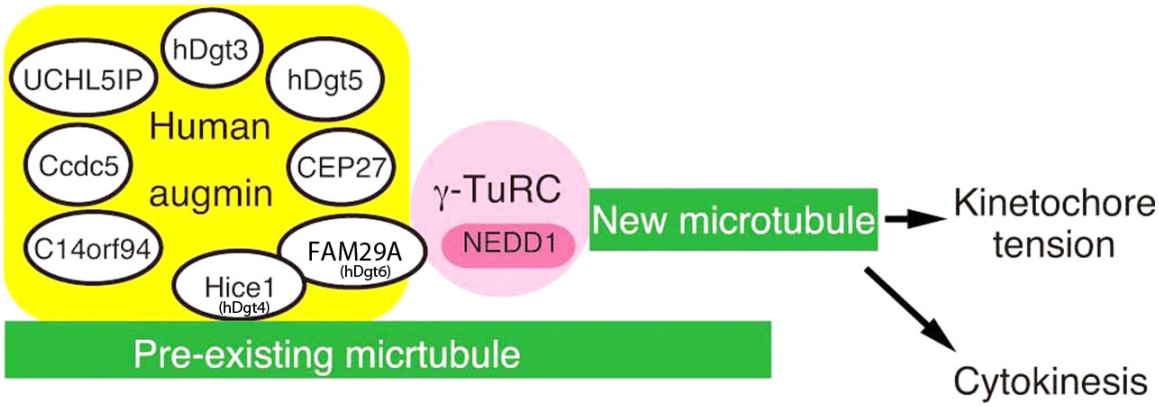

Figure 2.4 A Speculative Molecular Model of the Augmin/γ-TuRC-dependent Micrutubule Generation. (Human augmin subunits are described in this diagram) (Uehara et al. 2009).

Depletion of any of the eight subunits leads to destabilization of the complex and reduced microtubule density along the spindle, suggesting coregulation of the subunits (Goshima et al. 2008). These subunits cooperate to recruit γ-TuRC and increase microtubule density. In plant cells, Augmin-γ-Tubulin is important for postanaphase microtubule generation (Nakaoka et al. 2012) and subunit8 is shown to be a microtubule plus-end binding protein, which can promote microtubule polymerization *in vitro* (Cao et al. 2013). In interphase plant cells, Augmin is associated to interphase cortical microtubules and recruits γ-TuRC and thus initiates microtubule nucleation (Liu et al. 2014). In *Drosophila* embryos, it is also suggested that the Augmin complex contributes to centrosome-dependent astral microtubule assembly (Hayward et al. 2014). However, depletion of Wac, which is suggested to be a new Augmin component, does not affect microtubule assembly during female meiosis in *Drosophila* (Meireles et al. 2009). In general, Augmin complex is considered to associate with microtubule nucleation via γ-TuRC, but the mechanism underlying remains still unclear.

Furthermore, in Hela and U2Os cells, Augmin is evenly distributed along the microtubule lattice on spindles, which is determined by interaction between NEDD1 and γ-Tubulin (Lecland and Luders 2014). In human U2OS cells utilizing electron tomography, a 29nm rod-shaped structure was suggested to be the structure of the Augmin complex connecting the end of the newly formed microtubule to the wall of the existing microtubule (Kamasaki et al. 2013). These researches suggest a possible scenario of the augmin complex in mediating acentrosomal microtubule nucleation along existing microtubules.

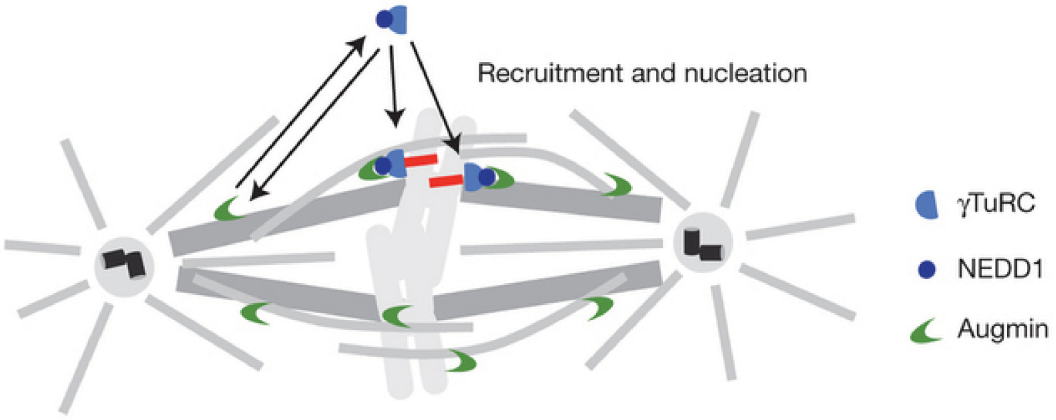

Figure 2.5 Model for spindle microtubule nucleation. γ-TuRC is recruited to the Augmin complex through its targeting subunit NEDD1 (Lecland and Luders 2014)**.**

In *Drosophila* S2 cells, immunoprecipitation has suggested an interaction between Dgt6 and Dgp71WD (Uehara et al. 2009). Interestingly, disrupting the interaction between NEDD1 (Dgp71WD) and γ-Tubulin results in a specific reduction of the amount of Augmin in pole-proximal spindle regions, suggesting a regulation function of NEDD1 in Augmin recruitment. It has been proposed that Dgt6 and its human homolog FAM29A recruit γ-TuRC via NEDD1 to spindle microtubules, indicating an important role of Dgt6 among the subunits of the augmin complex (Zhu, Coppinger et al. 2008, Uehara et al. 2009). Moreover, Hice1, the human homolog of *Drosophila* Dgt4, binds directly to microtubules and interacts with Hec1, a coiled-coil protein important for mitotic progression, to stabilize microtubules (Wu, Lin et al. 2008, Wu, Wei et al. 2009; Uehara el al. 2009). Aurora-A Phosphorylation of Hice1 regulated by Aurora-A is important for microtubule binding activity (Tsai, Ngo et al. 2011). RanGTP is also involved in stimulation of the interaction between the Augmin complex and the microtubule (Hsia et al. 2014). These researches

suggest interaction between Augmin and γ-TuRC may require the involvement of other molecules.

The processes underlying the formation of neuronal dendrite branches are fundamental to our understanding for the development, wiring and function of the nervous system. In this work, I identified the Augmin complex (Dgt5 and Dgt6) that co-functioned with γTub23C and Dgp71WD, which is the main microtubule nucleator in proper dendrite morphology establishment. Cell-autonomous RNAi-mediated depletion, as well as loss-of-function mutations led to a strong reduction in the number of terminal branchlets in *Drosophila* larvae class IV da neurons. This phenotype could be rescued by over expression of these molecules, which suggests a cell-autonomous function of the Augmin complex in maintaining proper dendritic morphology in the neuronal system. The reduction in the number of terminal branchlets was largely due to impairment of elongation of dendrite branching as revealed by in vivo time-lapse analysis of differentiating *Drosophila* da neurons, suggesting additional microtubule stabilization function of these molecules. Moreover, the organization of dendritic microtubules was disrupted in the Augmin complex components trans-heterozygous mutants. Taken together, a novel function of the Augmin complex in dendritic branch formation was suggested here in my thesis.

3 Results

3.1 γTub23C is necessary for proper establishment of class IV da neuron distal dendritic arbor

Microtubules are major architectural elements of neuronal dendrites and are nucleated primarily by γ-*tubulin*. Recently, a key role of γ*tub23C* in acentrosomal microtubule nucleation was suggested in the maintenance of the terminal dendrites of *Drosophila* PNS class IV da neurons (Ori-McKenney, Jan et al. 2012). However, the localization and nucleation sites for acentrosomal γ*tub23C* mediated microtubule nucleation in these neurons remain unclear.

To further investigate the function of γ*tub23C* in dendritic arbor establishment, I combined a loss of function allele, γ*Tub23C* $^{A15\text{-}2}$ (Vazquez et al. 2008) with a severe hypomorphic allele γ*Tub23C* ^{Pl} (Sunkel et al. 1995), to generate viable γ*Tub23C* mutant larvae. I analyzed the dendritic field of class IV ddaC da neurons and I found a simplified dendritic arbor (Figure 3.1A, B) displaying a significant reduction of the total number of dendritic branches (number of total branches control 654 ± 12.34; γ*Tub23C* mutant 504.6 ± 60.15; n=5; $p<0.01$) (Figure 3.1 C). This reduction in branch number could be rescued cell-autonomously by expressing GFP-tagged γ*Tub23C* (Chen et al. 2012) in class IV neurons using *ppkGal4* (Williams and Truman, 2005) (number of total branches 617.6 ± 22.45; n=5; compared to the γ*Tub23C* mutant $p<0.01$; compared to the control $p>0.1$) (Figure 3.1 C). The total length of the dendritic tree was only slightly modified (total length control 19063.582 μm ± 1065.69; γ*Tub23C* mutant 16602.853 μm ± 2349.96; n=5; $p>0.05$) (Figure 3.1 D). These data suggest γ*Tub23C* is required for proper dendrite number but not for dendrite length in class IV da neurons.

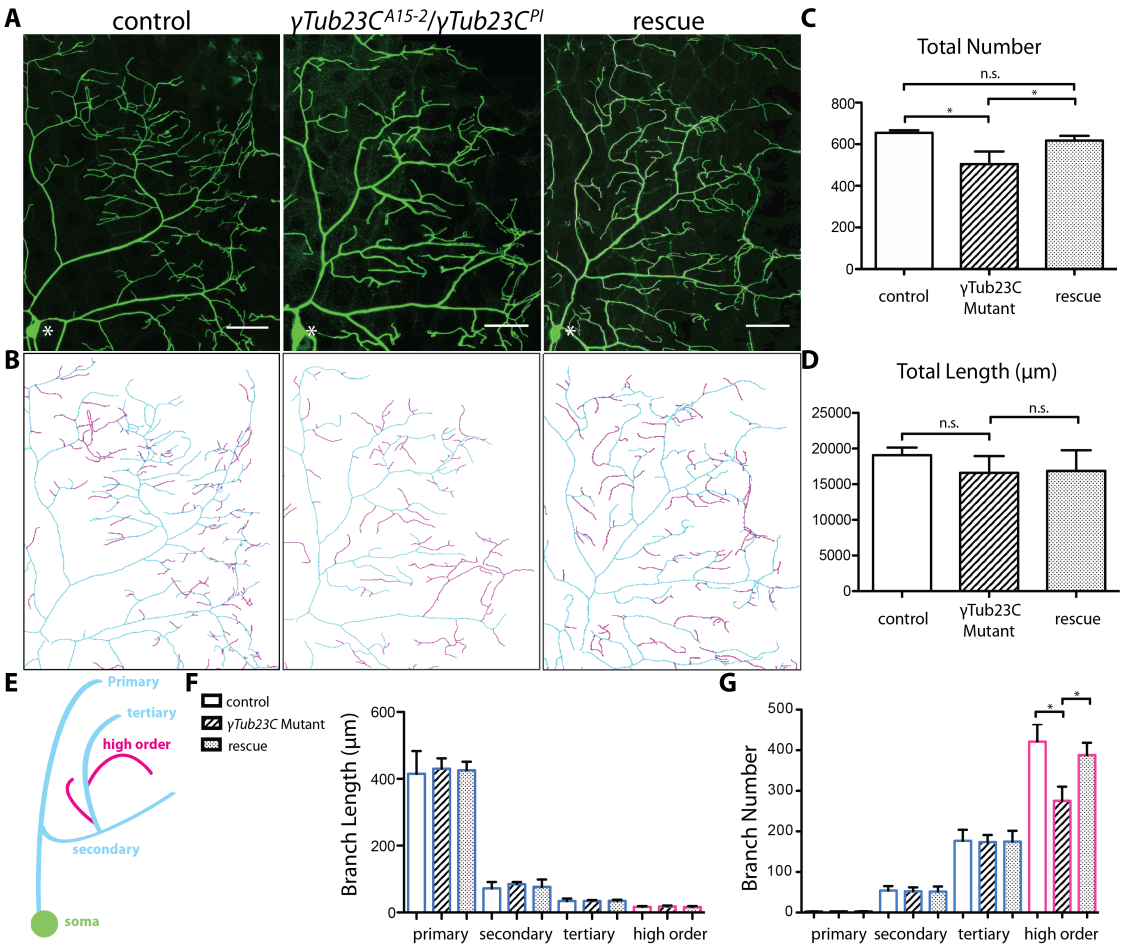

Figure 3.1 Loss of γ-Tubulin function alters the number of dendrites in class IV da neurons

(A) One quadrant of a class IV ddaC neuron of third instar larvae visualized with *mCD8GFP* under the control of *ppkGal4* in control animals, γ*Tub23C*$^{A15-2}$/γ*Tub23C*^{Pl} mutants or cell-autonomous rescue by *ppkGal4 expressing UAS-γTub23C-GFP.* White asterisk indicates the soma. Scale bar is 50 μm. (B) Tracing scheme of neurons shown in (A). Magenta indicates high order branches. Blue indicates other branch levels. (C) Quantification of total branch number in γ*Tub23C* mutant and rescue. (D) Quantification of total branch length in γ*Tub23C* mutant and rescue. (E) Tracing scheme of dendrite branches. Magenta indicates high order branches. Blue indicates other branch level. Green indicates cell body. (F) Quantification of branch length in γ*Tub23C* mutant and rescue. (G) Quantification of branch number in γ*Tub23C* mutant and rescue. Star indicates $p < 0.05$. Data is means ± SD; n = 5 neurons from individual animals per genotype.

To understand the dendrite number defect in more detail, I defined four dendritic branching orders from proximal (primary, starting at the cell body) to distal (high order, terminal branchlets) (Figure 3.1 B, E). A strong reduction was found in the number of high order branches (high order control 421.2 ± 41.97; γ*Tub23C* mutant 275.4 ± 34.77; n=5; $p<0.01$) but not in other branching levels (n=5; $p>0.05$) as shown in Table 3.1 and Figure 3.1 G.

Table 3.1 Number of branches of each branch level

	Primary	Secondary	Tertiary	High order
Control	2.4±0.55	54.2±11.26	177±27.24	421.2 ± 41.97
$\gamma Tub23C^{mutant}$	3±0	52.4±9.76	173.8±17.47	275.4 ± 34.77**

** indicates $p<0.01$

This is consistent with a previous report based on γ*Tub23C* RNAi that γ-*tubulin* is responsible for distal dendritic branching (Ori-Mckenney, Jan et al. 2012). The mean length of each branch level was not significantly modified as shown in Table 3.2 (n=5; $p>0.05$) and Figure 3.1 F.

Table 3.2 Mean lengths of each branch level (μm)

	Primary	Secondary	Tertiary	High order
Control	408.46±66.52	81.98±28.27	37.78±10.04	16.56±2.42
$\gamma Tub23C^{mutant}$	430.23±30.87	84.70±6.75	34.4±2.69	17.76±2.98

To better understand the high order branch reduction observed in the mutant, I performed time-lapse live imaging on late second instar larvae (approximately 72 h AEL) and monitored the initial establishment and dynamics of high order dendrites in class IV da neurons (Figure 3.2 A). I measured the number of branch initiations, extensions, retractions and branch loss events in newly formed branch events after 30 minutes. These numbers were normalized to the length of the basal dendrites and total initial branch number.

New branch formation in the γ*Tub23C* mutant was slightly reduced in comparison to the control (control 7.79 ± 4.07/100 μm, γ*Tub23C* mutant 2.98 ± 2.07/100 μm; n=5; $p<0.05$) (Figure 3.2 B). The percentage of branches elongating was slightly reduced (control 36.14 ± 13.21%; γ*Tub23C* mutant 19.1 ± 8.44%; n=5; $p<0.05$)) and the retraction events were increased (control 24.72 ± 7.09%; γ*Tub23C* mutant 55.20 ± 17.21%; n=5; $p<0.01$) (Figure 3.2 C, D). I also compared the percentage of branch number loss among newly formed branches within the time scale of 30 minutes. However, there was no significant difference (control 51.37 ± 11.81%; γ*Tub23C* mutant 28 ± 25.88%; n=5; $p>0.1$) (Figure 3.2 B), suggesting the stability of newly formed branches was not affected by loss of γ*Tub23C*. All the above data suggest that dendrite dynamics is altered by loss of γ*Tub23C* function and that the existing dendrite branches are less stable in the γ*Tub23C* mutant animals. They indicate that reduction in number of high order dendritic branch in γ-*tubulin* mutant class IV da neurons resulted from a defect of dendrite emergence and maintenance.

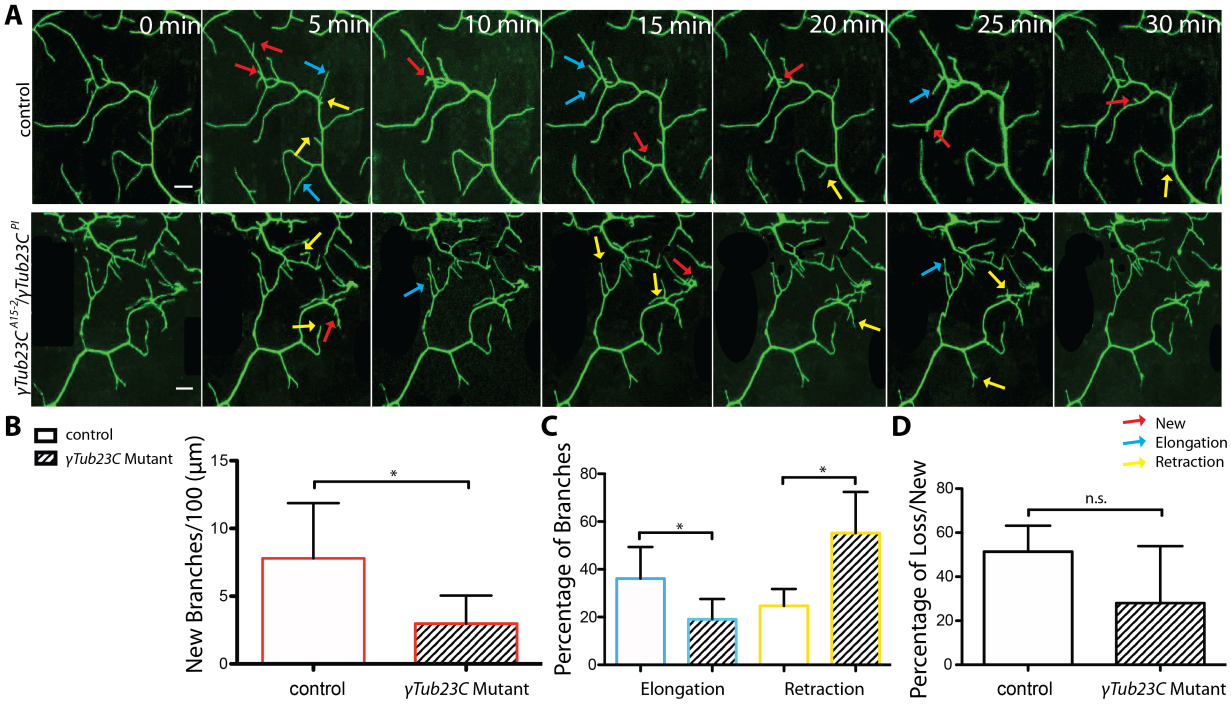

Figure 3.2 Dynamics of high order branches in ddaC neuron dendrites of γ*Tub23C*$^{A15\text{-}2}$/γ*Tub23C*^{Pl} mutants.

(A) Time-lapse imaging of high order branches of ddaC neurons in second instar larvae expressing *mCD8GFP* under the control of *ppkGal4* (total time: 30 min, interval between single images: 5 min). Red, blue and yellow arrows indicate new, elongating and retracting branches respectively. Scale bar is 10 μm. (B) Quantification of new branches per 100μm appearing during 30 minutes time-lapse imaging in wild type and γ*Tub23C*$^{A15\text{-}2}$/γ*Tub23C*^{Pl} neurons in second instar larvae. (C) Quantification of branch dynamics during 30 minutes time-lapse imaging in control and γ*Tub23C*$^{A15\text{-}2}$/γ*Tub23C*^{Pl} neurons. (D) Quantification of percentage of branch loss in newly formed branches during 30 minutes time-lapse imaging in control and γ*Tub23C*$^{A15\text{-}2}$/γ*Tub23C*^{Pl} neurons.

Stars indicate $p < 0.05$. Data is means ± SD; n = 5 neurons of individual animals per genotype.

To analyze the localization of γ*Tub23C,* I expressed GFP-tagged γ*Tub23C* (Chen et al. 2012) in class IV da neurons with *ppkGal4* (Williams and Truman, 2005). The functional construct localized in discontinuous stretches along the shafts of class IV ddaC da neuron dendrites, though barely detectable in more distal branches at this level of expression. The localization was not concentrated at the branching points as suggested in a previous publication (Nguyen, McCracken et al. 2014) (Figure 3.3).

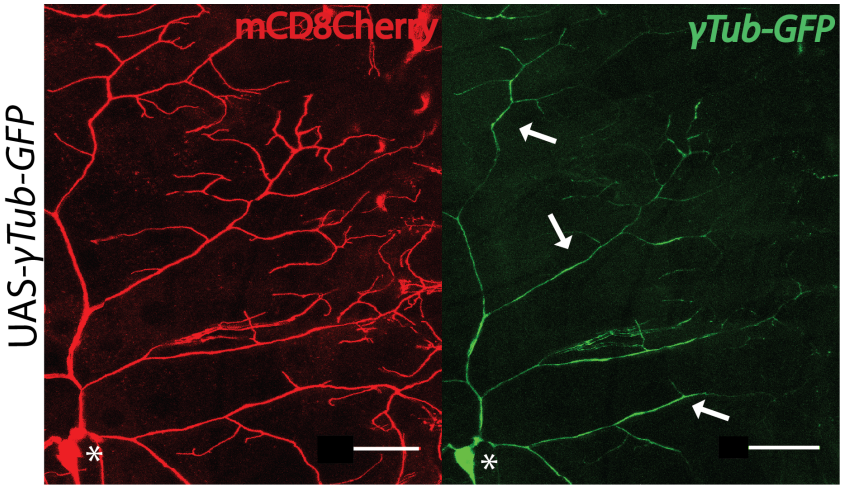

Figure 3.3 Localization of γ-Tub-GPF in *Drosophila* ddaC da neuron dendrites.

One quadrant of a class IV ddaC neuron of third instar larvae is shown. Red shows the dendrites of ddaC da neurons visualized with mCD8Cherry. Green shows the localization of γ-Tub-GPF expressed using *ppkGal4*. Scale bar is 50 μm.

Taken together, γ*tub23C* is required for establishing proper dendritic morphology especially in controlling the total number of high order dendrites. Moreover, γ*tub23C* function is important for new branch formation and dendrite maintenance. The localization pattern of γ*tub23C* along the dendrite shafts suggests a possible scenario in which it mediates microtubule nucleation within the dendrites.

3.2 Dgt5 controls number and length of class IV da neuron dendrites

Several studies have suggested the existence of acentrosomal microtubule nucleation in neurons, including the *Drosophila* PNS da neurons (Stiess et al. 2010; Nguyen et al. 2011). To address which molecules are involved in acentrosomal microtubule nucleation in differentiating dendrites, I performed a candidate-based RNAi screen. Specifically, I knocked down in class IV da neurons components of the γ-Tubulin ring complex (Dgp71WD, Dgrip128, Dgrip163 and Dgrip84) and of the Augmin complex (Dgt2-Dgt6), which is involved in acentrosomal γ-*tubulin*-mediated microtubule nucleation in dividing cells (for review see Teixidó-Travesa et al. 2012; Goshima et al. 2008). The conserved Augmin complex comprises 8 subunits (*dgt2-dgt9*) in *Drosophila* and the human orthologue is named as HAUS complex (Hotta et al. 2012; Goshima et al. 2008; Uehara et al. 2009; Goshima and Kimura, 2010) (Figure 3.4). I found a reduction of neuronal complexity, similar to the γ-*tubulin* mutant phenotype, upon RNAi-mediated knock-down of all tested Augmin complex components (data not shown).

To confirm the phenotype, we generated a *dgt5* mutant by imprecise mobilization of a P-element inserted in the 5'-UTR of the *dgt5* gene 30bp upstream of the initiating ATG (Ou, 2013) (Figure 3.4 A). A resulting lethal deletion line $dgt5^{LE10}$ was analyzed by genomic PCR analysis, which showed a 3kb deletion encompassing most exons of the gene (Figure 3.4 B). Furthermore, western blot analysis of embryo extracts probed with rabbit polyclonal anti-*dgt5* antibody (Goshima et al. 2008) revealed reduction of the protein level (Goshima et al. 2008) (Figure 3.4 C). Therefore, $dgt5^{LE10}$ was defined as a *dgt5* null allele.

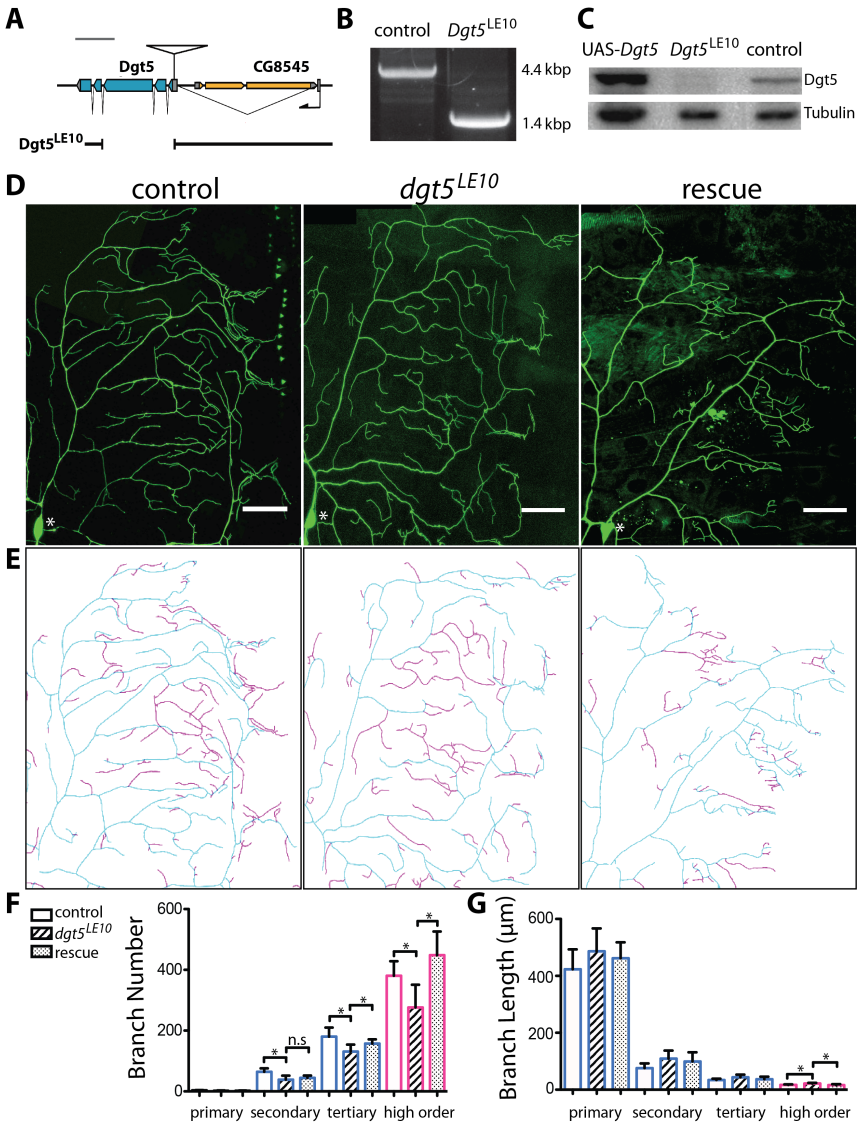

Figure 3.4 Dgt5 controls number and length of class IV da neuron dendrites

(A) Schematic view of the Dgt5 gene. Dgt5 coding sequences are indicated in blue and UTRs in gray; the inverted triangle represents the insertion site of *dgt5*^{EP2492} P-element. The interrupted black line indicates the deletion in the *dgt5*^{LE10} mutant. Scale bar is 1kb. (B) PCR of control, *dgt5*^{LE10} adult animals. (C) Western blots of control, *dgt5*^{LE10} and *UAS-dgt5* embryo extracts driven by *kruppelGal4*. (D) One quadrant of a ddaC clone obtained by MARCM of control, *dgt5*^{LE10} mutant or rescue with *UAS-dgt5*. White asterisk indicates the soma. Scale bar is 50 μm. (E) Tracing scheme of neurons in (C): MARCM control, *dgt5*^{LE10} mutant and rescue. Magenta indicates high order branches. Blue indicates other branch levels. (F) Quantification of dendritic branch number in control, *dgt5*^{LE10} and rescue MARCM clones. (G) Quantification of dendritic branch mean length in control, *dgt5*^{LE10} and rescue MARCM clones.

Stars indicate $p < 0.05$. Data is means ± SD; n = 5 neurons per genotype.

To analyze the function of *dgt5* in da neurons, single *dgt5*^{LE10} mutant ddaC neurons were obtained by MARCM (Lee and Luo, 1999). These clones displayed a significant reduction in the number of secondary, tertiary and high order branches as shown in Table 3.3 (n=5; p<0.05) and Figure 3.4 F.

Table 3.3 Number of branches in each branch level

	Primary	Secondary	Tertiary	High order
Control	3±0	75.84±11.39	180.2±29.88	380.6±47.71
dgt5^{LE10}	2.8±0.54	38.2±13.24*	131.2±22.91*	276.2±74.90*

* indicates p<0.05

The mean length of high order branches in *dgt5*^{LE10} neurons was increased comparing to the control (high order control 16.83 ± 1.96 μm; *dgt5*^{LE10} 21.49 ± 2.52 μm; n=5; p<0.05) while the mean length of branches of lower orders was not modified as shown in Table 3.4 (n=5; p>0.05) and Figure 3.5 G.

Table 3.4 Mean lengths of each branch level (μm)

	Primary	Secondary	Tertiary	High order
Control	423.23±59.71	75.84±16.53	33.88±4.57	16.83±1.96
dgt5^{LE10}	486.329±80.31	109.05±28.34	43.47±9.27	21.49±2.52*

* indicates p<0.05

3.3 Dgt6 controls number and length of class IV da neuron dendrites, similarly to Dgt5

The conserved Augmin complex component *dgt6* does not display known functional domains (Goshima et al. 2008; Lawo et al. 2009). Dgt6 interacts with γ-Tubulin in vivo and is important for kinetochore-microtubule regrowth during mitotic metaphase and anaphase (Goshima et al. 2008; Zhu et al. 2008; Bucciarelli et al. 2009; Uehara and Goshima, 2010).

To analyze the function of Dgt6, a *dgt6* mutant was generated by imprecise mobilization of the P-element in $dgt6^{\{GSV\}GS11802}$ (Ou, 2013). This line is lethal and contained a P-element insertion in the coding region of the *dgt6* gene 8bp downstream of the initiating ATG. This disrupts the expression of the protein as shown in Western Blot of third instar larvae extracts probed with a rabbit polyclonal anti-Dgt6 antibody described previously (Goshima et al. 2008) (Figure 3.5 E). The GSV6 P-element contained a UAS sequence and could potentially drive overexpression of *dgt6* in the presence of Gal4 drivers. The Dgt6 expression level was also tested in Western Blot (Figure 3.5 D). For this reason, deletion alleles were generated by imprecise remobilization of this original P-element. The $dgt6^{19A}$ allele obtained by imprecise excision still contained a fragment of 889bp from the original P-element (Figure 3.5 A). The Dgt6 protein level was clearly decreased in $dgt6^{19A}$ third instar larvae extracts probed with a rabbit polyclonal anti-Dgt6 antibody used as described previously (Bucciarelli et al. 2009) (Figure 3.5 B, C). Endogenous protein could not be detected in $dg6^{19A}$ larvae in da neurons with antibody staining (Figure 3.5 F). $Dgt6^{19A}$ flies were lethal but survived up to third instar larval stage.

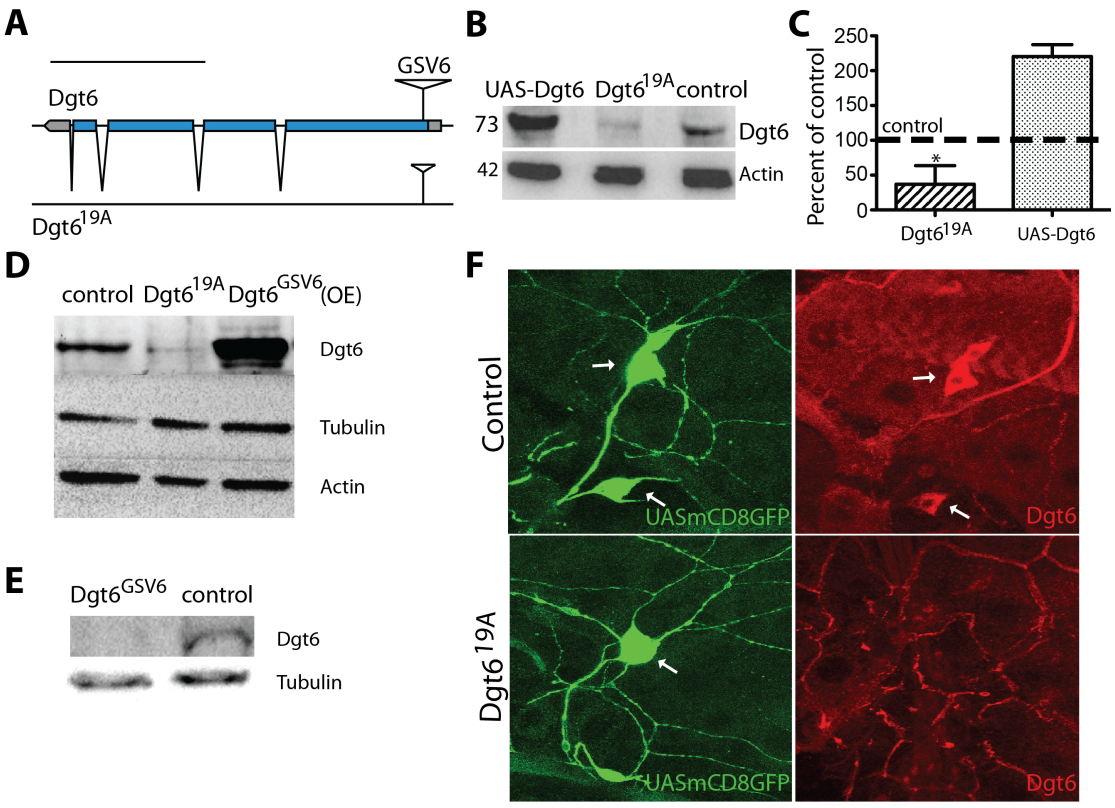

Figure 3.5 Localization of Dgt6 in *Drosophila* da neurons.

(A) Schematic view of *dgt6* gene. Dgt6 coding sequences are indicated in blue and UTRs in gray; the inverted triangle represents the insertion site of $dgt6^{GSV6}$ P-element. In $dgt6^{19A}$ after P-element remobilization, a fragment of the original GSV6 element was still present, schematized by the lower line and the smaller inverted triangle. The remaining fragment did not contain UAS sequences. Scale bar is 1kb. (B) Western blots of third instar larva extracts of control, $dgt6^{19A}$ or *UAS-Dgt6* expressed by *kruppelGal4* with polyclonal anti-Dgt6 antibody described previously (Bucciarelli et al. 2009). Blot was also probed with anti-actin antibodies as loading controls. (C) Quantification of protein level in $dgt6^{19A}$ and UAS-*dgt6* expressed by *kruppelGal4*. (D) Western blots of control, $dgt6^{19A}$ and $dgt6^{GSV6}$ third instar larvar extracts driven by *kruppelGal4* with polyclonal anti-Dgt6 antibody described previously (Bucciarelli et al. 2009). (E) Western blots of control and $dgt6^{GSV6}$ third instar larva extracts with anti-Dgt6 antibody described previously (Goshima et al. 2008). (F) Dgt6 staining in *Drosophila* da neurons. Green shows da neurons visualized with *mCD8GFP*. Red shows Dgt6 staining in da neurons.

To address the effect of loss of *dgt6* function on dendrite differentiation, I imaged class IV ddaC da neurons of *dgt6*^{19A} third instar larvae using *477Gal4 UASmCD8GFP* (Grueber et al. 2003) to highlight their morphology (Figure 3.6 A, B). I analyzed branch morphology and found a significant reduction in the number of high order branches comparing to the wild type (high order control 378.6 ± 21.44; *dgt6*^{19A} 222.8 ± 21.44; n=5; p<0.01), while the number of lower branch levels is not significantly modified as shown in Table 3.5 (n=5; p>0.05) and Figure 3.6 C.

Table 3.5 Number of branches of each branch level

	Primary	Secondary	Tertiary	High order
Control	2.2±0.45	45±4.18	150.4±35.96	378.6±21.44
Dgt6^{19A}	3±0	53±6.60	144.2±20.05	222.8±21.44**

** indicates p<0.01

This reduction in high order branch number could be rescued by expression of a UAS-*dgt6* transgene in class IV neurons using *477Gal4* (high order rescue 362 ± 35.04; n=5; compare to control p>0.1) (Grueber et al. 2003) (Figure 3.6 C). These data indicated a cell-autonomous function of *dgt6* in dendrite morphology. Similar to *dgt5*^{LE10} MARCM but different to γ*Tub23C* mutants, the total length of class IV neuron dendrites was significantly reduced in *dgt6*^{19A} due to the large number of dendrite loss (control 18614.22 ± 1019.29 μm; *dgt6*^{19A} 11454.72 ± 6641.02 μm; n=5; p<0.05) and this phenotype could be rescued with overexpression of full length Dgt6 (rescue 17771.38 ± 825.28 μm; n=5; compare to control p>0.1) (Figure 3.6 D). The mean length of each branch level remained unchanged (n=5; p>0.05) in *dgt6*^{19A} mutants except the secondary branch order (n=5; p<0.01) as shown in Table 3.6 and Figure 3.6 E.

Table 3.6 Mean length of each branch level (μm)

	Primary	Secondary	Tertiary	High order
Control	463.37±65.86	92.62±7.06	42.38±5.20	18.91±2.32
Dgt6^{19A}	392.60±59.53	69.62±11.40**	34.06±8.79	18.66±2.66

** indicates $p<0.01$

The reduction in mean length of secondary branches in *dgt6*^{19A} mutants could be further rescued (secondary rescue 87.25 ± 11.30 μm; n=5; $p>0.1$) (Figure 3.6 E). Thus, *dgt6* controls number and length of class IV neuron dendrites, which is similar to *dgt5* and overlapping with γ*Tub23C* function.

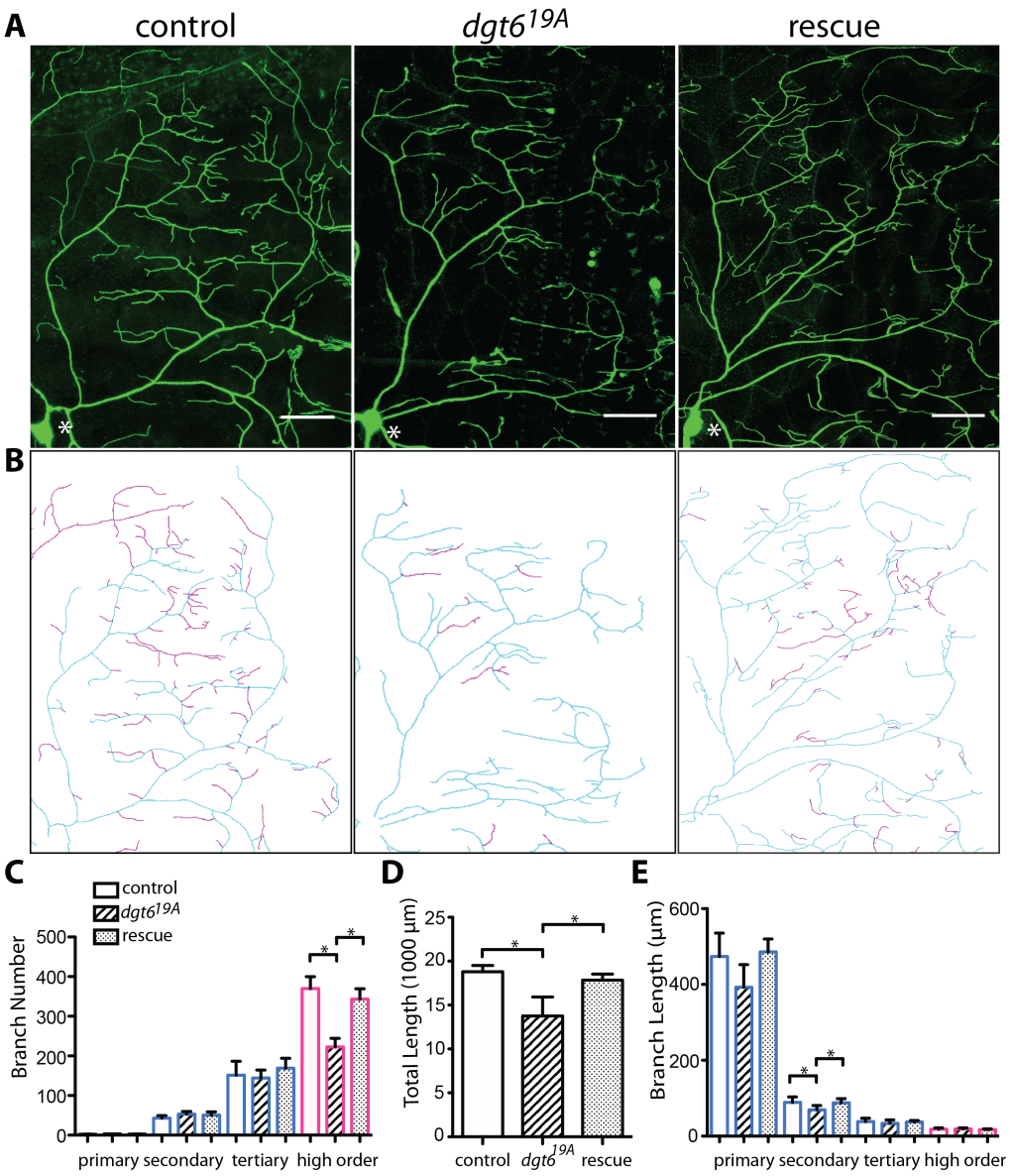

Figure 3.6 Loss of *dgt6* alters dendritic branch number.

(A) One quadrant of a class IV ddaC neuron visualized using *477Gal4 UASmCD8GFP* in third instar larvae of control, *dgt6*^{19A} or after cell-autonomous rescue of *dgt6*^{19A} with *UAS-Dgt6* under the control of *477Gal4*. White asterisk indicates the soma. Scale bar is 50 μm. (B) Tracing scheme of neurons shown in (A): control, *dgt6*^{19A} and rescue. Magenta indicates high order branches. Blue indicates other branch levels. (C) Quantification of dendritic branch number of *dgt6*^{19A} and rescue. (D) Quantification of total dendritic branch length of control, *dgt6*^{19A} and rescue. (E) Quantification of dendritic branch mean-length of control, *dgt6*^{19A} and rescue. Star indicates $p < 0.05$. Data is means ± SD; n = 5 neurons of individual animals per genotype. Magenta indicates high order branches. Blue indicates other branch levels.

I also performed time-lapse live imaging on late second instar larvae (approximately 72 h AEL) to analyze new branch formation and dynamics of high order dendrites (Figure 3.7 A). There were significantly less new branches formed in the *dgt6*^{19A} mutant (control 7.79±4.07/100 μm, *dgt6*^{19A} mutant 2.03±1.44/100 μm; n=5; $p<0.05$) (Figure 3.7 B). The percentage of branches elongating in the *dgt6*^{19A} mutant was significantly reduced (control 36.14±13.21%; *dgt6*^{19A} mutant 15.17±7.20%; n=5; $p<0.05$), whereas the number of retracting branches was unmodified (control 45.01±13.51%; *dgt6*^{19A} mutant 39.74±20.45%; n=5; $p>0.1$) (Figure 3.7 C). These data suggest that dendrite dynamics changed due to the loss of *dgt6*^{19A} function, leading to fewer new branch formation events and less stable branches in the *dgt6*^{19A} mutant animals. The phenotype of defective elongation was similar to γ*Tub23C* mutants. Moreover, there is a significant reduction in percentage of newly-formed branch loss (control 51.37±11.81%; *dgt6*^{19A} mutant 11.33±17.58%; n=5; $p<0.001$) (Figure 3.7 D). This data suggests most of the newly formed branches failed to elongate to stable branches, which indicates an additional function of Dgt6 in stabilizing newly formed dendritic branches.

To summarize, my data suggested a cell-autonomous requirement of Augmin complex in controlling proper dendrite morphology in both number and length of dendrites in *Drosophila* class IV da neurons.

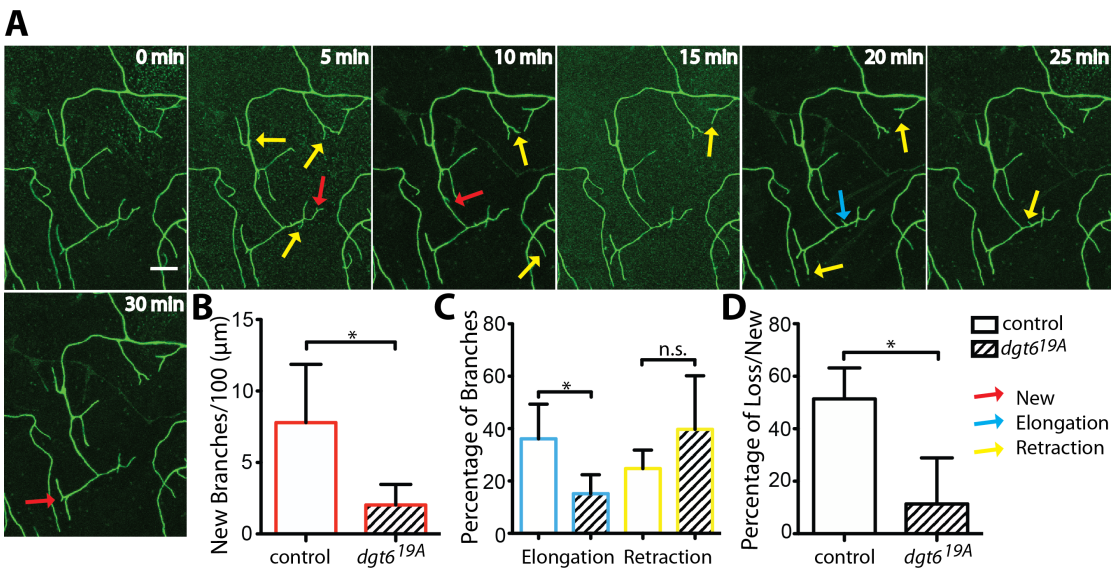

Figure 3.7 Time-lapse analysis of high order branches of ddaC neuron dendrites in *Dgt6^{19A}* mutant.

(A) Time-lapse imaging of high order branches of ddaC neurons in *dgt6^{19A}* second instar larvae (total time: 30 min, interval between single images: 5 min). Red, blue and yellow arrows indicate new, elongating and retracting branches, respectively. Scale bar is 10 µm. (B) Quantification of new branches per 100µm appearing during 30 minutes time-lapse imaging in control and *dgt6^{19A}* neurons in second instar larvae. (C) Quantification of branch dynamics during 30 minutes time-lapse imaging in control and *dgt6^{19A}* neurons. (D) Quantification of percentage of branch loss in newly formed branches during 30 minutes time-lapse imaging in control and *dgt6^{19A}* neurons.
Stars indicate $p < 0.05$. Data is means ± SD; n = 5 neurons of individual animals per genotype.

3.4 Dgt5 and Dgt6 cooperate to control appropriate dendrite morphology

Dgt5 and *dgt6* are part of the co-regulated Augmin complex (Goshima et al. 2008). The similarity of their phenotypes in class IV neuron dendrites suggests they might function together during neuronal dendrite differentiation.

I thus analyzed the phenotype of $dgt5^{LE10}$/+; $dgt6^{19A}$/ + trans-heterozygous animals in the background of *ppkGal4 UASmCD8GFP*. Animals of $dgt5^{LE10}$/+ or $dgt6^{19A}$/+ had similar dendrite number of different branch levels in class IV neurons compared to the control (n=5; p>0.1) (data shown in Table 3.7). In contrast, $dgt5^{LE10}$/+; $dgt6^{19A}$/+ trans-heterozygous third instar larvae showed a strong reduction in high order dendrite number and therefore simplified dendritic trees (high order $dgt5^{LE10}/dgt6^{19A}$ 297.8 ± 59.36; n=5; p<0.01; one-way ANOVA P<0.005) (Figure 3.8 A, C). The branch number of other branch levels remained unchanged (n=5; p>0.1) (data shown in Table 3.7) (Figure 3.8 A, C).

Table 3.7 Number of branches of each branch level

	Primary	Secondary	Tertiary	High order
Control	2.2±0.44	47.4±12.54	164.2±23.86	440.8±37.00
$dgt5^{LE10}$/+	2.6±0.89	49.2±10.64	167.2±41.00	382±32.95
$dgt6^{19A}$/+	3±0.71	66±18.44	193±43.83	376±24.78
$dgt5^{LE10}/dgt6^{19A}$	3.2±.84	64.8±16.33	187.8±31.91	297.8±59.36**

** indicates p<0.01 comparing to control, $dgt5^{LE10}$/+ and $gt6^{19A}$/+, respectively.

The total length of dendrites in trans-heterozygotes was also significantly reduced (*dgt5*^{LE10}/+ 18805.75 ± 390.31 μm; *dgt6*^{19A}/+ 19559.68 ± 990.18 μm; *dgt5*^{LE10}/*dgt6*^{19A} 16356.068 ± 1528.59 μm; n=5; p<0.01; one-way ANOVA P<0.005) (Figure 3.9 D). The average length of each branch level was not significantly modified as shown in Table 3.8 (n=5; p>0.05).

Table 3.8 Mean lengths of each branch level (μm)

	Primary	Secondary	Tertiary	High order
Control	433.37±25.86	90.33±5.26	32.36±7.13	17.49±0.32
dgt5^{LE10}/+	421.8±70.9	85.78±11.17	35.9±10.22	19.00±2.8
dgt6^{19A}/+	442.52±17.23	79.05±10.77	35.41±3.81	17.48±1.39
dgt5^{LE10}/*dgt6*^{19A}	438.32±0.71	71.32±16.12	30.43±3.56	16.06±2.2

These data suggest the defect in dendrite morphology in trans-heterozygous mutant is not due to the addition effect but a cooperation of Dgt5 and Dgt6. This cooperation is required for proper dendrite number and length in class IV da neurons.

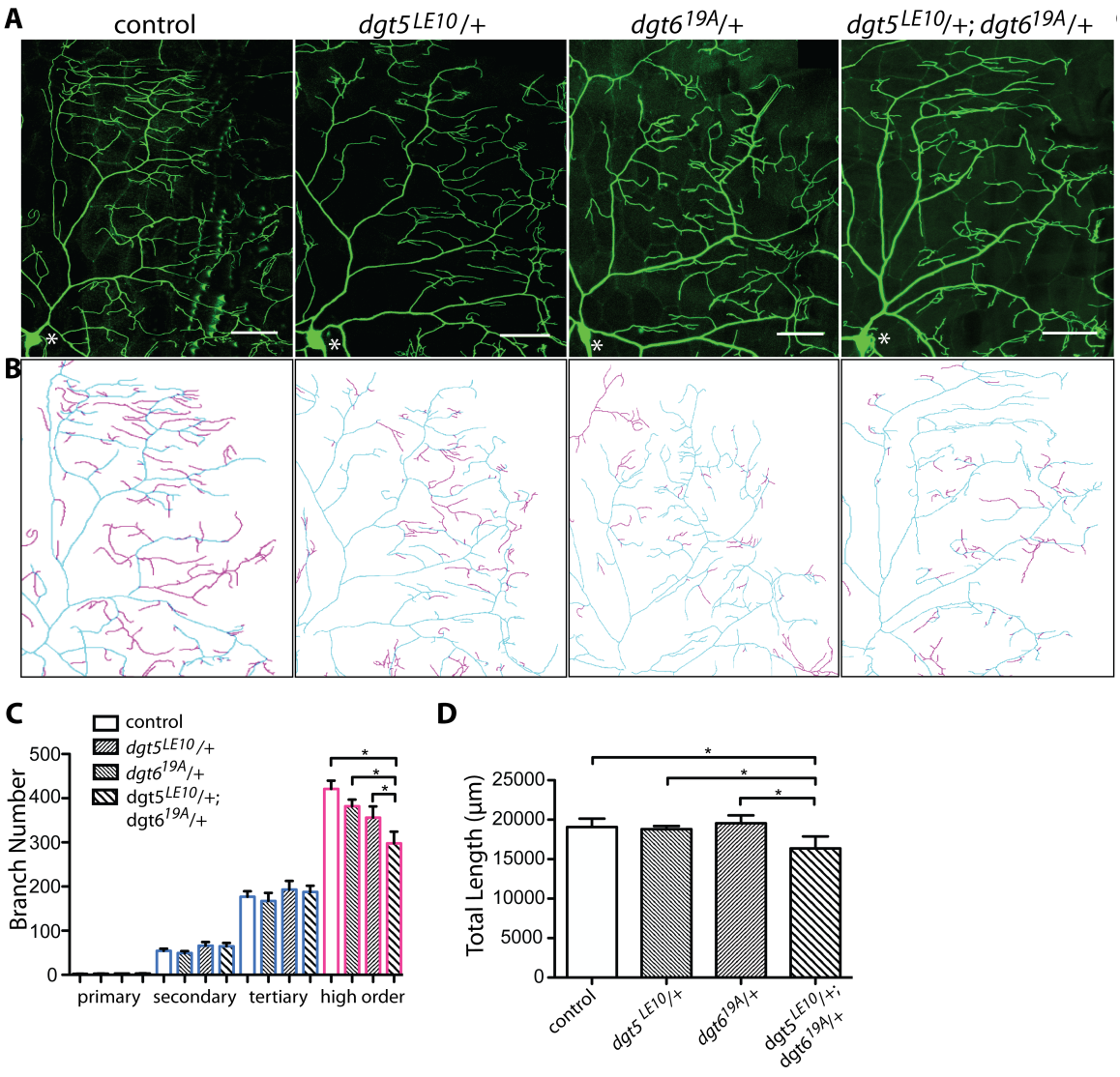

Figure 3.8 Normal *dgt5* and *dgt6* gene dosage is required for dendritic morphology.

(A) One quadrant of a class IV ddaC neuron of third instar of control, *dgt5*^{LE10}/+, *dgt6*^{19A}/+ and *dgt5*^{LE10}/+; *dgt6*^{19A}/+ trans-heterozygous mutant larvae. White asterisk indicates the soma. Scale bar is 50 μm. (B) (C) Quantification of branch number of control, *dgt5*^{LE10} heterozygous, *dgt6*^{19A} heterozygous, and *dgt5*^{LE10}/+; *dgt6*^{19A}/+ trans-heterozygous alleles. Star indicates $p < 0.05$. Data is means ± SD; n = 5 neurons per genotype. (D) Quantification of total dendritic length in control, *dgt5*^{LE10} heterozygous, *dgt6*^{19A} heterozygous and *dgt5*^{LE10}/+; *dgt6*^{19A}/+ trans-heterozygous animals.

Star indicates $p < 0.05$. Data is means ± SD; n = 5 neurons of individual animals per genotype.

To distinguish whether the reduction of branch number is due to a defect in new branch formation or branch maintenance and to better understand the dynamics of branching in *dgt5*^{LE10}/*dgt6*^{19A} trans-heterozygous mutants, I performed time-lapse imaging in late second instar larvae (approximately 72 h AEL) (Figure 3.9 A). The number of newly formed branches appearing within 100μm basal dendrite was comparable to control (control 7.79 ± 4.07/100 μm; *dgt5*^{LE10}/*dgt6*^{19A} 9.48 ± 4.16/100 μm; n=5; p>0.5) (Figure 3.9 B). Similar to the γ*tub23C* mutant, *dgt5*^{LE10}/*dgt6*^{19A} neurons showed an increase in the number of retracting branches (control 24.72 ± 7.09%; *dgt5*^{LE10}/*dgt6*^{19A} 45.01 ± 13.51%; n=5; p<0.05) while the number of elongated remained unmodified (Elongation events control 36.14 ± 13.21%, *dgt5*^{LE10}/+; *dgt6*^{19A}/ + 27.12 ± 6.71%; n=5; p>0.1) (Figure 3.9 C). The percentage of the loss of the new-formed branches was not modified (control 51.37 ± 11.81%; *dgt5*^{LE10}/*dgt6*^{19A} 34.67 ± 12.16%; n=5; p>0.05) (Figure 3.9 D).

These data suggest a defect in the maintenance of class IV da neuron dendritic branches, comparable to what is observed in γ*Tub23C* mutants. Reduction of the Augmin complex did not modify the stability of newly formed dendrites.

In S2 cells, Augmin is a co-regulated complex and reduction of one Dgt reduces the level of other Dgts (Goshima et al. 2008). Consistent with previous data, I found the level of *dgt6* was strongly reduced in *dgt5*^{LE10} allele embryo extracts (Figure 3.9 E). This data suggests Dgt5 and Dgt6 function as subunits within the complex. When comparing the phenotypes of *dgt6*^{19A} and *dgt5*^{LE10}/*dgt6*^{19A} animals, the reduction seen in *dgt6*^{19A} animals was stronger (high order branch number *dgt6*^{19A} 222.8 ± 21.44; *dgt5*^{LE10}/*dgt6*^{19A} 297.8 ± 59.36; n=5; p<0.05), suggesting the phenotype is a result of a more severe reduction of Augmin complex. Moreover, the *dgt5*^{LE10}/*dgt6*^{19A} phenotype is similar comparing to the phenotype of γ*Tub23C* mutants (high order branch number *dgt5*^{LE10}/*dgt6*^{19A} 297.8 ± 59.36; γ*Tub23C* mutant 275.4 ± 34.77; n=5; p>0.1), suggesting a similar level of reduction of microtubules in both mutant animals.

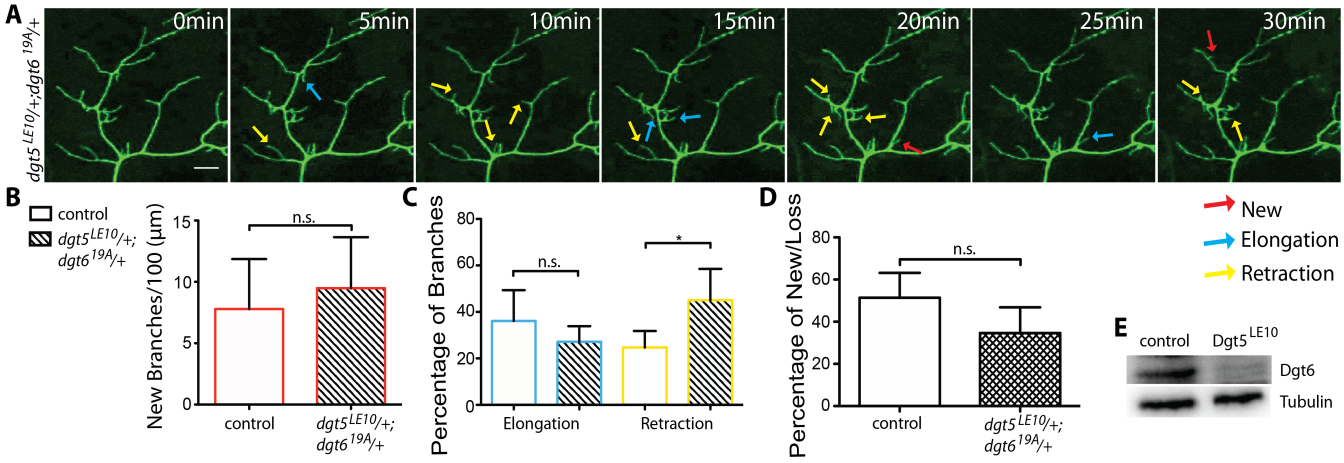

Figure 3.9 Time-lapse analysis of high order dendritic branches in *dgt5^{LE10}/dgt6^{19A}* trans-heterozygous mutant.

(A) Time-lapse imaging of high order branches of ddaC in *dgt 5^{LE10}*/+; *dgt6^{19A}*/+trans-heterozygous second instar larvae (total time: 30 min, interval between single images: 5 min). Red, blue and yellow arrows indicate new, elongating and retracting branches, respectively. Scale bar is 10 μm. (B) Quantification of new branches per 100μm appearing during 30 minutes time-lapse imaging in ddaC neurons of *dgt5^{LE10}*/+; *dgt6^{19A}*/+ trans-heterozygous mutant second instar larvae. Star indicates $p < 0.05$. Data is means ± SD; n = 5 neurons of individual animals per genotype. (C) Quantification of branch dynamics of ddaC dendrites of *dgt5^{LE10}*/+; *dgt6^{19A}*/+ trans-heterozygous mutant second instar larvae. Star indicates $p < 0.05$. Data is means ± SD; n = 5 neurons of individual animals per genotype. (D) Quantification of percentage of branch loss in newly formed branches during 30 minutes time-lapse imaging in control and *dgt5^{LE10}*/+; *dgt6^{19A}*/+ trans-heterozygous mutant neurons. Stars indicate $p < 0.05$. Data is means ± SD; n = 5 neurons of individual animals per genotype. (E) Western blot of control or *dgt5^{LE10}* embryo extracts, probed with polyclonal anti-Dgt6 antibody (Bucciarelli et al. 2009).

3.5 Dgt5 and Dgt6 cooperate to control appropriate microtubule organization in dendrites

Given the role of the Augmin complex in promoting microtubule nucleation in dividing cells, the question arose whether the organization of the microtubule cytoskeleton is altered upon impairment of Augmin complex function in class IV da neurons. I thus investigated the localization of GFP-tagged α-*tubulin* (Hummel et al. 2000; Nagel et al. 2011).

Consistent with previous reports, endogenous α-*tubulin* was detected in proximal branches but not in distal dendrites (Nagel et al. 2011) (Figure 3.10 A). Nonetheless, in *dgt5*^{LE10}/+; *dgt6*^{19A}/ + trans-heterozygotes, α-Tubulin-GFP could be detected even in terminal branches and the signal was stronger comparing to the control (Figure 3.10). These data suggest a potential increase in the number of Tubulin monomers or an alteration in the organization of the microtubule cytoskeleton.

Figure 3.10 Localization of α-Tubulin in *dgt5*^{LE10}/*dgt6*^{19A} trans-heterozygous mutant.

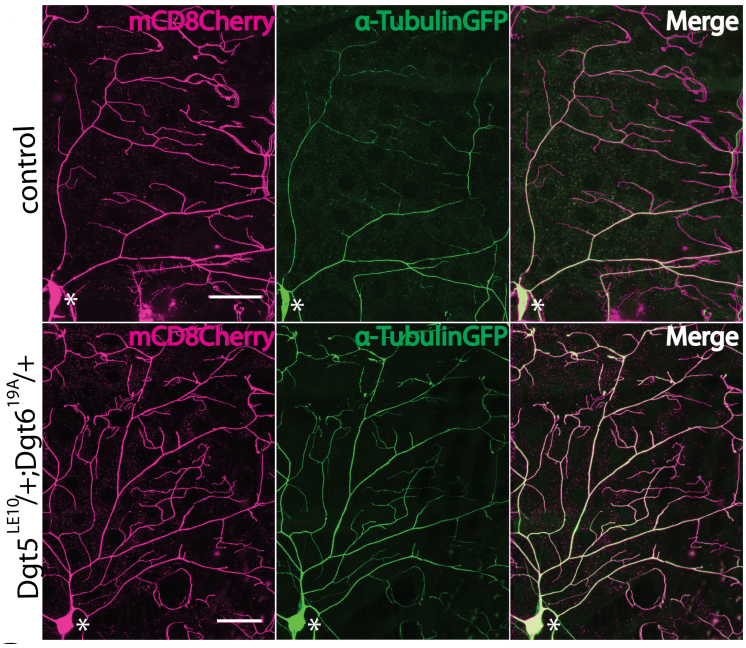

One quadrant of a class IV ddaC neuron of third instar of control and *dgt5*^{LE10}/*dgt6*^{19A} trans-heterozygous mutant larvae was shown here. Red shows dendrites of class IV da neurons labeled with *mCD8Cherry*. Green shows α-*Tubulin-GFP*. Scale bar is 50 μm. n = 10 neurons of individual animals per genotype.

I thus addressed whether the orientation of microtubules might be modified in the *dgt5*^{LE10}*/dgt6*^{19A} genotype. To address this question, I investigated the orientation of growing microtubules by imaging GFP-tagged Nod localization in *Drosophila* class IV da neurons as described before (Andersen et al., 2005). The Nod-GFP reporter construct accumulates at the minus-end of microtubules both *in vitro* and *in vivo*, and is therefore used as a microtubule polarity marker (Cui et al. 2005; Rolls et al. 2007). I found Nod-GFP localized in the cell body, along the proximal segments of primary branches, accumulated at dendrite branching points and within the terminal branchlets of class IV neurons, which is consistent with previous research (Rolls et al. 2007). In particular, the signal of Nod-GFP was weaker at branching points and in the terminal branches comparing to control (n=5) (Figure 3.11). Due to the lack of an indicator marker of the dendrites, I could not perform statistic analysis to this phenotype.

In *dgt5*^{LE10}*/dgt6*^{19A} trans-heterozygous mutants, the amount of Nod was reduced, potentially suggesting the presence of less microtubules. In particular, though, Nod-GFP was less enriched at branching points and in the terminal branches and was rather more distributed along the dendrite branch length (Figure 3.11). This supported the view that microtubule organization is modified in these mutants. Nonetheless, the reduction of the Nod-GFP signal could due to a reduction of microtubule number.

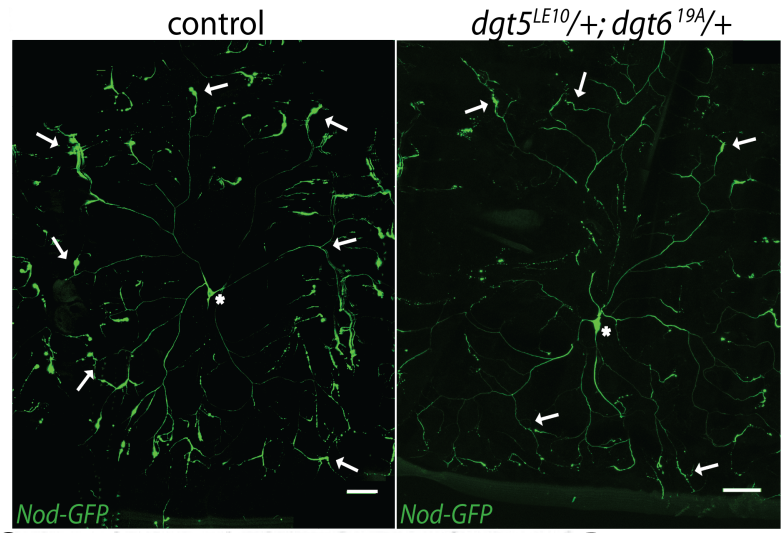

Figure 3.11 Localization of Nod-GFP in *dgt5^{LE10}/dgt6^{19A}* trans-heterozygous mutant.

Class IV ddaC neuron of third instar of control and *dgt5^{LE10}/dgt6^{19A}* trans-heterozygous mutant larvae was shown here. Green shows Nod-GFP expression pattern. White arrow indicates Nod-GFP localization. Scale bar is 50 μm. n = 5 neurons of individual animals per genotype.

I also checked the polarity of microtubules in the heterozygous mutant by observing the GFP-tagged EB1 movements in class IV da neurons between two branching points using spinning disc microscopy (Zheng et al. 2008; Stone et al. 2008; Hill et al. 2012), and less EB1 movements were found in *dgt5^{LE10}/dgt6^{19A}* trans-heterozygous mutant animals within 100 μm basal dendrite (control 37.62±13.86/100 μm; *dgt5^{LE10}/dgt6^{19A}* 11.47±7.69/100 μm; n=10; $p<0.01$) (Figure 3.12 B). These data suggest that the amount of growing microtubule was reduced due to the reduction of the Augmin complex. However, whether the orientation was changed remained unclear.

In summary, my data indicate that the Augmin complex controls morphology and dynamics of high order branches in *Drosophila* class IV da neurons, potentially through the regulation of microtubule regulation.

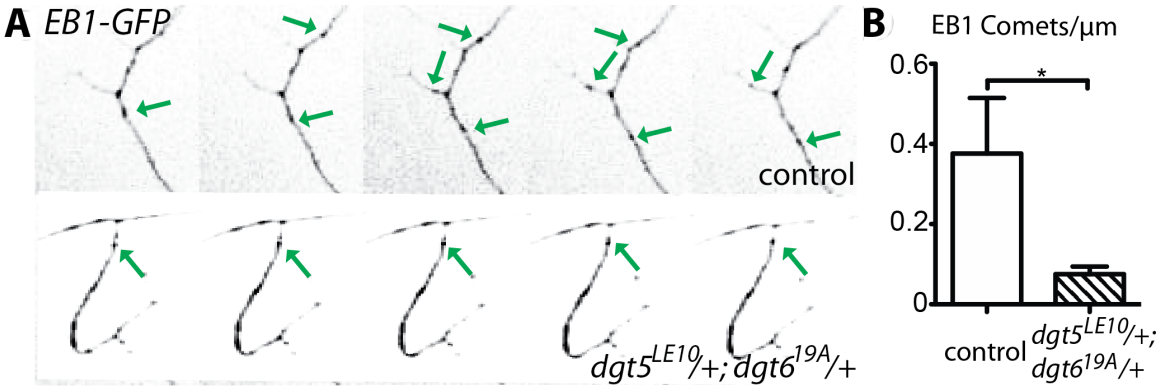

Figure 3.12 EB1 movements in *dgt5*^{LE10}/*dgt6*^{19A} trans-heterozygous mutant.

(A) EB1 Movements in *Drosophila* ddaC da neurons distal dendrites of third instar of control and *dgt5*^{LE10}/*dgt6*^{19A} trans-heterozygous mutant. Green arrow indicates EB1 moving dots. (B) Quantification of number of EB1 moving dots in control and *dgt5*^{LE10}/*dgt6*^{19A} trans-heterozygous mutant. Data is means ± SD; n = 10 neurons of individual animals per genotype.

3.6 The Augmin complex genetically interacts with γTub23C

Previous data have suggested possible interactions between Dgts and γ-Tubulin (Goshima et al. 2008; Bucciarelli et al. 2009). To address whether the Augmin complex and γ*tub23C* function together to control dendrite differentiation, I performed genetic interaction experiments between *dgt5*, *dgt6* and γ*tub23C*.

Class IV ddaC da neurons of γ$Tub23C^{A15\text{-}2}$/+, $dgt5^{LE10}$/+ or $dgt6^{19A}$/+ animals showed normal dendrite morphology (total number control 654.8 ± 12.34; γ$Tub23C^{A15\text{-}2}$/+ 641.8 ± 73.34; $dgt5^{LE10}$/+ 630 ± 32.66; $dgt6^{19A}$/+ 618 ± 52.45; n=5; p>0.5) (Figure 3.11 A, C). Trans-heterozygous γ$Tub23C^{A15\text{-}2}$/$dgt5^{LE10}$ or γ$Tub23C^{A15\text{-}2}$/+; $dgt6^{19A}$/ + displayed dramatically simplified dendritic trees (Figure 3.11 A, B). I found a significant reduction in number of high order branches (high order γ$Tub23C^{A15\text{-}2}$/+ 436.2 ± 93.63; $dgt5^{LE10}$/+ 382 ± 32.95; $dgt6^{19A}$/+ 376 ± 24.78; γ$Tub23C^{A15\text{-}2}$/$dgt5^{LE10}$ 183.4±29.73; γ$Tub23C^{A15\text{-}2}$/+; $dgt6^{19A}$/ + 193.6±21.27; n=5; p<0.001) while all other branch levels were comparable to wild type (n=5; p>0.05) as shown in Table 3.9 and Figure 3.13 D.

Table 3.9 Number of branches of each branch level

	Primary	Secondary	Tertiary	High order
Control	2.2±0.44	47.4±12.54	164.2±23.86	440.8±37.00
γTub^{-}/+	2.8±0.45	52.6±19.50	178.2±19.97	436.2±93.36
γTub^{-}/$dgt5^{-}$	3.8±0.84	60.2±10.33	144.6±12.58	183.4±29.73**
γTub^{-}/$dgt6^{-}$	3±0	50.4±5.59	138.6±18.81	193.6±21.27**

** indicates p<0.01 comparing to control and γTub^{-}/+, respectively.

The total dendrite length was nonetheless strongly reduced, due to the loss of high order branches (γ*Tub23C*$^{A15-2}$/+ 19665.239 ± 1031.81 μm; *dgt5*^{LE10}/+ 18805.75 ± 390.31 μm; *dgt6*^{19A}/+ 19559.68 ± 990.18 μm; γ*Tub23C*$^{A15-2}$/*dgt5*^{LE10} 13614.613 ± 2020.60 μm; γ*Tub23C*$^{A15-2}$/+; *dgt6*^{19A}/ + 13275.71 ± 1760.70 μm; n=5; p<0.01) (Figure 3.13 E). The mean length of each branch order was not modified as shown in Table 3.10 (n=5; p>0.05) and Figure 3.13 F. Thus, the reduction in total length is due to a dramatic reduction in the number of branches.

Table 3.10 Mean lengths of each branch level (μm)

	Primary	Secondary	Tertiary	High order
Control	433.37±25.86	90.33±5.26	32.36±7.13	17.49±0.32
γ*Tub*$^{-}$/+	403.42±44.88	92.83±33.03	37.14±6.05	18.91±1.62
γ*Tub*$^{-}$/*dgt5*$^{-}$	385.95±60.75	70.51±11.92	32.44±4.36	17.88±2.45
γ*Tub*$^{-}$/*dgt6*$^{-}$	386.05±46.42	74.59±3.51	33.74±2.30	18.96±1.78

These data indicate that both *dgt5* and *dgt6* can genetically interact with γ-*tub23C* to control distal dendrite number, suggesting Dgt5 and Dgt6 function together with γTub23C to control dendrite morphology in *Drosophila* class IV da neurons.

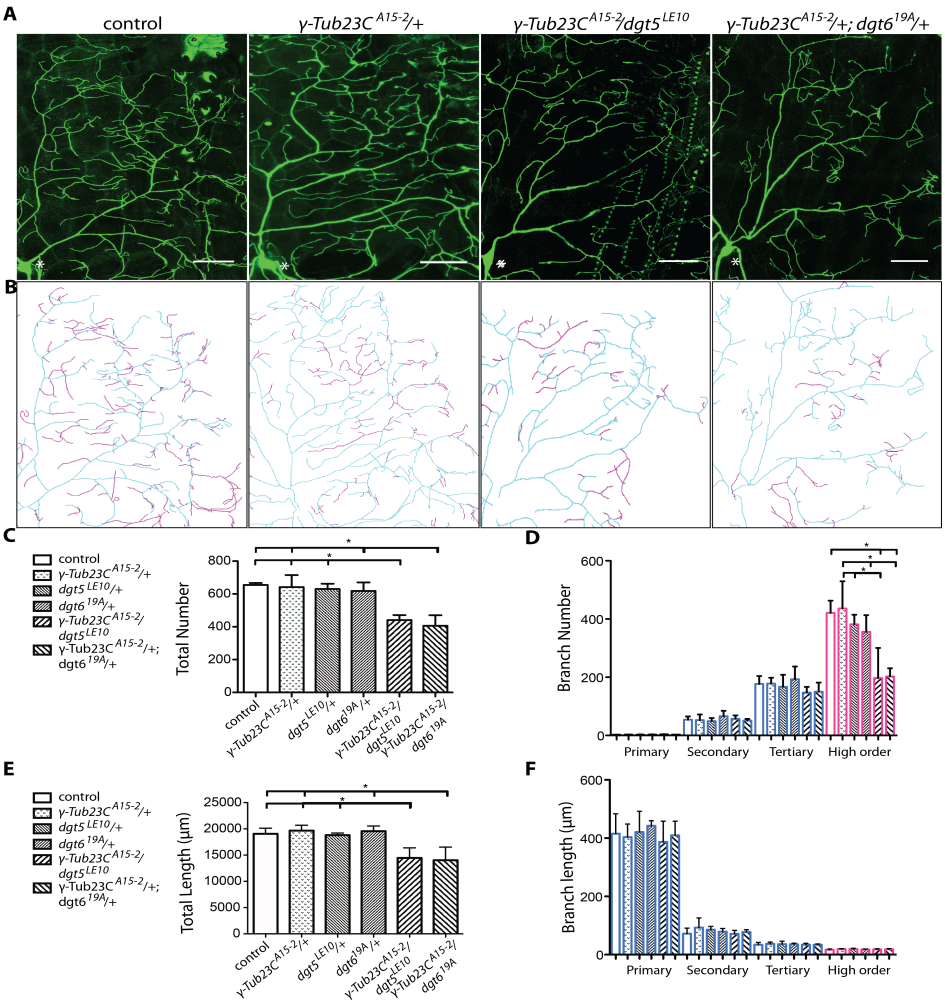

Figure 3.13 γ*Tub23C*, *dgt5* and *dgt6* display genetic interactions.

(A) One quadrant of a class IV ddaC neuron in third instar larva of control, γ*Tub23C*$^{A15\text{-}2}$ heterozygous, *dgt5*^{LE10} heterozygous, *dgt6*^{19A} heterozygous, or trans-heterozygous mutants of γ*Tub23C*$^{A15\text{-}2}$/ *dgt5*^{LE10} or γ*Tub23C*$^{A15\text{-}2}$/ *dgt6*^{19A}. White asterisk indicates the soma. Scale bar is 50 μm. (B) Tracing scheme of the neurons shown in (A). Magenta indicates high order branches. Blue indicates other branch levels. (C) Quantification of total branch number in control, heterozygous and trans-heterozygous mutants of γ*Tub23C*$^{A15\text{-}2}$ and *dgt5*^{LE10} or *dgt6*^{19A}. (D) Quantification of branch number in control, heterozygous and trans-heterozygous mutants of γ*Tub23C*$^{A15\text{-}2}$ and *dgt5*^{LE10} or *dgt6*^{19A}. Magenta indicates high order branches. Blue indicates other branch levels. (E) Quantification of total branch length in control, heterozygous and trans-heterozygous mutants of ©*Tub23C*$^{A15\text{-}2}$ and *dgt5*^{LE10} or *dgt6*^{19A}. (F) Quantification of branch mean-length in control, heterozygous and trans-heterozygous mutants of γ*Tub23C*$^{A15\text{-}2}$ and *dgt5*^{LE10} or *dgt6*^{19A}. Magenta indicates high order branches. Blue indicates other branch levels. Star indicates $p < 0.05$. Data is means ± SD; n = 5 neurons of individual animals per genotype.

3.7 *Dgp71WD/Nedd1* controls maintenance of class IV da neuron dendrites, similarly to γ-Tub23C

Previous research suggests that γ-Tubulin and the γ-TuRC are important for microtubule nucleation and the Augmin complex is involved in mediating the recruitment of the γ-TuRC (Schnorrer et al. 2002; Goshima et al., 2008; Fisher et al., 2009; Buster et al., 2009; Pellacani et al., 2009). Identified as a component of the γ-*tubulin* complex γ-TuRC, Dgp71WD*,* known also as NEDD1*,* is a conserved centrosomal protein (Gunawardane et al. 2003) and essential for targeting the γ-TuRC to the centrosome (Lüders et al. 2006; Haren et al. 2006). In S2 cells Dgp71WD targets the γ-TuRC to the spindle through the Augmin complex thus promoting microtubule nucleation within the spindle (Lüders et al. 2006; Uehara et al. 2009; Zhu et al. 2008; Johmura et al. 2011).

I therefore investigated the organization of class IV da neuron dendrites in larvae carrying the *Dgp71WD*^{120} null mutation (Reschen et al. 2012). Dendrites of class IV ddaC neurons *Dgp71WD*^{120} homozygous third instar larvae were simplified (total number control 654.8 ± 12.34; *Dgp71WD*^{120} 436.4 ± 64.65; n=5; $p<0.01$) (Figure 3.14 A, B). Similarly to what I observed in γ*Tub23C*, *dgt5* or *dgt6* mutant, the number of high order branches was clearly reduced (high order control 421.2±41.97; *Dgp71WD*^{120} 236±49.52; n=5; $p<0.001$), while the number of other branch orders were unchanged (n=5; $p>0.05$) as shown in Table 3.11 and Figure 3.14 D.

Table 3.11 Number of branches of each branch level

	Primary	Secondary	Tertiary	High order
Control	2.2±0.45	47.4±12.54	164.2±23.86	421.2±41.97
Dgp71WD^{120}	3±0.71	49.4±12.20	148±14.92	236±49.52***

*** indicates p<0.001

The length of the entire dendritic tree of the homozygote was also significantly reduced (control 16602.85 ± 2349.96 μm; *Dgp71WD*^{120} 13223.57 ± 1862.43 μm; n=5; p<0.01), while the mean length of each branch level remained unmodified (n=5; p>0.1) as shown in Table 3.12 and Figure 3.14 C, F.

Table 3.12 Mean lengths of each branch level (μm)

	Primary	Secondary	Tertiary	High order
Control	408.46±66.52	81.98±28.27	37.78±10.04	16.56±2.42
Dgp71WD^{120}	371.71±50.23	73.51±20.52	30.20±2.57	18.03±3.15

These data suggest Dgp71WD has a similar function as γTub23C, Dgt5 or Dgt6 in controlling the dendrite number of class IV da neurons.

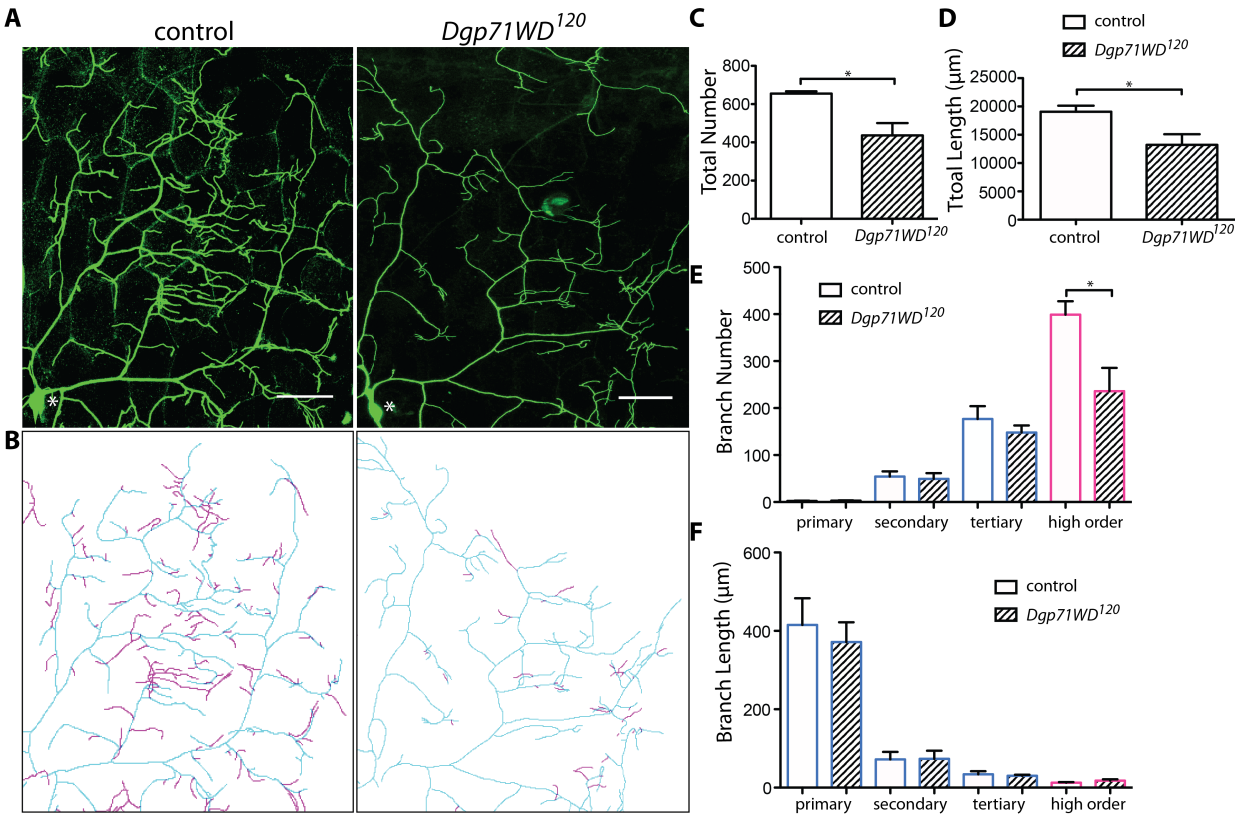

Figure 3.14 *Dgp71WD* controls dendritic morphology of *Drosophila* ddaC da neurons.

(A) One quadrant of a class IV ddaC neuron of third instar of control and *Dgp71WD*^{120} animals with expression of *UASmCD8GFP* under the control of *ppkGal4*. White asterisk indicates the soma. Scale bar is 50μm. (B) Tracing scheme of the neurons shown in (A): control and *Dgp71WD*^{120} homozygote. Magenta indicates high order branches. Blue indicates other branch levels. (C) Quantification of total branch number of control and *Dgp71WD*^{120} mutant. (D) Quantification of total branch length of control and *Dgp71WD*^{120} mutant. (E) Quantification of branch number of control and *Dgp71WD*^{120} homozygote. (F) Quantification of branch length of control and *Dgp71WD*^{120} homozygote.

Star indicates $p < 0.05$. Data is means ± SD; n = 5 neurons of individual animals per genotype.

To analyze the dynamics of dendrite differentiation in *Dgp71WD*^{120} mutants, I performed time-lapse images in late second instar larvae (approximately 72 h AEF) (Figure 3.15 A), counted the number of branches that were newly formed, elongated, retracted and number that disappeared in newly formed branches. These were normalized to the basal dendrite length and to the initial number of branches.

Comparing to the wild type, I found significant reduction in the number of elongating branches (control 36.14 ± 13.21%; *Dgp71WD*^{120} 13.32 ± 8.64%; n=5; $p<0.05$). The number of retracted branches was increased (control 24.72 ± 7.09%; *Dgp71WD*^{120} 39.01 ± 10.77%; n=5; $p<0.05$), while the number of newly formed branches was comparable to the wild type (control 7.79 ± 4.07/100 μm, *Dgp71WD*^{120} 2.67 ± 3.36/100 μm; n=5; $p>0.05$) (Figure 3.15 B, C). The percentage of lost newly formed branches was significantly reduced (control 51.37 ± 11.81%; *Dgp71WD*^{120} 11.33 ± 17.58%; n=5; $p<0.01$) (Figure 3.15 D). These data suggest that the dendritic defect in the *Dgp71WD*^{120} mutant was due to defective maintenance, which is similar to what was observed in *γTub23C* and *dgt5*^{LE10}*/dgt6*^{19A} mutants. Dgp71WD^{120} and *γTub23C*$^{A15-2}$*/γTub23C*^{PI} mutants are characterized as null mutants, and *dgt5*^{LE10}*/dgt6*^{19A} mutant is trans-heterozygous mutant. They all showed a same defect in existing dendrite maintenance. For *dgt5*^{LE10}*/dgt6*^{19A} mutant, this phenotype may more due to the disorganization of microtubules. Moreover, *Dgp71WD*^{120} mutants failed maintaining the newly formed branches, which is likewise to *dgt6*^{19A} mutants.

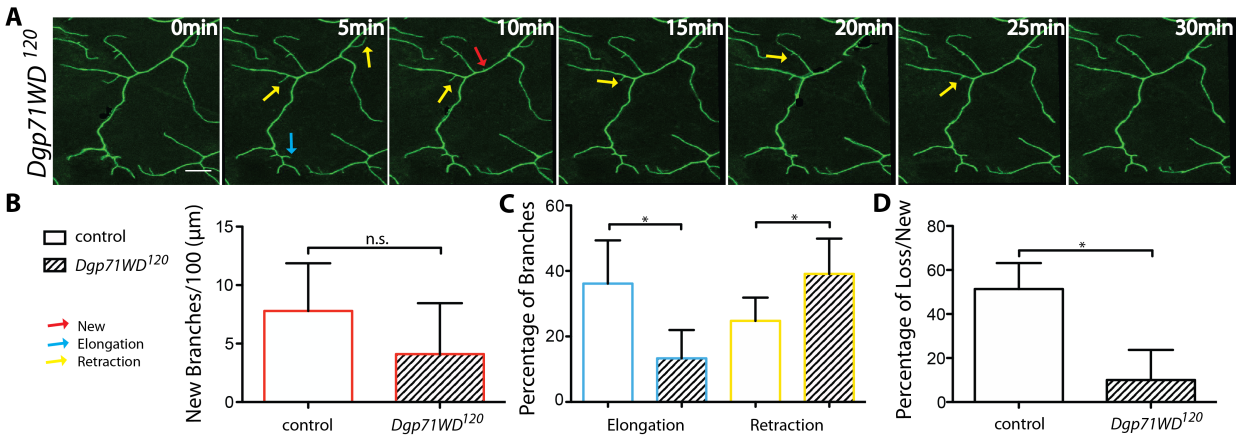

Figure 3.15 Dynamics of high order dendritic branches in *Dgp71WD*^{120} mutant.

(A) Time-lapse imaging of ddaC neuron terminal dendrite branches of control and *Dgp71WD*^{120} second instar larvae carrying *ppkGal4* UASmCD8GFP (total time: 30 min, interval between single images: 5 min). Red, blue and yellow arrows indicate new, elongating and retracting branches respectively. Scale bar is 10 µm. (B) Quantification of new branches per 100µm appearing during 30 minutes time-lapse imaging in ddaC neurons of control or *Dgp71WD*^{120} homozygous second instar larvae. (C) Quantification of branch dynamics of ddaC dendrites of control or *Dgp71WD*^{120} homozygous second instar larvae. (D) Quantification of percentage of branch loss in newly formed branches during 30 minutes time-lapse imaging in control and *Dgp71WD*^{120} mutant neurons.

Stars indicate $p < 0.05$. Data is means ± SD; n = 5 neurons of individual animals per genotype.

3.8 *Dgp71WD/Nedd1* genetically interacts with Dgt6 and Dgt5 in controlling the dendrite number and length respectively

To test whether *Dgp71WD* interacts with the Augmin complex within *Drosophila* class IV da neuron dendrites, I performed genetic interaction analysis between Dgt5, Dgt6 and Dgp71WD (Figure 3.15 A, B). $Dgp71WD^{120}$ heterozygous larvae did not show defects in dendrite morphology (total number control 654.8 ± 12.34; $Dgp71WD^{120}$/+ 636 ± 66.14; n=5; p>0.5) (Figure 3.16 C). In contrast, in $Dgp71WD^{120}$ /$dgt6^{19A}$ trans-heterozygotes the number of dendrites was reduced (total number $Dgp71WD^{120}$/$dgt6^{19A}$ trans-heterozygote 450.8 ± 63.83; n=5; p<0.01) (Figure 3.16 A, C). In particular, the number of high order branches was significantly reduced in trans-heterozygous $Dgp71WD^{120}$/$dgt6^{19A}$ (high order 228.6 ± 69.27; n=5; p<0.01) (Figure 3.16 D). The total number and the number of high order branches of trans-heterozygotes $Dgp71WD^{120}$ /$dgt5^{LE10}$ were comparable to the control (total number 614.2 ± 76.95; n=5; p>0.5; high order number 341.2 ± 51.25; n=5; p>0.05) (Figure 3.16 C, D). Nonetheless, the high order branches of $Dgp71WD^{120}$/$dgt5^{LE10}$ trans-heterozygous were shorter ($Dgp71WD^{120}$/+ 17.52 ± 2.08 μm; $dgt5^{LE10}$/+ 18.10 ± 2.80 μm; $Dgp71WD^{120}$/$dgt5^{LE10}$ trans-heterozygote 12.14 ± 1.94 μm; n=5; p<0.01) (Figure 3.16 F). The total length of the dendritic tree was also dramatically reduced in the trans-heterozygotes of $Dgp71WD^{120}$/$dgt5^{LE10}$ and $Dgp71WD^{120}$/$dgt6^{19A}$ as shown in Table 3.13 (n=5; p<0.01) and Figure 3.16 E.

Table 3.13 Total lengths of each genotype (μm)

	Total length
Control	18808.45±711.32
Dgp71WD^{120}/+	18421.64±2439.78
Dgp71WD^{120}/*dgt5*$^{-}$	14811.49±2360.65**
Dgp71WD^{120}/*dgt6*$^{-}$	14281.65±1160.55**

** indicates p<0.01 comparing to control and *Dgp71WD*^{120}/+, respectively.

The mean length of each branch level of *Dgp71WD*^{120}/*dgt6*^{19A} trans-heterozygote was comparable to the control (n=5; p>0.05). However, the mean length of high order branches of *Dgp71WD*^{120}/*dgt5*^{LE10} trans-heterozygote showed a significant reduction (high order *Dgp71WD*^{120}/*dgt5*^{LE10} trans-heterozygote 12.14 ± 1.94 μm; n=5; p<0.01) while the mean length of other branch level remained unmodified. Data are shown in Table 3.14 (n=5; p>0.05) and Figure 3.16 F.

Table 3.14 Mean lengths of each branch level (μm)

	Primary	Secondary	Tertiary	High order
Control	433.37±25.86	90.33±5.26	32.36±7.13	17.49±0.32
Dgp71WD^{120}/+	407.07±53.74	78.50±6.39	35.20±5.54	17.52±2.08
Dgp71WD^{120}/*dgt5*$^{-}$	382.22±48.04	66.60±17.62	25.88±5.98	12.14±1.94**
Dgp71WD^{120}/*dgt6*$^{-}$	418.53±55.48	78.30±14.93	31.72±7.58	16.57±2.81

** indicates p<0.01 comparing to control and *Dgp71WD*^{120}/+, respectively.

These data suggest *Dgp71WD* genetically interacts with *dgt5* in class IV da neuron for dendrite length especially in the length of high order branches, while it interacts with *dgt6* in both dendrite number and length especially in the number of high order branches. The difference we found between the trans-heterozygotes of *Dgp71WD* with *dgt5* or *dgt6* may be due to potential different function of *dgt5* and *dgt6* in microtubule nucleation within the Augmin complex as dgt6 is suggested to perform a core function in the Augmin complex in a recent paper (Hsia et al. 2014). Future work is required to address this question. These data support the involvement of the Augmin complex and Dgp71WD in controlling the morphology of the distal dendrites in *Drosophila* class IV da neurons. The similarity in γ*tub23C*, *dgt5*, *dgt6* and *Dgp71WD* mutant phenotypes as well as their genetic interactions provides a possible scenario of γ-Tubulin-Augmin acentrosomal microtubule nucleation pathway in neuronal dendrites.

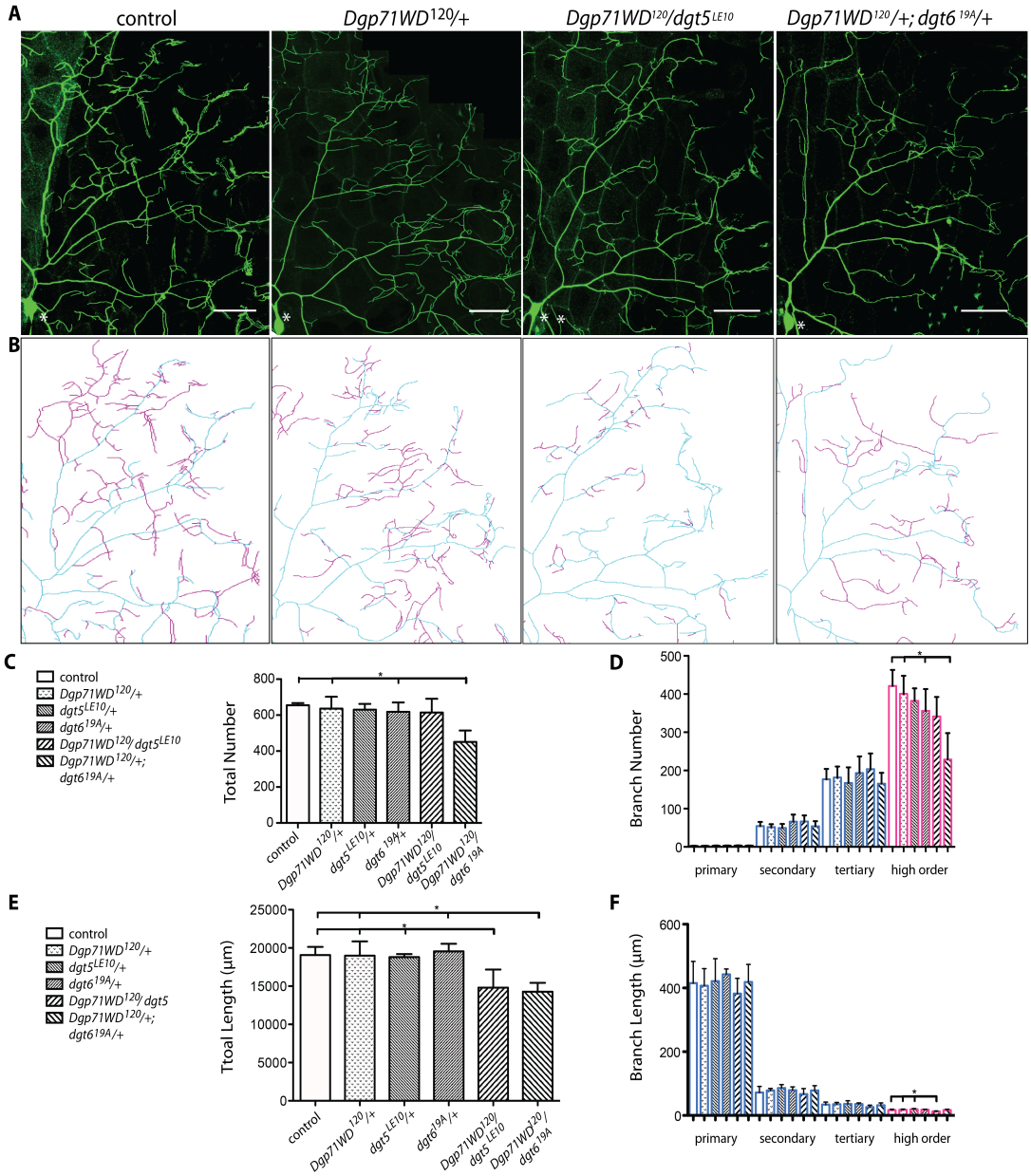

Figure 3.16 *Dgp71WD*, *dgt5* and *dgt6* display genetic interactions.

(A) One quadrant of a class IV ddaC neuron of third instar larvae of control, heterozygous *Dgp71WD*^{120}, *dgt5*^{LE10} or *dgt6*^{19A} and trans-heterozygous *Dgp71WD*^{120} and *dgt5*^{LE10} or *dgt6*^{19A} carrying *ppkGal4 UASmCD8GFP*. White asterisk indicates the soma. Scale bar is 50µm. (B) Tracing scheme of neurons shown in (A). Magenta indicates high order branches. Blue indicates other branch levels. (C), (D), (E) and (F) Quantification of total branch number, branch number, total branch length and branch length of ddaC neurons of control, heterozygotes and trans-heterozygotes *Dgp71WD*^{120} and *dgt5*^{LE10} or *dgt6*^{19A} third instar larvae. Magenta indicates high order branches. Blue indicates other branch levels.

Star indicates $p < 0.05$. Data is means ± SD; n = 5 neurons of individual animals per genotype

4 Discussion

4.1 Summary of the Results

Here, I have investigated the function of Augmin complex and γ-TuRC in the establishment of dendrites in class IV da neurons in *Drosophila*. By loss of function and cell-autonomous rescue, I have provided evidence for the cell-autonomous function of *γtub23C*, the Augmin complex (here *dgt5* and *dgt6*) and *Dgp71WD* in dendrite morphology. Further, my experiments addressing genetic interactions between *γtub23C*, the Augmin complex (here *dgt5* and *dgt6*) and *Dgp71WD* suggest that these molecules play coordinated roles in dendrite branching. Taken together, I have provided a possible pathway of acentrosomal microtubule nucleation during neuronal dendritic differentiation in *Drosophila* Class IV da neurons. I propose that the Augmin complex regulates acentrosomal microtubule nucleation by interaction with *γtub23C* and *Dgp71WD*, thus controls the maintenance of the dendritic field.

4.2 γTub23C regulates dendrite morphology of class IV da neurons

In many cell types, centrosome is considered to be the main MTOC and microtubule minus-ends were found anchored at it. In neurons, recent researches have given evidence that the centrosome loses its function as a microtubule nucleation site during development (Stiess et al. 2010; Nguyen et al. 2011). There are several described mechanisms for noncentrosomal microtubule nucleation. For instance, pre-existing microtubules severed by Katanin or Spastin can be transported from the soma and are suggested to serve as local microtubule nucleation sites by γ-*tubulin* and other centrosomal proteins (Kapitein and Hoogenraad 2015).

In *Drosophila*, class IV da neurons have the highest dendritic complexity with fine high order branches covering the entire target field (Grueber et al. 2002). It is provided to be a useful tool to uncover relation between cytoskeleton structure and dendritic morphology. In this work, I have demonstrated the importance of γTub23C in *Drosophila* class IV da neuron dendritic differentiation by showing that the number of high order branches was strongly reduced as a result of reduced levels of γTub23C. This result is consistent with a previous report utilizing γTub23C RNAi (Chen et al. 2012; Ori-McKenney et al. 2012; Nguyen et al. 2014). The main phenotype is a strong reduction in high order branch number, while the branch number of other levels is not affected. There is no effect on total dendritic length or on mean length of each branch order. These data suggest an effect of γ*tub23C* in maintenance of the distal dendritic branches. Considering the fact that very few of the loss-of function animals survive until the second instar or sometimes even the early third instar, it is possible that maternal γ*-tubulin* contributes to microtubule nucleation in early stages, which allows primary branch formation. In *Drosophila* there is a second γ*-tubulin* isoform, γ*Tub37C,* required for *Drosophila* female meiosis (Tavosanis et al., 1997; Oegema et al., 1999). This second isoform is present in oocytes and may contribute to

microtubule nucleation in dendrite development at embryonic stages, allowing for the establishment of dendrite branches of lower level.

Previous studies have showed that, in the second instar larvae, terminal branches in class IV da neurons undergo dynamic extension and retraction (Nagel et al. 2012). To investigate whether the defect of high order branches in *γ-tubulin* mutant animals is due to a defect in branch initiation or branch maintenance, I have performed time-lapse experiments visualizing terminal branches in mutant animals. A reduction in the number of new branch formation in the mutant animals was analyzed, suggesting γ-Tu23C may promote new branch formation in distal region. Moreover, a reduction in the number of extended branches and an increase in retracted branches were found. These data further support the effect of *γtub23C* in maintenance of the distal dendritic branches. And they are consistent with the previous research using *γtub23C* RNAi (Ori-McKenney, Jan et al. 2012), which suggest a function of *γtub23C* in dendrite maintenance in distal region.

In summary, *γTub23C* mutant phenotype has suggested an important role of *γTub23C* in establishing proper dendritic field in distal region. Time-lapse data indicate a defect of branch maintenance in the existing dendrites and a failure in new branch formation in *γTub23C* mutants. Therefore, *γ-tubulin* cell-autonomously controls the emergence and maintenance of high order branches and thus affects the dendritic morphology independently of the centrosome in *Drosophila* neurons as suggested by other researchers (Nguyen et al. 2011).

4.3 γTub23C targeting in class IV da neurons

To understand the mechanism of acentrosomal microtubule nucleation by *γ-tubulin*, one important aspect is whether other microtubule nucleation sites exist while the centrosome loses its microtubule nucleation function in mature neurons. One potential site is the Golgi complex. Microtubule nucleation was reported to occur on Golgi membranes *in vitro* (Chabin-Brion et al. 2001) and *in vivo*, which requires the association of *AKAP450* and *CLASP2* (Rivero et al. 2009). Additionally, in *Drosophila* da neurons, Golgi outposts are suggested to be the nucleation site for local microtubule nucleation in dendrites and thus involved in shaping the dendritic morphology (Ori-McKenney et al. 2012). In this work, the localization of a GFP-tagged γTub23C construct in class IV da neurons was clearly detectable in proximal dendrites, but only weakly in distal dendrites, suggesting a possible scenario that γTub23C is transported to distal dendrites in da neurons. It is possible that the Golgi complex mediates this transportation. However, while other researchers agree that there is local microtubule nucleation in dendrites, their data do not support the idea of Golgi as a nucleation site (Nguyen et al. 2014).

Another important aspect is to understand the recruitment of *γ-tubulin*. In centrosome dependent microtubule nucleation, *γ-tubulin* is recruited at the centrosome from a soluble cytoplasmic pool (Khodjakov and Rieder, 1999). In animal cells, *γ-tubulin* associates with spindle microtubules, which suggests *γ-tubulin* can be bound to the ends of those microtubules that are not anchored in the centrosome (Lajoie-Mazenc et al. 1994). Components in γ-TuRC have played a crucial role in anchoring *γ-tubulin*. To address the interaction between γ-TuRC components, I started first by examining RNAi phenotypes in da neuron dendrites. In class IV da neurons, I have found a similar phenotype to loss of *γtub23C* function upon the RNAi-mediated knockdown of *Dgp71WD, Dgrip128, Dgrip163* and *Dgrip84* (data now shown). I then focused on *Dgp71WD* since this molecule is the potential linker between γ-Tubulin and microtubule nucleation sites (Reschen, Colombie et al. 2012; Gunawardane et al. 2003). In *Dgp71WD* loss of function animals I

found significant reduction in dendritic number, which is stronger than the number reduction phenotype observed in other molecular mutants. A UAS-Dgp71WD full-length transgene will be generated to complete these genetic studies and address whether Dgp71WD is required cell autonomously. Time-lapse imaging showed a defect in dendrite elongation and maintenance in the *Dgp71WD* loss of function animal, which is similar to the γ*tub23C* mutant. However, loss of *Dgp71WD* did not reduce the new branch formation events, suggesting that unlike γ*tub23C, Dgp71WD* is not important for branch emergence. Moreover, within the newly formed branches, there were more stable new branches in the *Dgp71WD*^{120} mutant, suggesting a similar function of Dgp71WD with γTub23c in dendrite maintenance. Whether the actin cytoskeleton plays a role in emergence of new branches remains an interesting question.

In both zebrafish and human cells, *Nedd1/GCP-WD* (*Dgp71WD* homologue) is essential for targeting the γ-TuRC to the spindle and promoting microtubule nucleation (Lüders et al. 2006; Uehara et al. 2009). In this work, γ*tub23C* and *Dgp71WD* mutants showed similar phenotype in high order branches. Therefore, I suggest that *Dgp71WD* recruites γ*tub23C* for local dendritic microtubule nucleation in this study.

Another possible γ-Tubulin anchoring site is the side of existing microtubules. As shown in spindles of human U2OS cells, Augmin-dependent microtubule outgrowth is found to attach to the adjacent microtubule walls (Kamasaki et al. 2013). This data suggests a possible way of γ-Tu23C targeting through Augmin complex within the dendrites. The function of Augmin components in da neurons will be discussed in the following chapters.

The severed microtubule end is suggested to serve as nucleation site for microtubule outgrowth. CAMSAPs, which are important for microtubule minus-end nucleation, are considered to play an important role in this scenario as Katanin can bind to it (Jiang, Hua et al. 2014). I have tested the function of Kat-60L1 and confirmed its function in controlling dendrite complexity in

Drosophila class IV da neurons (data not shown) as reported previously (Stewart, Tsubouchi et al. 2012). I have also performed genetic analysis between Kat-60L1, Dgp71WD, γ-Tu23C and Dgt5 (data not shown). However, I could only find a genetic interaction between Kat-60L1 and Dgp71WD but not the other two molecules. One possible explanation is that Kat-60L1-Dgp71WD mediated γ-Tu23C recruitment pathway other than Augmin-mediated γ-Tu23C recruitment. It would be interesting to explore further the function CAMSAPs, Kat-60L1 and Dgp71WD in targeting γ-Tu23C during acentrosomal microtubule minus-end nucleation within dendrites.

4.4 The Augmin complex affects high order dendrite branching in class IV neurons

Previous report has suggested *Nedd1 (Dgp71WD)* is required to link γ-TuRC and the Augmin complex for microtubule nucleation (Zhu et al. 2008). The Augmin complex, consisting of 8 subunits, was first discovered by high-throughput RNAi screens in *Drosophila* S2 cells. It was later shown to recruit γ-TuRC through Dgp71WD in the spindle (for review see Goshima and Kimura, 2010). I have found a cell-autonomous function of *dgt5* in controlling the number and length of dendritic branches in class IV da neurons. The phenotype was different than in γ*-tubulin* and *DGP71WD* mutants as the branch number in all branch levels are significantly reduced as well as the mean length of high order branches in *dgt5* mutant, while in γ*-tubulin* and *Dgp71WD* mutants the branch number in other branch level was not strongly affected but the high order branches. The difference may due to different technics utilized in different molecules or due to the extremely severe reduction in the distal branches in the *dgt5* null mutant. The difference could also due to different functions of these molecules in dendrite.

I have also analyzed *dgt6,* which is considered to interact with γ*-tubulin* (Bucciarelli et al. 2009). Although $dgt6^{19A}$ mutant is not a clean null mutant, similar phenotype as $dgt5^{null}$ was found in mutant animals. The reduction in dendrite number is quite similar as seen in γ*tub23C* and *Dgp71WD* mutants. The stronger reduction in branch number in *Dgp71WD* and *dgt6* mutants comparing to γTub23C mutant suggests *dgt6* has similar function *as Dgp71WD* in microtubule stability. Time-lapse imaging of the $dgt6^{19A}$ mutant showed a defect in new branch formation and branch elongation, which is similar to the γ*tub23C* mutant. Within the new branches, there were more stable new branches in the $dgt6^{19A}$ mutant that is comparable to the $Dgp71WD^{120}$ null mutant. In general, these data indicate a correlation between these molecules.

Genetic interaction analysis suggested cooperation between the Augmin complex (*dgt5* and *dgt6*), γ*tub23C* and *Dgp71WD*. The severe reduction phenotype in either branch length or branch number of the trans-heterozygous mutants has suggested a potential pathway in regulating development of dendrites in da class IV neurons. This phenotype is not due to additive effect as is proved by one-way ANOVA analysis. The result suggests that Augmin complex (here *dgt5* and *dgt6*) functions with γ-TuRC (here γ*tub23C* and *Dgp71WD*) in regulating dendrite development, especially in high order branch formation, possibly through the same pathway. This hypothesis fits to the previous suggestions that the Augmin complex recruits *γ-tubulin* for new microtubule nucleation through the link to *Dgp71WD* (Zhu et al. 2008; Lawo et al. 2009; Bucciarelli et al. 2009).

Statistic analysis has also shown difference between Dgts. Combined with Dgp71WD, *dgt5* trans-heterozygous mutant has shown a reduction in mean length of high order dendrite, while *dgt6* trans-heterozygous mutant has shown a reduction in number of high order dendrites. This difference is hard to explain. Although the Augmin complex functions as a unit (Goshima et al. 2008), biochemical reconstitution suggests that Dgt4 and Dgt6 are the core components within the complex (Hsia et al. 2014). Therefore, it is conceivable that different Dgt subunits have in addition their own specific functions, which fits to delicate difference in phenotypes observed by dgt5 and dgt6 respectively. It also potentially support the suggestion that Dgt6 binds directly to Dgp71WD as suggested before (Uehara et al. 2009), so that a decrease of Dgp71WD with Dgt6 will result in a severe phenotype than with other Dgts. Considering the Augmin complex functions in acentrosomal microtubule nucleation of other cell types, a function of the Augmin complex in controlling proper patterning of dendrites in local microtubule nucleation in neuronal dendrites is here suggested. And it requires the interaction with *γ-tubulin* and *Dgp71WD.*

4.5 Augmin components jointly regulate microtubule organization in dendrites of class IV da neurons.

Reduction of one component in the Augmin complex results in reduction of other components in S2 cells, suggesting the whole complex functions as a unit (Goshima et al. 2008). In this work, *dgt5*^{LE10}*/dgt6*^{19A} trans-heterozygote animals also showed a strong reduction in branch number, suggesting these two molecules regulate dendrite morphology jointly. The reduction phenotype in trans-heterozygote animals is comparable to the reduced phenotype seen in the γ*tub23C* mutant but weaker than the *dgt6*^{19A} mutant. One possible explanation is the different reduction level of Augmin complex in these mutants. Time-lapse imaging of *dgt5*^{LE10}*/dgt6*^{19A} trans-heterozygote animals showed a defect in branch maintenance, which was similarly observed in γ*tub23C* mutants and the *Dgp71WD*^{120} null allele. Thus, it is possible that the defect in branch maintenance in trans-heterozygous *dgt5*^{LE10}*/dgt6*^{19A} mutant animals is due to the reduction of microtubule mass, which is a result of the decreasing level of the Augmin complex.

To further explore the change in microtubule structure, I have observed an increased distribution of α-*tubulin* in trans-heterozygous *dgt5*^{LE10}*/dgt6*^{19A} mutant animals comparing to the control. This result is contradicted to my hypothesis as a decreased intensity was expected. One possible explanation is that with less Augmin attached to pre-existing microtubules, the over-expressed α-*tubulin* could not be nucleated and the increased monomer intensity could therefore be detected in the high order branches. Another possible explanation is that besides the microtubule nucleation function of Augmin, the complex can also act as a regulation factor for α-*tubulin* polymerization that certain dosage of Augmin complex is required for proper microtubule polymerization. Future work to detect endogenous α-*tubulin* distribution is needed to address this question. The distribution of actin in both control and experimental groups was also examined by using actin over-expression. However, I did not find any significant changes in actin distribution (data not shown).

One important character of dendritic microtubule is its mixed polarity. In *Drosophila* da neurons, the orientation of microtubules in dendrites is also mixed but with most (>90%) plus-ends pointing towards the soma (Stone et al. 2008). A recent study in *Xenopus* egg extracts showed that the Augmin complex conducted microtubule branching from pre-existing microtubules (Petry et al. 2013). Later, people suggested that the Augmin complex is required for connections between mother and daughter microtubules at the microtubule walls in microtubule branching with same orientation (Kamasaki et al. 2013).

To check whether the microtubule polarity was changed in Augmin mutants, I first utilized Nod (Cui et al. 2005; Rolls et al. 2007) to detect microtubule minus-ends in dendrites in class IV da neurons. Although the localization of Nod is weaker in distal dendrites in trans-heterozygous animal, without labeled dendrites, it is hard to conclude whether the polarity is changed statistically. The reduction of Nod localization in $dgt5^{LE10}/dgt6^{19A}$ mutant animals suggests two possibilities: (i) the reduction of the microtubule mass as a result of the reduction of microtubule nucleation; (ii) the change in microtubule polarity because there are less microtubules orientating with their plus-ends towards the soma.

To address this question, I have performed time-lapse imaging of GFP targeted EB1, a microtubule +TIPs protein. The movements of EB1 illustrate the orientation of growing microtubule as is used in pervious studies (Nguyen et al. 2014; Chen et al. 2014; Hill et al. 2012). The time-lapse imaging has showed less EB1 dots in trans-heterzygous mutant. However, as a small amount of moving EB1 dots along the distal dendrites was observed, it is difficult to conclude a change in orientation comparing to the control. Nontheless, this result suggests interruption of Augmin complex can not disrupt microtubule polarity in *Drosophila* da neuron dendrites, which is consistent with previous studies using cell cultures (Petry et al. 2013; Kamasaki et al. 2013). This result strongly supports the first scenario that there are less microtubules in the Augmin trans-heterozygotes.

4.6 A Model of Augmin–γ–TuRC function in dendrite formation

In this work, I have characterized for the first time the function of Augmin complex (here *dgt5* and *dgt6*) and Dgp71WD in γ-TuRC in dendrite formation in *Drosophila* Class IV da neurons. I have also confirmed the role of γ*tub23C* in dendrite maintenance in the same system. All the molecules described in this work contribute to establishment of proper dendritic field especially in distal dendrites. Knockdown or knockout of any of them results in reduction in dendritic number or dendrite length, which leads to a defect in dendrite complexity. As γ*tub23C* is considered to be the main microtubule nucleator, an interaction between Augmin complex, Dgp71WD and γTub23C is implied by genetic interaction analysis, which may contribute to non-centrosomal microtubule nucleation along the dendrites. Therefore, my data suggests a model in which the Augmin complex interacts with γTub23C and Dgp71WD, and thus cell-autonomously controls the dendritic morphology without changing the microtubule polarity. Nevertheless, the mechanisms how non-centrosomal microtubule is mediated and whether Augmin mediated microtubule nucleation occurs locally or by transportation remain to be elucidated.

Regarding the abnormality of over-expressed α-*tubulin* in Augmin trans-heterozygoes, it is also likely that Augmin complex acts as a regulator for α-*tubulin* polymerization in microtubule nucleation or α-*tubulin* transportation. Considering the wide expression of Augmin complex in different organisms, further studies on Augmin complex in dendrite development as well as in microtubule organization would help to understand the mechanisms underlying dendrite formation.

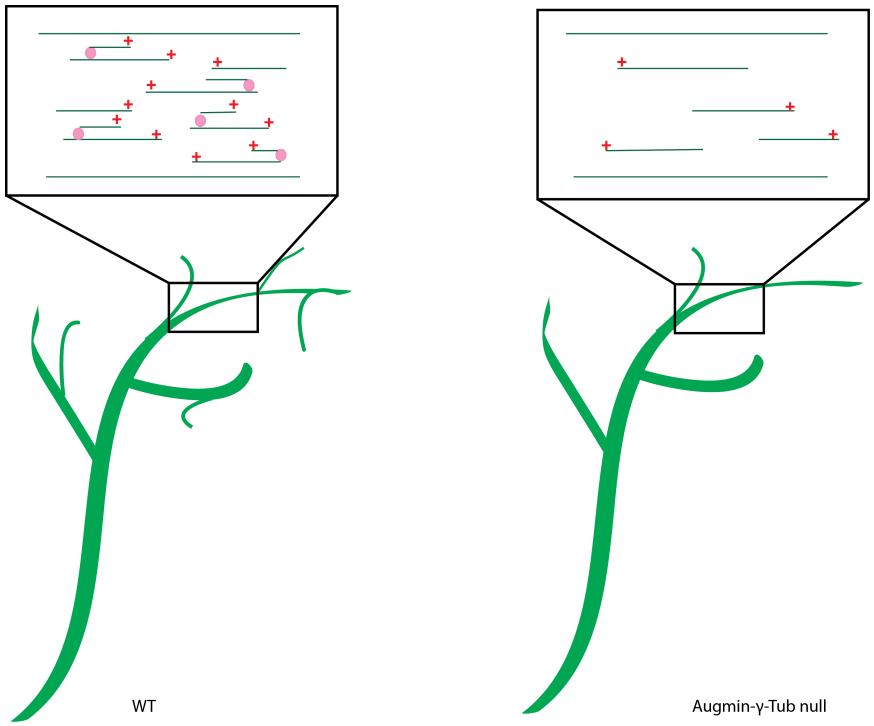

Figure 4.1 Model of Augmin−γ−Tubulin function in dendrite formation

In *Drosophila* class IV da neuron dendrites, reduction of Augmin- γ-Tubulin complex results in reduction of dendritic branches. Green lines indicate microtubules. Pink oval indicates Augmin−γ−Tubulin complex. Red cross indicates microtubule orientation.

5 Materials and Methods

5.1 Materials

5.1.1 Chemicals

Table 5.1 Chemicals

Chemical	Supplier
Agarose,	Roth
Ampicillin	Roche
dNTP set	Roche
Glycerine	MERCK
Triton-X100	Roth
Tris	Bio-Rad
Potassium chloride (KCl)	MERCK
Methanol	Roth
Halocarbon oil Volatef S3	Lehmann & Voss Co.
Sodium chloride (NaCl)	Roth
Syber Green	Bio-Rad
Glycerol	Roth
Bromopherol	Roth
TEMED	Bio-Rad
Acrylamide	Roth
Ammonium Persulfate (APS)	Roth
Sodium dodecyl sulfate (SDS)	Roth
Methanol	Roth
Coomassie Blue	Roth
Acetic acid	Roth
EDTA	Roth

Hydrochlorie acid (HCl)	Roth
Natriumchlorid (NaCl)	Roth
Potassium acetate (KAc)	Roth
Ethanol	Roth
Isopropanol	Roth
Beta-mercaptoethanol	Roth
Heptane	Roth
Formaldehyd	Polysciences
Sodiumhypochlorid (Bleach)	MERCK
Fetal Calf Serum (FCS)	Perbio
Sodium hydroxide (NaOH)	Roth
Milk powder	Roth

5.1.2 Buffers and Solutions

Phosphate buffered saline (PBS)

NaCl (137mM)

KCl (2.7mM)

Na_2HPO_4 (8mM)

KH_2PO_4 (1.5mM)

8 g NaCl, 0.2g KCl, 1.15g Na_2HPO_4, and 0.24g KH_2PO_4 were dissolved in 800 ml distilled water. The pH was adjusted with HCl to 7.4 and the volume with distilled water to 1 L. The final solution was sterilized by autoclaving and stored at RT.

PBT (0.1%)

0.1% Tween20 was dissolved in PBS

10% APS

1g APS was dissolved in 10 mL distilled water and the final solution was stored at 4°C.

Running buffer (10x)

Tris base

Glycine

SDS

151g Tris, 720g Glycine and 10g SDS were dissolved in 5 L distilled water. The pH was adjusted to 8.3. The final solution was stored at 4°C.

Laemmli buffer (4x)

Tris-Hcl (pH 6.8) (1M)

SDS

Glycerol

Bromophenol blau

Beta-mercaptoethanol

24mL 1M Tris-Hcl with pH 6.8, 8g SDS, 32mL Glycerol and 16 mg Bromophenol blau were dissolved in 80 mL distilled water, then 20 mL beta-mercaptoethanol was added to make the final solution and stored at -20°C.

10% SDS

10g SDS was dissolved in 100 mL distilled water and stored at RT.

1.5 M Tris-HCl pH8.8

Tris base

HCl (1N)

182g Tris was dissolved in 700 mL distilled water. The pH was adjusted to 8.8 with 1N HCl and the volume with distilled water to 1 L. The final solution was filtered through a 0.45 µ filter and stored at 4°C.

1 M Tris-HCl pH6.8

Tris base

NHCl (1N)

60.7g Tris was dissolved in 300 mL distilled water. The pH was adjusted to 6.8 with 1N NHCl and the volume with distilled water to 500 mL. The final solution was filtered through a 0.45 µ filter and stored at 4°C.

Transfer buffer (10x)

Tris base

Glycine

SDS

154.5g Tris, 721g Glycine and 50g SDS were dissolved in 10L distilled water to make the 10x solution and stored at RT. 1x running buffer was made freshly out of 10x solution every time. For 100mL 1x buffer, 20mL 10x buffer and 40mL Methanol were mixed and the volume was added to 200ml with distilled water.

Coomassie blue buffer

Coomassie Blue R-250

Methanol

Acetic acid

DTT (1M)

1g coomassie blue, 500mL distilled water, 400mL Methanol and 100mL Acetic acid were mixed. Aliquots were made and stored at -20°C. 1.54g Dithiothreitol was dissolved in 10 mL distilled water and stored at -20°C. For use of each time, 80µl fresh DTT was add to 400µl 2x laemmili buffer.

Coomassie blue distain buffer

Acetic acid

Methanol

100mL Acetic acid was mixed with 500 mL H_20 and then mixed with 400 mL Methanol. The final solution was stored at RT.

TAE buffer (50x)

Tris base

Glacial acetic acid

EDTA (0.5 m, pH8.0)

242g Tris, 57.1 ml Glacial acetic acid, 100 mL EDTA were dissolved in distilled water to obtain a final volume of 1L. For 1xTAE buffer, 20 mL of the 50x buffer were mixed with 980 mL distilled water and stored at RT.

Squishing buffer

Tris-HCl (10mM, pH8.2)

EDTA 1mM

NaCl 25mM

Proteinase K

1.2114g Tris was dissolved to 700mL water. The pH was adjusted to 8.2 by HCl to make to final solution with 10mM. 1.461g NaCl was and 0.29224g EDTA were dissolved in Tris-HCl and the final volume was 1L with distilled water. The final solution was stored at RT.

Proteinase K was added freshly to a final concentration of 200 µg/ml.

Blocking buffer

2g milk powder was dissolved in 50 mL PBT buffer. The solution was made freshly every time.

5.1.3 Media

Table 5.2 Media

Medium	**Supplier**
Instant blue Drosophila medium	Fisher Scientific
Instant dry yeast	Fermipan Inc.

Apple agar plates

Apple juice 500mL

H_2O 480mL

Agar 40g

Ethanol 10.5mL

Glacial acetic acid 10mL

Apple juice, H2O and Agar were mixed and boiled until agar was dissolved completely. After the solution cooled down to 60°C, Ethanol and Glacial acetic acid were added and the pH was adjust to 4.25-4.40 with 100% NaOH. The final solution was poured immediately to plates and stored at 4°C.

Fly food (7L)

Agar 117g

Melasse 800g

Maismehl 600g

Hefe150g

Propionic acid 63mL

Methylparaben 24g

Agar was dissolved in boiled water for about 40-50% of finial volume while maismehl and yeast were dissolved in cold water. The cold homogenious broth was added after Melasse was added to the agar. The temperature of the kettle was heated to 96°C. After cooked for 1.5 hours, the broth was cooled down to 60°C and propionic acid and Methylparaben were added and mixed well. The final broth was aliquot, covered immediately and stored in 4°C.

LB medium and plates

LB medium and plates were supplemented with 1.5% Agar before autoclave. For Ampicillin resistant bacteria, Ampicillin was added to LB media and plates with working concentration of 100 µg/mL.

5.1.4 Enzymes and DNA standards

Table 5.3 Enzymes and DNA standards

Enzyme/Standard	Supplier
Phusion DNA polymerase	NEB
Proteinase K	Sigma
Restriction endonucleases	NEB
T4 DNA Ligase	NEB
Taq Polymerase	Roche
1 kb ladder	NEB

5.1.5 Plasmids and DNA library

Table 5.4 Plasmids and DNA library

Plasmid	**Supplier/Donor**
Drosophila DGC cDNA clone LD47477	DGRC
Drosophila DGC cDNA clone LD14121	DGRC
Drosophila DGC cDNA clone RE05579	DGRC
pP{UAST}	Juh Nung Jan
pP{UAST}attB	Jonannes Bischof

5.1.6 Primers

Table 5.5 Primers

Primer	**Sequence 5'-3'**	**Use**
1	TTAAGAATTCATGAAATGTGCC	UAS-Dgt5 forward
2	GATCTCTAGATCATTCTAACAG	UAS-Dgt5 reverse
3	CCGGAATTCATGGATCGGACCATAATTGCAC	UAS-Dgt6 forward
4	CTAGTCTAGACTAAAAGATAATATCCTTG	UAS-Dgt6 reverse
5	TTCCTTTTTTGCGGCCGCATGCATGTT	UAS-Dgp71WD forward
6	CTAGTCTAGATTACTCTCCGCATGATT	UAS-Dgp71WD reverse

All primers were synthesized by Eurofins MWG Operon.

5.1.7 Antibodies

Table 5.6 Antibodies

Antibody	**Supplier/Donor**
Rabbit anti-Dgt5 (Goshima et al. 2008)	Gohta Goshima
Rabbit anti-Dgt6 (Goshima et al. 2008)	Gohta Goshima
Rabbit anti-Dgt6 (Bucciarelli et al. 2009)	Maria Patrizia Somma
Anti-α-Tubulin	DSHB
Anti-Actin	DSHB
Mouse anti-GFP	DSHB

5.1.8 Commercial kits

Table 5.7 Commercial kits

Commercial Kit	**Supplier**
QIAquick Gel Extraction Kit	Qiagen
QIAprep Spin Miniprep Kit	Qiagen
QIAGEN Plasmid Midi Kit	Qiagen
GFP-Trap® _M Kit	Chromotek

5.1.9 Equipments

Table 5.8 Microscope systems

Microscope	**Supplier**
Zeiss LSM780 confocal microscope under a 40x/NA 1.4 oil immersion objective	Zeiss GmbH
Zeiss Fluorescent Dissectoscope	Zeiss GmbH
Yokogawa Spinning-disc confocal microscope with a EM-CCD camera	Nikon
Zeiss Stemi 2000-C Dissectoscope	Zeiss GmbH

Table 5.9 Consumables

Consumables	**Supplier**
Electrocompetent cells TOP10	Invitrogen
Doppelband Fotostrip (Double sided tape)	Tesa AG
Forcep DuMont Nr.5	Zeiss
Immersion oil	Zeiss
Insect pins	FST
Microscope cover glasses 24 mmx 40 mm	Menzel Gläser
Microscope cover glasses 24 mmx 24 mm	Menzel Gläser
Microscope sildes 76 mmx 26 mm	Menzel Gläser
Small petri dishes	Mat Tek Corporation

5.2 *Drosophila* stocks

5.2.1 *Drosophila* stocks

Table 5.10 *Drosophila* stocks

Stock	**Source**
γ*Tub23C*$^{A15\text{-}2}$ (Vazquez et al. 2008)	Bloomington Stock Center
γ*Tub23C*^{Pl} (Sunkel et al. 1995)	Bloomington Stock Center
UAS-γ*Tub23C-GFP* (Nguyen et al. 2011)	Rolls M.M.
UAS-α*-Actin-GFP*	Bloomington Stock Center
dgt5^{LE10}42D	Tadashi Uemura
dgt6^{19A}	Generated in the lab
dgt6^{GSV6}	Bloomington Stock Center
DGP71WD^{120} (Reschen et al. 2012)	Jordan W. Raff
ppkGal4 (Ainsley et al. 2003)	Bloomington Stock Center
477Gal4 (Grueber et al. 2003)	Bloomington Stock Center
elav Gal4	Bloomington Stock Center
FRT42D tub Gal 80	Bloomington Stock Center
OregonR	Bloomington Stock Center
UASmCD8Cherry	Bloomington Stock Center
UASmCD8GFP	Bloomington Stock Center
UAS-dgt5	Generated in the lab
UAS-dgt6	Generated in the lab
UAS-EB1-GFP	Rolls M.M.
UAS-Nod-GFP	Bloomington Stock Center
Dr Δ{2-3}/ TM6	Bloomington Stock Center

5.2.2 Genotypes

Table 5.11 Analyzed genotypes

ppkGal4 UASmCD8GFP/+
477Gal4 UASmCD8GFP/+
hs-FLp, elav Gal4, UAS mCD8-GFP/ +; FRT42D tub Gal 80/ +
γTub23 $^{A15-2}$/γ*Tub23C* ^{PI}*; ppkGal4 UASmCD8GFP/+*
γ*Tub23C* $^{A15-2}$/γ*Tub23C* ^{PI}*; ppkGal4 UASmCD8GFP/UAS-* γ*Tub23C-GFP*
UASmCD8Cherry/+; ppkGal4/UAS- γ*Tub23C-GFP*
hs-FLp,elav Gal4,UAS mCD8-GFP/ dgt5^{LE10}*42D; FRT42D tub Gal 80/ +*
hs-FLp,elav Gal4,UAS mCD8-GFP/dgt5^{LE10}*42D; FRT42D tub Gal 80/UAS-dgt5*
ppkGal4 UASmCD8GFP/+; dgt6^{19A}
ppkGal4 UASmCD8GFP/UAS-dgt6; Dgt6^{19A}
ppkGal4 UASmCD8GFP/+; dgt6^{19A}*/+*
ppkGal4 UASmCD8GFP/dgt5^{LE10}*; dgt6*^{19A}*/+*
ppkGal4/+; UAS-EB1-GFP/+
ppkGal4/Dgt5^{LE10}*; UAS-EB1-GFP/Dgt6*^{19A}
ppkGal4/+; UAS-Nod-GFP/+
ppkGal4/Dgt5^{LE10}*; UAS-Nod-GFP/Dgt6*^{19A}
ppkGal4,UASmCD8Cherry/+; UAS- α*Tub23C-GFP/+*
ppkGal4,UASmCD8Cherry/+; UAS- α*Tub23C-GFP/+*
γ*Tub23C* $^{A15-2}$*/+; ppkGal4 UASmCD8GFP/+*
γ*Tub23C* $^{A15-2}$*/Dgt5*^{LE10}*; ppkGal4 UASmCD8GFP/+*
γ*Tub23C* $^{A15-2}$*/+; ppkGal4 UASmCD8GFP/Dgt6*^{19A}
dgp71WD^{120}*/+; ppkGal4 UASmCD8GFP/+*
dgp71WD^{120}*/Dgt5*^{LE10}*; ppkGal4 UASmCD8GFP/+*
dgp71WD^{120}*; ppkGal4 UASmCD8GFP/+*
dgp71WD^{120}*/+; ppkGal4 UASmCD8GFP/Dgt6*^{19A}

5.3 Methods

5.3.1 MARCM

The MARCM (mosaic analysis with a repressible cell marker) system is used to generate genetic mosaics. The initial cells carry the Gal4, UAS-target gene, and Gal80 suppressor. During mitotic recombination, Gal80 suppressor will be removed from one daughter cell and therefore allow the expression of the target gene under Gal4-UAS system. The *FLP* recombinase is used to catalyze the mitotic recombination at specific *FRT* site. The gene of interest is located in trans of the *Gal80* at the same chromosome and the labeled cells will go homozygous with the gene of interest after mitotic recombination (Lee and Luo. 1999).

To analyze Dgt5 loss-of-function phenotype, Dgt5*LE10* line was combined with FRT42D. The procedure of MARCM was carried as described before (Grueber et al. 2002). *hsFLP, elavGal4 UASmCD8GFP; FRT42D tubGal80/Cyo* virgins were collected and crossed to $Dgt5^{LE10}$ *FRT42D* males. Eggs from this cross were collected on apple agar plates for 2 hours at 25°C. Later, the plates were incubated in 25°C for 3 hours. Heat shock was performed at 38°C in the water bath afterwards for 45 min and followed by 30 min incubation time at RT and again heat shocked at 38°C for 45 min. The plates were kept in 25°C till third instar larvae were selected and imaged under the confocal microscope (Zeiss).

5.3.2 Molecular procedures

5.3.2.1 Molecular cloning

Dgt5, Dgt6 and Dgp71WD were cloned into pP{UAST} attB vector (Bischof et al. 2007). Primers including the sites for restriction endonucleases and over-hang nucleotides were designed using Primer3 software. For Dgt5, restriction sites XbaI and EcoRI were added. For Dgt6, restriction sites EcoRI and XbaI

were added. For Dgp71WD, restriction sites NotI and XbaI were added. For each construct, 5 independent lines were generated by embryonic injection into different attP lines by Best Gene.

5.3.2.2 PCR (Polymerase Chain Reaction)

PCR was used to amplify the gene of interest.
The template for the PCR amplification of Dgt5 was the Drosophila BDGP DGC cDNA clone LD47477. For Dgt6, the template was the Drosophila BDGP DGC cDNA clone LD14121. For Dgp71WD, the template was Drosophila BDGP DGC cDNA clone RE05579. Phusion high-fidelity DNA Polymerase was used in all the PCR.

PCR Dgt5

1 µl cDNA clone LD47477
2 µl Primer (10 pmol/µl)
2 µl Primer (10 pmal/µl)
1 µl dNTPs (10mM)
0.5 µl Phusion DNA Polymerase
10 µl Phusion Buffer
add dH_2O to 50 µl in total

Cycling conditions

98 °C	30sec	
98 °C	10sec	
56 °C	30sec	30 cycles
72 °C	2.5min	
72 °C	10min	
4 °C	∞	

PCR Dgt6

1 µl cDNA clone LD14121
2 µl Primer (10 pmol/µl)
2 µl Primer (10 pmal/µl)
1 µl dNTPs (10mM)
0.5 µl Phusion DNA Polymerase
10 µl Phusion Buffer
add dH_2O to 50 µl in total

Cycling conditions

98 °C	30sec	
98 °C	10sec	
62 °C	30sec	30 cycles
72 °C	2.5min	
72 °C	10min	
4 °C	∞	

5.3.2.3 Generation of transgenic flies

To generate UAS-Dgt5, UAS-Dgt6 and UAS-Dgp71WD, amplified genes of interest were subcloned into the pP{UAST} attB vector. The bacteria were sent to Best Gene to make transgenic flies. 5 independent lines were generated by the company and sent back to the lab for further analysis.

5.3.2.4 Gelelectrophoresis

0.8% agarose in TAE buffer was used for the gels. Syber Green was added to the DNA samples to run together with electrophoresis. The gel was run for 40-60 min at 200V in TAE buffer. Chemi-doc was used then for documentation a picture of the gel.

5.3.2.5 Gel extraction of DNA

To purify specific DNA fragment after electrophoresis, the separated DNA fragment was checked and cut out of the gel under UV-light with a sterile razor blade and purified with QIAquick Ger Extraction Kit following the manufacturer's instruction. DNA was eluted with 50 µl Sigma water instead of elution buffer provided by the Kit. The concentration of the DNA was later checked by Nano-drop.

5.3.2.6 Restriction digests of DNA

Restriction digest with specific restriction endonucleases was carried under 37°C in a 20-50 µl reaction volume for 1.5 hours. Enzymes were heat inactivated at 65°C for 5 min.

5.3.2.7 Ligation

Ligations were carried in 10-20 µl reaction volumes, containing 1 µl T4 DNA ligase, 1-2 µl T4 DNA ligase buffer, vector and gene of interest. The concentration of vector and DNA of gene of interest was checked by Nano-drop. In the reaction, the ratio of the amount of vector and gene DNA was 1:9. The reaction was incubated at 16°C overnight and inactivated at 65°C for 5 min the next day.

5.3.2.8 Transformation

50 µl Competent cells were taken from -80°C fridge and thawed to liquid on ice. 50-100 ng DNA were added and incubated 30 min on ice. Afterward, the mixture was heated at 42°C in the water bath for precisely 1 min and placed on ice for 2-3 min right afterward. Then 400 µl S.O.C medium was added to the mixture and incubated in 37°C for 1 hour to allow expression of resistance genes in transformed cells. The mixture was then centrifuged for 5min at 6000

rpm. After aspirate 300 μl supernatant, re-suspended bacteria were plated on selective LB plates and incubated at 37°C overnight.

5.3.2.9 DNA miniprep

Single colony was selected from the overnight cultured LB plates and cultured in 3ml LB medium for 8 hours as a starter. Then 3μl starter culture was put in 5μl LB medium and incubated overnight. The DNA of a 5 ml bacteria LB culture was extracted using the QIAprep Spin Miniprep Kit as described in the manufacturer's instruction. DNA was eluted with Sigma water and purification was carried after electrophoresis. Digestion was carried later to check for positive transformation.

5.3.2.10 Cultrue and conservation of E.coli strains

Bacteria were cultured in LB medium with selective antibiotics in a shaking incubator at 37 °C or on LB agar plates containing selective antibiotics in an incubator at 37°C. For short time periods, bacteria were stored at 4°C, for long period they were stored in 50% Glycerol at -80°C.

5.3.2.11 Sequencing

All the cloned vectors were sent to Seqlab for sequencing.

5.3.2.12 Hopping out

The P-element has not only been used for germline transformation to make transgenic flies, but also been used to induce imprecise excision to delete the flanking sequence. We have generated Dgt6 mutant using P-element excision. Males of $Dgt6^{\{GSV\}GS11802}$ P-element insertion line were crossed to virgins of *yw; Pin/ Cyo; Dr Δ{2-3}/ TM6, Ubx*. Males *of* $dgt6^{\{GSV\}GS11802}$*/ Dr Δ{2-3}* were selected in the next generation and crossed to Tm3/Tm6 balance line. Single male progeny with white-eye color (indicating miniwhite in the P-

element was gone in) was selected and crossed back to virgins of Tm3/Tm6 balancer line to create a stable line. Each single line was sequenced and checked by western blot to select the Dgt6 excision line.

5.3.2.13 Western blot

5 third instar larvae of the right genotype were selected and grinded in 100 µl 2x Laemmli buffer plus DTT and boiling for 5min with thermo block at 95°C. Protein separation by SDS-PAGE was done under standard procedure and protein was transferred to nitrocellulose membrane with Trans-blot Turbo (Bio-Rad). After block with 5% powdered mile and 0.1%Tween in PBS for 1 hour at RT, the membrane was incubated with first antibody overnight at 4°C. For Dgt5, the antibody was a gift from Dr. Goshima's lab (1:1000 diluted in PBS with 0.1%Tween; Goshima et al. 2008). For Dgt6, the antibody was a gift from Dr. Somma's lab and Dr. Goshima's lab (1:1000 diluted in PBS with 0.1%Tween; Goshima et al. 2008; Bucciarelli et al. 2009). After incubation, the membrane was washed with PBS with 0.1%Tween 3x 5 min and incubated with secondary antibody (1:1000) for 1 hour at RT. After wash the membrane 15-30min in PBS with 0.1%Tween, the membrane was imaged under Chemi-doc (Bio-Rad) using ECL detection reagents.

5.3.3 Gal4 UAS system

Gal4 UAS system is utilized to control the expression of genes spatially and temporally (Brand and Perrimon, 1993). Therefore, Gal4 enhancer trap lines combined with UAS is used in this work to visualize da neurons in the living animals with coupled fluorophores. Membrane marker lines can specifically label the membrane in the neurons of interest. Moreover, the Gal4 UAS system was utilized to ectopically expression gene of interest for rescue.

5.3.4 Confocal imaging

5.3.4.1 Confocal imaging

Wandering third instar larvae were selected to image the Class IV da ddaC neuron at dorsal segment A4-A5 under fluorescent microscope. Selected larvae were then immerged in 90% glycerol and pressed between glass slide and cover slip. Confocal microscope (Zeiss) was used to obtain confocal images of class IV ddaC da neurons with a 40x objective. 561nm laser and 488nm laser were used to detect different fluorescent signal. Stacks of images were processed with ImageJ software (National Institutes of Health, Bethesda, Maryland, USA, http://rsb.info.nih.gov/ij/) to make maximum projections and modifications.

5.3.4.2 Time lapse

Second instar larvae were mounted in halocarbon oil and immobilized beteween a metal sieve and cover slip. Images were taken under confocal microscope (Zeiss) with a 40x objective for 30 min interval of 5 min. stacks of images were then processed with ImageJ software (National Institutes of Health, Bethesda, Maryland, USA, http://rsb.info.nih.gov/ij/) and photoshop (Adobe) for maximum projections and modifications.

5.3.4.3 Image analysis and statistics

Images were analyzed with ImageJ software (National Institutes of Health, Bethesda, Maryland, USA, http://rsb.info.nih.gov/ij/) with the NeuronJ Plug-in (Meijering, Jacob et al. 2004). All the dendritic branches were traced and classified into four classes. The long dendrites emerged from the soma were defined as primary dendrite. Dendrites emerged from the primary dendrites were defined as secondary dendrite. Tertiary dendrites were defined as the dendrites emerged from the secondary dendrites and the rest were defined as high order branches. The number and length of each branch were measured

with NeuronJ. 5 different larvae were quantified per each genotype. Statistical analysis was done using Student's t-test.

For time lapse, NeuronJ was used to trace and measure the image at each time point. New branches were defined as branches appeared for the first time within 30 min imaging period. Number of new branches was counted and normalized to the basal dendrite length. Elongated and retracted branches were defined by comparing the length of the branches in the first image to the last image. Number of elongation, retraction and loss of branches were normalized to the initial branch number.

6 References

Ainsley, J. A., et al. (2003). "Enhanced Locomotion Caused by Loss of the Drosophila DEG/ENaC Protein Pickpocket1." Current Biology 13(17): 1557-1563.

Ageta-Ishihara, N., et al. (2013). "Septins promote dendrite and axon development by negatively regulating microtubule stability via HDAC6-mediated deacetylation." Nat Commun 4: 2532.

Aldaz, H., et al. (2005). “Insights into microtubule nucleation from the crystal structure of human gamma-tubulin.” Nature 435(7041): 523-527

Alves-Silva, J., et al. (2012). "Spectraplakins promote microtubule-mediated axonal growth by functioning as structural microtubule-associated proteins and EB1-dependent +TIPs (tip interacting proteins)." J Neurosci 32(27): 9143-9158.

Andersen, R., et al. (2005). "Calcium/calmodulin-dependent protein kinase II alters structural plasticity and cytoskeletal dynamics in Drosophila." J Neurosci 25(39): 8878-8888.

Ahmad, F., et al. (1999). "An essential role for katanin in severing microtubules in the neuron." J Cell Biol 145(2): 305-315.

Baas, P. W., et al. (1989). "Changes in microtubule polarity orientation during the development of hippocampal neurons in culture." J Cell Biol. 109(6): 3085-3094.

Baas, P. W. and H. Joshi (1992). "Gamma-tubulin distribution in the neuron: implications for the origins of neuritic microtubules." J Cell Biol 119(1): 171-178.

Baas, P. W. and S. Lin (2011). "Hooks and comets: The story of microtubule polarity orientation in the neuron." Dev Neurobiol 71(6): 403-418.

Baas, P. W. and O. I. Mozgova (2012). "A novel role for retrograde transport of microtubules in the axon." Cytoskeleton (Hoboken) 69(7): 416-425.

Bartolini, F. and G. G. Gundersen (2006). "Generation of noncentrosomal microtubule arrays." J Cell Sci 119(Pt 20): 4155-4163.

Bischof, J., et al. (2007). “An optimized transgenesis system for *Drosophila* using germ-line-specific phiC31 integrases.” Proc Natl Acad Sci 104(9): 3312-3317.

Bechstedt, S. and G. J. Brouhard (2012). "Doublecortin recognizes the 13-protofilament microtubule cooperatively and tracks microtubule ends." Dev Cell 23(1): 181-192.

Bodmer, R., et al. (1987). "Transformation of sensory organs by Mutations of the cut locus of D. melanogaster." Cell 51(2): 293-307.

Brand, A. and N. Perrimon (1993). "Targeted gene expression as a means of altering cell fates and generating dominant phenotypes." Development 118(2): 401-415.

Brot, S., et al. (2010). "CRMP5 interacts with tubulin to inhibit neurite outgrowth, thereby modulating the function of CRMP2." J Neurosci 30(32): 10639-10654.

Brown, C. E., et al. (2010). "Longitudinal in vivo imaging reveals balanced and branch-specific remodeling of mature cortical pyramidal dendritic arbors after stroke." J Cereb Blood Flow Metab 30(4): 783-791.

Bucciarelli, E., et al. (2009). "Drosophila Dgt6 interacts with Ndc80, Msps/XMAP215, and gamma-tubulin to promote kinetochore-driven MT formation." Curr Biol 19(21): 1839-1845.

Campellone, K. G. and M. D. Welch (2010). "A nucleator arms race: cellular control of actin assembly." Nat Rev Mol Cell Biol 11(4): 237-251.

Cao, L., et al. (2013). "Arabidopsis AUGMIN subunit8 is a microtubule plus-end binding protein that promotes microtubule reorientation in hypocotyls." Plant Cell 25(6): 2187-2201.

Charalambous, D. C., et al. (2013). "KIF1Bbeta transports dendritically localized mRNPs in neurons and is recruited to synapses in an activity-dependent manner." Cell Mol Life Sci 70(2): 335-356.

Chabin-Brion, K., et al. (2001). "The Golgi complex is a microtubule-organizing organelle." Mol Biol Cell 12(7): 2047-2060.

Chen, H. and B. L. Firestein (2007). "RhoA regulates dendrite branching in hippocampal neurons by decreasing cypin protein levels." J Neurosci 27(31): 8378-8386.

Chen, L., et al. (2012). "Axon injury and stress trigger a microtubule-based neuroprotective pathway." Proc Natl Acad Sci 109(29): 11842-11847.

Chen, Y., et al. (2014). "An EB1-kinesin complex is sufficient to steer microtubule growth in vitro." Curr Biol 24(3): 316-321.

Conde, C and Cáceres, A (2009). “Microtubule assembly, organization and dynamics in axons and dendrites.” Nat Rev Neurosci. 10(5): 319-332.

Corty, M. M., et al. (2009). "Molecules and mechanisms of dendrite development in Drosophila." Development 136(7): 1049-1061.

Crino, P. B. and J. Eberwine (1996). "Molecular characterization of the dendritic growth cone: regulated mRNA transport and local protein synthesis." Neuron Vol. 17: 1173–1187.

Cui, W., et al. (2005). “D*rosophila* Nod protein binds preferentially to the plus ends of microtubules and promotes microtubule polymerization *in vitro.”* Mol Bio Cell Vol. 16:5400-5409

Dailey, M. E. and S. J. Smith (1996). "The Dynamics of Dendritic Structure in Developing Hippocampal Slices." J Neurosci. 16(9): 2983-2994.

Dehmelt, L. and S. Halpain (2004). "Actin and microtubules in neurite initiation: are MAPs the missing link?" J Neurobiol 58(1): 18-33.

Dehmelt, L. and S. Halpain (2005). "The MAP2/Tau family of microtubule-associated proteins." Genome Biol. 6(1): 204.

Dent, E. W. and P. W. Baas (2014). "Microtubules in neurons as information carriers." J Neurochem 129(2): 235-239.

Dent, E. W., et al. (2011). "The dynamic cytoskeleton: backbone of dendritic spine plasticity." Curr Opin Neurobiol 21(1): 175-181.

Dong, X., et al. (2014). "Intrinsic and Extrinsic Mechanisms of Dendritic Morphogenesis." Annu Rev Physiol 77: 271-300.

Doodhi, H., et al. (2014). "Mechanical and geometrical constraints control kinesin-based microtubule guidance." Curr Biol 24(3): 322-328.

Ejlerskov, P., et al. (2013). "Tubulin polymerization-promoting protein (TPPP/p25alpha) promotes unconventional secretion of alpha-synuclein through exophagy by impairing autophagosome-lysosome fusion." J Biol Chem 288(24): 17313-17335.

Espinosa, J. S., et al. (2009). "Uncoupling dendrite growth and patterning: single-cell knockout analysis of NMDA receptor 2B." Neuron 62(2): 205-217.

Farah, C. A. and N. Leclerc (2008). "HMWMAP2: new perspectives on a pathway to dendritic identity." Cell Motil Cytoskeleton 65(7): 515-527.

Fourniol, F. J., et al. (2010). "Template-free 13-protofilament microtubule-MAP assembly visualized at 8 A resolution." J Cell Biol 191(3): 463-470.

Fujishima, K., et al. (2012). "Principles of branch dynamics governing shape characteristics of cerebellar Purkinje cell dendrites." Development 139(18): 3442-3455.

Gao, F. B. (2007). "Molecular and cellular mechanisms of dendritic morphogenesis." Curr Opin Neurobiol 17(5): 525-532.

Gao, F. B., et al. (1999). "Genes regulating dendritic outgrowth, branching, and routing in Drosophila." Genes Dev 13: 2549-2561.

Georges, P. C., et al. (2008). "The yin-yang of dendrite morphology: unity of actin and microtubules." Mol Neurobiol 38(3): 270-284.

Gomez-Ferreria, M. A., et al. (2012). "Novel NEDD1 phosphorylation sites regulate gamma-tubulin binding and mitotic spindle assembly." J Cell Sci 125(Pt 16): 3745-3751.

Gonzalez-Billault, C., et al. (2012). "The role of small GTPases in neuronal morphogenesis and polarity." Cytoskeleton (Hoboken) 69(7): 464-485.

Goodwin, S. S. and R. D. Vale (2010). "Patronin regulates the microtubule network by protecting microtubule minus ends." Cell 143(2): 263-274.

Gorczyca, D. A., et al. (2014). "Identification of Ppk26, a DEG/ENaC channel functioning with Ppk1 in a mutually dependent manner to guide locomotion behavior in Drosophila." Cell Rep 9(4): 1446-1458.

Gorski, J. A., et al. (2003). "Brain-Derived Neurotrophic Factor Is Required for the Maintenance of Cortical Dendrites." The Journal of Neuroscience 23(17): 6856 – 6865.

Gotoh, A., et al. (2013). "Gas7b (growth arrest specific protein 7b) regulates neuronal cell morphology by enhancing microtubule and actin filament assembly." J Biol Chem 288(48): 34699-34706.

Goshima, G., et al. (2008). "Augmin: a protein complex required for centrosome-independent microtubule generation within the spindle." J Cell Biol 181(3): 421-429.

Goshima and Kimura (2010). "New look inside the spindle: microtubule-dependent microtubule generation within the spindle." Curr Opin Cell Biol 22(1): 44-49

Grueber, W. B., et al. (2002). "Tiling of the Drosophila epidermis by multidendritic sensory neurons." Development 129(12): 2867-2878.

Grueber, W. B., et al. (2003). "Different levels of the homeodomain protein Cut regulate distinct dendrite branching patterns of Drosophila multidendritic neurons." Cell 112(6): 805–818.

Grueber, W. B., et al. (2003). "Dendrites of distinct classes of Drosophila sensory neurons show different capacities for homotypic repulsion." Current Biology 13(8): 618–626.

Gunawardane, R., et al. (2003). "Characterization of a new gammaTuRC subunit with WD repeats." Mol Biol Cell 14(3): 1017-1026.
Guo, Y., et al. (2014). "The Role of PPK26 in Drosophila Larval Mechanical Nociception." Cell Rep 9(4): 1183-1190.

Halpain, S. and L. Dehmelt (2006). "The MAP1 family of microtubule-associated proteins." Genome Biology 7(6): 224.

Hammer, J. A., 3rd and J. R. Sellers (2012). "Walking to work: roles for class V myosins as cargo transporters." Nat Rev Mol Cell Biol 13(1): 13-26.

Hammer, J. A., 3rd and W. Wagner (2013). "Functions of class V myosins in neurons." J Biol Chem 288(40): 28428-28434.

Hanus, C. and M. D. Ehlers (2008). "Secretory outposts for the local processing of membrane cargo in neuronal dendrites." Traffic 9(9): 1437-1445.

Hayward, D. and J. G. Wakefield (2014). "Chromatin-mediated microtubule nucleation in Drosophila syncytial embryos." Commun Integr Biol 7: e28512.

Heiman, M. G. and S. Shaham (2010). "Twigs into branches: how a filopodium becomes a dendrite." Curr Opin Neurobiol 20(1): 86-91.

Henriquez, D. R., et al. (2012). "The light chain 1 subunit of the microtubule-associated protein 1B (MAP1B) is responsible for Tiam1 binding and Rac1 activation in neuronal cells." PLoS One 7(12): e53123.

Hsia, K. C., et al. (2014). "Reconstitution of the augmin complex provides insights into its architecture and function." Nat Cell Biol 16(9): 852-863.

Hill, S. E., et al. (2012). "Development of dendrite polarity in Drosophila neurons." Neural Dev. 7: 34.

Hodges, J. L., et al. (2011). "Myosin IIb activity and phosphorylation status determines dendritic spine and post-synaptic density morphology." PLoS One 6(8): e24149.

Hoogenraad, C. C. and A. Akhmanova (2010). "Dendritic spine plasticity: new regulatory roles of dynamic microtubules." Neuroscientist 16(6): 650-661.

Hoogenraad, C. C. and F. Bradke (2009). "Control of neuronal polarity and plasticity--a renaissance for microtubules?" Trends Cell Biol 19(12): 669-676.

Hossain, S., et al. (2012). "Dynamic morphometrics reveals contributions of dendritic growth cones and filopodia to dendritogenesis in the intact and awake embryonic brain." Dev Neurobiol 72(4): 615-627.

Hotta, T., et al. (2012). "Characterization of the Arabidopsis augmin complex uncovers its critical function in the assembly of the acentrosomal spindle and phragmoplast microtubule arrays." Plant Cell 24(4): 1494-1509.

Hsieh, P. C., et al. (2012). "DDA3 stabilizes microtubules and suppresses neurite formation." J Cell Sci 125(Pt 14): 3402-3411.

Ho, C. M., et al. (2011). "Augmin plays a critical role in organizing the spindle and phragmoplast microtubule arrays in Arabidopsis." Plant Cell 23(7): 2606-2618.

Hu, J., et al. (2012). "Septin-driven coordination of actin and microtubule remodeling regulates the collateral branching of axons." Curr Biol 22(12): 1109-1115.

Huang, J., et al. (2011). "Interaction between very-KIND Ras guanine exchange factor and microtubule-associated protein 2, and its role in dendrite growth-structure and function of the second kinase noncatalytic C-lobe domain." FEBS J 278(10): 1651-1661.
Huang, Y. A., et al. (2013). "Microtubule-associated type II protein kinase A is important for neurite elongation." PLoS One 8(8): e73890.

Hughes, C. L. and J. B. Thomas (2007). "A Sensory Feedback Circuit Coordinates Muscle Activity in Drosophila." Mol Cell Neurosci 35(2): 383–396.

Hughes, S. E., et al. (2011). "Gamma-tubulin is required for bipolar spindle assembly and for proper kinetochore microtubule attachments during prometaphase I in Drosophila oocytes." PLoS Genet 7(8): e1002209.

Hummel, T., et al. (2000). "Drosophila Futsch/22C10 is a MAP1B-like protein required for dendritic and axonal development." Neuron 26(2): 357-370.

Hutchinson, K. M., et al. (2014). "Dscam1 is required for normal dendrite growth and branching but not for dendritic spacing in Drosophila motoneurons." J Neurosci 34(5): 1924-1931.

Hwang, R. Y., et al. (2007). "Nociceptive neurons protect Drosophila larvae from parasitoid wasps." Curr Biol 17(24): 2105-2116.

Iyer, S. C., et al. (2012). "The RhoGEF trio functions in sculpting class specific dendrite morphogenesis in Drosophila sensory neurons." PLoS One 7(3): e33634.

Jan, Y. N. and Jan, L. Y. (2003). "The Control of Dendrite Development." Neuron 40(2): 229–242.

Jan, Y. N. and Jan, L. Y. (2010). "Branching out: mechanisms of dendritic arborization." Nat Rev Neurosci 11(5): 316-328.

Janke, C. and J. C. Bulinski (2011). "Post-translational regulation of the microtubule cytoskeleton: mechanisms and functions." Nat Rev Mol Cell Biol 12(12): 773-786.

Jiang, K., et al. (2014). "Microtubule minus-end stabilization by polymerization-driven CAMSAP deposition." Dev Cell 28(3): 295-309.

Jinushi-Nakao, S., et al. (2007). "Knot/Collier and cut control different aspects of dendrite cytoskeleton and synergize to define final arbor shape." Neuron 56(6): 963-978.

Johnson, W. A. and J. W. Carder (2012). "Drosophila nociceptors mediate larval aversion to dry surface environments utilizing both the painless TRP channel and the DEG/ENaC subunit, PPK1." PLoS One 7(3): e32878.

Joshi, H., et al. (1992). "Gamma-tubulin is a centrosomal protein required for cell cycle-dependent microtubule nucleation." Nature 356(6364): 80-83.

Kahn, O. I., et al. (2014). "Effects of kinesin-5 inhibition on dendritic architecture and microtubule organization." Mol Biol Cell.

Kamasaki, T., et al. (2013). "Augmin-dependent microtubule nucleation at microtubule walls in the spindle." J Cell Biol 202(1): 25-33.

Kapitein, L. C. and C. C. Hoogenraad (2011). "Which way to go? Cytoskeletal organization and polarized transport in neurons." Mol Cell Neurosci 46(1): 9-20.

Kapitein, L. C. and C. C. Hoogenraad (2015). "Building the Neuronal Microtubule Cytoskeleton." Neuron 87(3): 492-506.

Kapitein, L. C., et al. (2010). "Mixed microtubules steer dynein-driven cargo transport into dendrites." Curr Biol 20(4): 290-299.

Kaufmann, W. E. and H. W. Moser (2000). "Dendritic Anomalies in Disorders Associated with Mental Retardation." Cerebral Cortex 10(10)(10): 981-991.

Kerr, B., et al. (1999). "Brain-Derived Neurotrophic Factor Modulates Nociceptive Sensory Inputs and NMDA-Evoked Responses in the Rat Spinal Cord." 19 12(5138-5148).

Kerrisk, M. E. and A. J. Koleske (2013). "Arg kinase signaling in dendrite and synapse stabilization pathways: memory, cocaine sensitivity, and stress." Int J Biochem Cell Biol 45(11): 2496-2500.

Kevenaar, J. T. and C. C. Hoogenraad (2015). "The axonal cytoskeleton: from organization to function." Front Mol Neurosci 8: 44.

Khanna, R., et al. (2012). "Opening Pandora's jar: a primer on the putative roles of CRMP2 in a panoply of neurodegenerative, sensory and motor neuron, and central disorders." Future Neurol 7(6): 749-771.

Khodjakov, A. and C. Rieder (1999). "The sudden recruitment of gamma-tubulin to the centrosome at the onset of mitosis and its dynamic exchange throughout the cell cycle, do not require microtubules." J Cell Biol 146(3): 585-596.

Kim, M. E., et al. (2012). "Integrins establish dendrite-substrate relationships that promote dendritic self-avoidance and patterning in drosophila sensory neurons." Neuron 73(1): 79-91.

Kim, M. J. and W. A. Johnson (2014). "ROS-mediated activation of Drosophila larval nociceptor neurons by UVC irradiation." BMC Neurosci.

Kim, Y. T., et al. (2011). "Role of GSK3 Signaling in Neuronal Morphogenesis." Front Mol Neurosci 4: 48.

Kimura, T., et al. (2005). "Tubulin and CRMP-2 complex is transported via Kinesin-1." J Neurochem 93(6): 1371-1382.

Kinoshita, M., et al. (2002). "Self- and actin-templated assembly of Mammalian septins." Dev Cell 3(6): 791-802.

Kishore, S. and J. R. Fetcho (2013). "Homeostatic regulation of dendritic dynamics in a motor map in vivo." Nat Commun 4: 2086.

Kneussel, M. and W. Wagner (2013). "Myosin motors at neuronal synapses: drivers of membrane transport and actin dynamics." Nat Rev Neurosci 14(4): 233-247.

Koleske, A. J. (2013). "Molecular mechanisms of dendrite stability." Nat Rev Neurosci 14(8): 536-550.

Kollman, J. M., et al. (2011). "Microtubule nucleation by gamma-tubulin complexes." Nat Rev Mol Cell Biol 12(11): 709-721.

Korulu, S., et al. (2013). "Protein kinase C activation causes neurite retraction via cyclinD1 and p60-katanin increase in rat hippocampal neurons." Eur J Neurosci 37(10): 1610-1619.

Kremer, M. C., et al. (2010). "Structural long-term changes at mushroom body input synapses." Curr Biol 20(21): 1938-1944.

Kuijpers, M. and C. C. Hoogenraad (2011). "Centrosomes, microtubules and neuronal development." Mol Cell Neurosci 48(4): 349-358.

Kulkarni, V. A. and B. L. Firestein (2012). "The dendritic tree and brain disorders." Mol Cell Neurosci 50(1): 10-20.

Kuramoto, K., et al. (2009). "Regulation of dendrite growth by the Cdc42 activator Zizimin1/Dock9 in hippocampal neurons." J Neurosci Res 87(8): 1794-1805.

Kwon, M., et al. (2011). "BDNF-promoted increases in proximal dendrites occur via CREB-dependent transcriptional regulation of cypin." J Neurosci 31(26): 9735-9745.

Labonte, D., et al. (2013). "TRIM3 regulates the motility of the kinesin motor protein KIF21B." PLoS One 8(9): e75603.

Lansbergen, G. and A. Akhmanova (2006). "Microtubule plus end: a hub of cellular activities." Traffic 7(5): 499-507.

Lajoie-Mazenc, I., et al. (1994). "Recruitment of antigenic gamma-tubulin during mitosis in animal cells: presence of gamma-tubulin in the mitotic spindle." J Cell Sci 107(10): 2825-2837.

Lawo, S., et al. (2009). "HAUS, the 8-subunit human Augmin complex, regulates centrosome and spindle integrity." Curr Biol 19(10): 816-826.

Lecland, N. and J. Luders (2014). "The dynamics of microtubule minus ends in the human mitotic spindle." Nat Cell Biol 16(8): 770-778.

Lee, H., et al. (2004). "The microtubule plus end tracking protein Orbit/MAST/CLASP acts downstream of the tyrosine kinase Abl in mediating axon guidance." Neuron 42(6): 913-926.

Lee, H. H., et al. (2009). "Drosophila IKK-related kinase Ik2 and Katanin p60-like 1 regulate dendrite pruning of sensory neuron during metamorphosis." Proc Natl Acad Sci U S A 106(15): 6363-6368.

Lee, L. J., et al. (2005). "NMDA receptor-dependent regulation of axonal and dendritic branching." J Neurosci 25(9): 2304-2311.

Lee, S., et al. (2011). "Pathogenic polyglutamine proteins cause dendrite defects associated with specific actin cytoskeletal alterations in Drosophila." Proc Natl Acad Sci 108(40): 16795-16800.

Lee, T. and L. Luo (1999). "Mosaic analysis with a repressible cell marker for studies of gene function in neuronal morphogenesis." Neuron 22(3): 451-461.

Leemhuis, J. and H. H. Bock (2011). "Reelin modulates cytoskeletal organization by regulating Rho GTPases." Commun Integr Biol 4(3): 254-257.

Lewis, T. L., Jr., et al. (2009). "Myosin-dependent targeting of transmembrane proteins to neuronal dendrites." Nat Neurosci 12(5): 568-576.

Lewis, T. L., Jr. and F. Polleux (2012). "Neuronal morphogenesis: Golgi outposts, acentrosomal microtubule nucleation, and dendritic branching." Neuron 76(5): 862-864.

Li, J., et al. (2011). "In vivo time-lapse imaging and serial section electron microscopy reveal developmental synaptic rearrangements." Neuron 69(2): 273-286.

Li, Q. and H. Joshi (1995). "Gamma-Tubulin Is a Minus End-specific Microtubule Binding Protein." J Cell Biol 131(1): 207-214.

Li, W. and F. B. Gao (2003). "Actin Filament-Stabilizing Protein Tropomyosin Regulates the Size of Dendritic Fields." The Journal of Neuroscience 23(15): 6171– 6175.

Licznerski, P. and R. S. Duman (2013). "Remodeling of axo-spinous synapses in the pathophysiology and treatment of depression." Neuroscience 251: 33-50.
Lin, S., et al. (2012). "Mitotic motors coregulate microtubule patterns in axons and dendrites." J Neurosci 32(40): 14033-14049.

Lin, T. C., et al. (2014). "Targeting of gamma-tubulin complexes to microtubule organizing centers: conservation and divergence." Trends Cell Biol.

Lin, W. H., et al. (2013). "Myosin X and its motorless isoform differentially modulate dendritic spine development by regulating trafficking and retention of vasodilator-stimulated phosphoprotein." J Cell Sci 126(Pt 20): 4756-4768.

Lin, W. H., et al. (2010). "Vasodilator-stimulated phosphoprotein (VASP) induces actin assembly in dendritic spines to promote their development and potentiate synaptic strength." J Biol Chem 285(46): 36010-36020.

Lin, Y. C. and A. J. Koleske (2010). "Mechanisms of synapse and dendrite maintenance and their disruption in psychiatric and neurodegenerative disorders." Annu Rev Neurosci 33: 349-378.

Liu, T., et al. (2014). "Augmin triggers microtubule-dependent microtubule nucleation in interphase plant cells." Curr Biol 24(22): 2708-2713.

Lom, B. and S. Cohen-Cory (1999). "Brain-Derived Neurotrophic Factor Differentially Regulates Retinal Ganglion Cell Dendritic and Axonal Arborization In Vivo." The Journal of Neuroscience 19(22): 9928–9938.

Lu, W., et al. (2013). "Initial neurite outgrowth in Drosophila neurons is driven by kinesin-powered microtubule sliding." Curr Biol 23(11): 1018-1023.

Lüders et al. (2006). “GCP-WD is a γ-tubulin targeting factor required for centrosomal and chromatin-mediated microtubule nucleation.” Nat Cell Biol 8: 137-147

Ma, L., et al. (2011). "CRP1, a protein localized in filopodia of growth cones, is involved in dendritic growth." J Neurosci 31(46): 16781-16791.

Maniar, T. A., et al. (2012). "UNC-33 (CRMP) and ankyrin organize microtubules and localize kinesin to polarize axon-dendrite sorting." Nat Neurosci 15(1): 48-56.

Manning, J. A. and S. Kumar (2010). "A potential role for NEDD1 and the centrosome in senescence of mouse embryonic fibroblasts." Cell Death Dis 1: e35.

Manning, J. A., et al. (2010). "An essential function for the centrosomal protein NEDD1 in zebrafish development." Cell Death Differ 17(8): 1302-1314.

Manning, J. A., et al. (2010). "A direct interaction with NEDD1 regulates gamma-tubulin recruitment to the centrosome." PLoS One 5(3): e9618.

Mattie, F. J., et al. (2010). "Directed microtubule growth, +TIPs, and kinesin-2 are required for uniform microtubule polarity in dendrites." Curr Biol 20(24): 2169-2177.

Meng, W., et al. (2008). "Anchorage of microtubule minus ends to adherens junctions regulates epithelial cell-cell contacts." Cell 135(5): 948-959.

Merriam, E. B., et al. (2013). "Synaptic regulation of microtubule dynamics in dendritic spines by calcium, F-actin, and drebrin." J Neurosci 33(42): 16471-16482.

Meireles, A. M., et al. (2009). "Wac: a new Augmin subunit required for chromosome alignment but not for acentrosomal microtubule assembly in female meiosis." J Cell Biol 184(6): 777-784.

Meijering, E., et al. (2004). "Design and validation of a tool for neurite tracing and analysis in fluorescence microscopy images." Cytometry A 58(2): 167-176.

Moores, C. A., et al. (2004). "Mechanism of microtubule stabilization by doublecortin." Mol Cell 14(6): 833-839.

Moritz, M., et al. (2000). "Structure of the gamma-tubulin ring complex: a template for microtubule nucleation." Nat Cell Biol 2: 365-370.

Mumm, J. S., et al. (2006). "In vivo imaging reveals dendritic targeting of laminated afferents by zebrafish retinal ganglion cells." Neuron 52(4): 609-621.

Nakaoka, Y., et al. (2012). "An inducible RNA interference system in Physcomitrella patens reveals a dominant role of augmin in phragmoplast microtubule generation." Plant Cell 24(4): 1478-1493.

Nagel, J., et al. (2012). "Fascin controls neuronal class-specific dendrite arbor morphology." Development 139(16): 2999-3009.

Nagendran, T. and L. R. Hardy (2011). "Calcium/calmodulin-dependent protein kinase IV mediates distinct features of basal and activity-dependent dendrite complexity." Neuroscience 199: 548-562.

Namba, T., et al. (2011). "The role of selective transport in neuronal polarization." Dev Neurobiol 71(6): 445-457.

Newey, S. E., et al. (2005). "Rho GTPases, dendritic structure, and mental retardation." J Neurobiol 64(1): 58-74.

Nguyen, M. M., et al. (2014). "Gamma-tubulin controls neuronal microtubule polarity independently of Golgi outposts." Mol Biol Cell 25(13): 2039-2050.

Nguyen, M. M., et al. (2011). "Microtubules are organized independently of the centrosome in Drosophila neurons." Neural Dev 6: 38.

Niblock, M. M., et al. (2000). "Insulin-Like growth factor I stimulates dendritic growth in primary somatosensory cortex." J Neurosci. 20(11): 4165–4176.

Niell, C. M., et al. (2004). "In vivo imaging of synapse formation on a growing dendritic arbor." Nat Neurosci 7(3): 254-260.

Niell, C. M. and S. J. Smith (2004). "Live optical imaging of nervous system development." Annu Rev Physiol 66(1): 771-798.

Niisato, E., et al. (2013). "Phosphorylation of CRMP2 is involved in proper bifurcation of the apical dendrite of hippocampal CA1 pyramidal neurons." Dev Neurobiol 73(2): 142-151.

Noack, M., et al. (2014). "HDAC6 inhibition results in tau acetylation and modulates tau phosphorylation and degradation in oligodendrocytes." Glia 62(4): 535-547.

Oakley, B., et al. (1990). "Gamma-Tubulin Is a component of the spindle pole body that Is essential for microtubule function in Aspergillus nidulans." Cell 61(7): 1289-1301.

Oegema, K., et al. (1999). "Characterization of two related Drosophila gamma-tubulin complexes that differ in their ability to nucleate microtubules." J Cell Biol 144(4): 721-733.

Ohtani, A., et al. (2014). "Serotonin 2A receptor regulates microtubule assembly and induces dynamics of dendritic growth cones in rat cortical neurons in vitro." Neurosci Res 81-82: 11-20.

Okumura, M., et al. (2015). "Linking cell surface receptors to microtubules: tubulin folding cofactor D mediates Dscam functions during neuronal morphogenesis." J Neurosci 35(5): 1979-1990.

Ori-McKenney, K. M., et al. (2012). "Golgi outposts shape dendrite morphology by functioning as sites of acentrosomal microtubule nucleation in neurons." Neuron 76(5): 921-930.

Ou, H. L. (2013). "Gene knockout by inducing P-element transposition in Drosophila." Genet Mol Res 12(3): 2852-2857.

Parrish, J. Z., et al. (2007). "Polycomb genes interact with the tumor suppressor genes hippo and warts in the maintenance of Drosophila sensory neuron dendrites." Genes Dev 21(8): 956-972.

Peris, L., et al. (2009). "Motor-dependent microtubule disassembly driven by tubulin tyrosination." J Cell Biol 185(7): 1159-1166.

Petry, S., et al. (2013). "Branching microtubule nucleation in Xenopus egg extracts mediated by augmin and TPX2." Cell 152(4): 768-777.

Pertz, O. (2010). "Spatio-temporal Rho GTPase signaling - where are we now?" J Cell Sci 123(Pt 11): 1841-1850.

Pinyol, R., et al. (2013). "The role of NEDD1 phosphorylation by Aurora A in chromosomal microtubule nucleation and spindle function." Curr Biol 23(2): 143-149.

Preitner, N., et al. (2014). "APC is an RNA-binding protein, and its interactome provides a link to neural development and microtubule assembly." Cell 158(2): 368-382.

Reiner, o. (2013). "LIS1 and DCX: Implications for brain development and human disease in relation to microtubules." Scientifica (Cairo) 2013: 393975.

Reschen, R. F., et al. (2012). "Dgp71WD is required for the assembly of the acentrosomal Meiosis I spindle, and is not a general targeting factor for the gamma-TuRC." Biol Open 1(5): 422-429.

Rivero, S., et al. (2009). "Microtubule nucleation at the cis-side of the Golgi apparatus requires AKAP450 and GM130." EMBO J 28(8): 1016-1028.

Roberts, A. J., et al. (2013). "Functions and mechanics of dynein motor proteins." Nat Rev Mol Cell Biol 14(11): 713-726.

Rolls, M. M., et al. (2007). "Polarity and intracellular compartmentalization of *Drosophila* neurons." Neural Dev 2: 7.

Roubin, R., et al. (2013). "Myomegalin is necessary for the formation of centrosomal and Golgi-derived microtubules." Biol Open 2(2): 238-250.

Sakakibara, A., et al. (2013). "Microtubule dynamics in neuronal morphogenesis." Open Biol 3(7): 130061.

Sasaki, S., et al. (1983). "Serial reconstruction of microtubular arrays within dendrites of the cat retinal ganglion cell: The cytoskeleton of a vertebrate dendrite." Brain Res. 259(2): 193-206.

Satoh, D., et al. (2008). "Spatial control of branching within dendritic arbors by dynein-dependent transport of Rab5-endosomes." Nat Cell Biol 10(10): 1164-1171.

Schlager, M. A. and C. C. Hoogenraad (2009). "Basic mechanisms for recognition and transport of synaptic cargos." Mol Brain 2: 25.

Schwenk, B. M., et al. (2014). "The FTLD risk factor TMEM106B and MAP6 control dendritic trafficking of lysosomes." EMBO J 33(5): 450-467.
Scott, E. K., et al. (2003). "Dendritic development of Drosophila high order visual system neurons is independent of sensory experience." BMC Neuroscience 4(14).

Sharp, D. J. and J. L. Ross (2012). "Microtubule-severing enzymes at the cutting edge." J Cell Sci 125(Pt 11): 2561-2569.

Sharp, D. J., et al. (1995). "Transport of dendritic microtubules establishes their nonuniform polarity orientation." J Cell Biol 130(1): 93-103.

Shashikala, S., et al. (2013). "Fodrin in centrosomes: implication of a role of fodrin in the transport of gamma-tubulin complex in brain." PLoS One 8(10): e76613.

Shin, E., et al. (2013). "Doublecortin-like kinase enhances dendritic remodelling and negatively regulates synapse maturation." Nat Commun 4: 1440.

Sin, W. C., et al. (2002). "Dendrite growth increased by visual activity requires NMDA receptor and Rho GTPases." Nature 419(6906): 475-480.

Singh, A. P., et al. (2010). "Dendritic refinement of an identified neuron in the Drosophila CNS is regulated by neuronal activity and Wnt signaling." Development 137(8): 1351-1360.

Soba, P., et al. (2007). "Drosophila sensory neurons require Dscam for dendritic self avoidance and proper dendritic field organization." Neuron.

Stearns, T. and M. Kirschner (1994). "In vitro reconstitution of centrosome assembly and function: the central role of gamma-tubulin." Cell 76(4): 623-637.

Stepanova, T., et al. (2003). "Visualization of microtubule growth in cultured neurons via the use of EB3-GFP (end-binding protein 3-green fluorescent protein)." J Neurosci. 23(7): 2655-2664.

Stewart, A., et al. (2012). "Katanin p60-like1 promotes microtubule growth and terminal dendrite stability in the larval class IV sensory neurons of Drosophila." J Neurosci 32(34): 11631-11642.

Stiess, M., et al. (2010). "Axon extension occurs independently of centrosomal microtubule nucleation." Science 327(5966): 704-707.

Stone, M., et al. (2008). "Microtubules have opposite orientation in axons and dendrites of Drosophila neurons." Mol Biol Cell 19(10): 4122-4129.

Stone, M. C., et al. (2010). "Global up-regulation of microtubule dynamics and polarity reversal during regeneration of an axon from a dendrite." Mol Biol Cell 21(5): 767-777.

Stone, M. C., et al. (2012). "Normal spastin gene dosage is specifically required for axon regeneration." Cell Rep 2(5): 1340-1350.

Sudo, H. and P. W. Baas (2010). "Acetylation of microtubules influences their sensitivity to severing by katanin in neurons and fibroblasts." J Neurosci 30(21): 7215-7226.

Sudo, H. and P. W. Baas (2011). "Strategies for diminishing katanin-based loss of microtubules in tauopathic neurodegenerative diseases." Hum Mol Genet 20(4): 763-778.

Sugimura, K., et al. (2003). "Distinct developmental modes and lesion-Induced reactions of dendrites of two classes of Drosophila sensory neurons." J Neurosci. 23(9): 3752-3760.

Sunkel, C., et al. (1995). "Gamma-Tubulin is required for the structure and function of the microtubule organizing centre in Drosophila neuroblasts." EMBO J 14(1): 28-36.

Sweet, E. S., et al. (2011). "PSD-95 alters microtubule dynamics via an association with EB3." J Neurosci 31(3): 1038-1047.

Sweet, E. S., et al. (2011). "To branch or not to branch: How PSD-95 regulates dendrites and spines." Bioarchitecture 1(2): 69-73.

Swiech, L., et al. (2011). "CLIP-170 and IQGAP1 cooperatively regulate dendrite morphology." J Neurosci 31(12): 4555-4568.

Szebenyi, G., et al. (2005). "Activity-driven dendritic remodeling requires microtubule-associated protein 1A." Curr Biol 15(20): 1820-1826.

Tada, T., et al. (2007). "Role of Septin cytoskeleton in spine morphogenesis and dendrite development in neurons." Curr Biol 17(20): 1752-1758.

Tan, J., et al. (2010). "N-cadherin-dependent neuron-neuron interaction is required for the maintenance of activity-induced dendrite growth." Proc Natl Acad Sci 107(21): 9873-9878.

Tavosanis, G. (2012). "The computing dendrite." 23-40.

Teixido-Travesa, N., et al. (2012). "The where, when and how of microtubule nucleation - one ring to rule them all." J Cell Sci 125(Pt 19): 4445-4456.

Tokesi, N., et al. (2010). "TPPP/p25 promotes tubulin acetylation by inhibiting histone deacetylase 6." J Biol Chem 285(23): 17896-17906.

Topalidou, I., et al. (2012). "Genetically separable functions of the MEC-17 tubulin acetyltransferase affect microtubule organization." Curr Biol 22(12): 1057-1065.

Toriumi, K., et al. (2013). "SHATI/NAT8L regulates neurite outgrowth via microtubule stabilization." J Neurosci Res 91(12): 1525-1532.

Tortosa, E., et al. (2011). "Microtubule-associated protein 1B (MAP1B) is required for dendritic spine development and synaptic maturation." J Biol Chem 286(47): 40638-40648.

Tripodi, M., et al. (2008). "Structural homeostasis: compensatory adjustments of dendritic arbor geometry in response to variations of synaptic input." PLoS Biol 6(10): e260.

Tsai, C. Y., et al. (2011). "Aurora-A phosphorylates Augmin complex component Hice1 protein at an N-terminal serine/threonine cluster to modulate its microtubule binding activity during spindle assembly." J Biol Chem 286(34): 30097-30106.

Uehara, R., et al. (2009). "The augmin complex plays a critical role in spindle microtubule generation for mitotic progression and cytokinesis in human cells." Proc Natl Acad Sci U S A 106(17): 6998-7003.

Vaillant, A., et al. (2002). "Signaling mechanisms underlying reversible, activity-dependent dendrite formation." Neuron 34(6): 985-998.

van Spronsen, M., et al. (2013). "TRAK/Milton motor-adaptor proteins steer mitochondrial trafficking to axons and dendrites." Neuron 77(3): 485-502.

Vazquez, M., et al. (2008). "gammaTub23C interacts genetically with brahma chromatin-remodeling complexes in Drosophila melanogaster." Genetics 180(2): 835-843.

Verhey, K. J. and J. Gaertig (2014). "The Tubulin Code." Cell Cycle 6(17): 2152-2160.

Vidal, R. L., et al. (2012). "RNA interference of Marlin-1/Jakmip1 results in abnormal morphogenesis and migration of cortical pyramidal neurons." Mol Cell Neurosci 51(1-2): 1-11.

Vignjevic, D., et al. (2003). "Formation of filopodia-like bundles in vitro from a dendritic network." J Cell Biol 160(6): 951-962.

Vinh, D. B., et al. (2002). "Reconstitution and characterization of budding yeast gamma-tubulin complex." Mol Biol Cell 13(4): 1144-1157.

Walia, A., et al. (2014). "GCP-WD mediates gamma-TuRC recruitment and the geometry of microtubule nucleation in interphase arrays of Arabidopsis." Curr Biol 24(21): 2548-2555.

Wen, Y., et al. (2004). "EB1 and APC bind to mDia to stabilize microtubules downstream of Rho and promote cell migration." Nat Cell Biol 6(9): 820-830.

Westermann, S. and K. Weber (2003). "Post-translational modifications regulate microtubule function." Nat Rev Mol Cell Biol 4(12): 938-947.

Wong, W. T. and R. O. Wong (2000). "Rapid dendritic movements during synapse formation and rearrangement." Curr Opin Neurobiol 10(1): 118-124.

Wong-Riley, M. T. and J. C. Besharse (2012). "The kinesin superfamily protein KIF17: one protein with many functions." Biomol Concepts 3(3): 267-282.

Wu, G., et al. (2008). "Hice1, a novel microtubule-associated protein required for maintenance of spindle integrity and chromosomal stability in human cells." Mol Cell Biol 28(11): 3652-3662.

Wu, G., et al. (2009). "Hec1 contributes to mitotic centrosomal microtubule growth for proper spindle assembly through interaction with Hice1." Mol Biol Cell 20(22): 4686-4695.

Wu, G. Y., et al. (1999). "Dendritic dynamics In vivo change during neuronal maturation." The Journal of Neuroscience 19(11): 4472–4483.

Xiang, Y., et al. (2010). "Light-avoidance-mediating photoreceptors tile the Drosophila larval body wall." Nature 468(7326): 921-926.

Yacoubian, T. A. and D. C. Lo (2000). "Truncated and full-length TrkB receptors regulate distinct modes of dendritic growth." Nat Neurosci 3(4): 342-349.

Yamashita, N., et al. (2012). "Phosphorylation of CRMP2 (collapsin response mediator protein 2) is involved in proper dendritic field organization." J Neurosci 32(4): 1360-1365.

Yan, J., et al. (2013). "Kinesin-1 regulates dendrite microtubule polarity in Caenorhabditis elegans." Elife 2: e00133.

Yan, Z., et al. (2013). "Drosophila NOMPC is a mechanotransduction channel subunit for gentle-touch sensation." Nature 493(7431): 221-225.

Yau, K. W., et al. (2014). "Microtubule minus-end binding protein CAMSAP2 controls axon specification and dendrite development." Neuron 82(5): 1058-1073.

Ye, B., et al. (2011). "Differential regulation of dendritic and axonal development by the novel Kruppel-like factor Dar1." J Neurosci 31(9): 3309-3319.

Ye, B., et al. (2007). "Growing dendrites and axons differ in their reliance on the secretory pathway." Cell 130(4): 717-729.

Yu, W., et al. (1993). "Microtubule nucleation and release from the neuronal centrosome." J Cell Biol 122(2): 349-359.

Yuan, Q., et al. (2011). "Light-induced structural and functional plasticity in Drosophila larval visual system." Science 333(6048): 1458-1462.

Zheng Y., et al (1995). “Nucleation of microtubule assembly by a gamma-tubulin-containing ring complex.” Nature 378(6557): 578-583.

Zheng, Y., et al. (2008). "Dynein is required for polarized dendritic transport and uniform microtubule orientation in axons." Nat Cell Biol 10(10): 1172-1180.

Zhu, H., et al. (2008). "FAM29A promotes microtubule amplification via recruitment of the NEDD1-gamma-tubulin complex to the mitotic spindle." J Cell Biol 183(5): 835-848.

Zipursky, S. L. and W. B. Grueber (2013). "The molecular basis of self-avoidance." Annu Rev Neurosci 36: 547-568.

Ziv, N. E. and S. J. Smith (1996). "Evidence for a role of dendritic filopodia in synaptogenesis and spine formation." Neuron 17(1): 91–102.

7 Acknowledgement

There are many people to thank for helping me during my stay in Germany.

I would express my sincere gratitude to Dr. Gaia Tavosanis for her support and encouragement to my research with her patience and immense knowledge. I would like to thank all the previous and current lab members in the Tavosanis lab for the helpful discussions and the wonderful working atmosphere you have created. I have had a wonderful time to work with you. For experimental support, I would like to especially thank Komal Bhandari.

I would also like to thank all the people in DZNE and LIMES for the useful discussions and scientific advices. Also, thanks to all the friends I made during my life in Germany for the pleasure and help you bring to me.

Last but not the least, I would like to thank my family for supporting me spiritually. Wo ai nimen.